

# 國立交通大學

## 電子物理學系

### 碩 士 論 文

量子點光源中精細結構分裂與光學特性之研究

**Fine Structure Splitting and Optical Properties of Single  
Neutral Excitons in Quantum Dot Light Sources**

研 究 生：林佩儀

指導教授：鄭舜仁 教授

中 華 民 國 一 百 零 一 年 十 月

量子點光源中精細結構匹裂與光學特性之研究

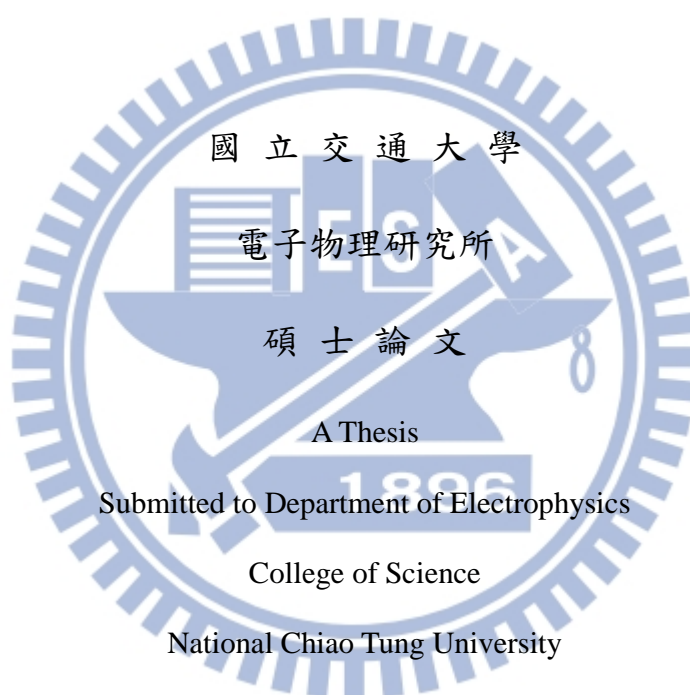
**Fine Structure Splitting and Optical Properties of Single Neutral  
Excitons in Quantum Dot Light Sources**

研 究 生：林佩儀

Student：Pei-Yi Lin

指導教授：鄭舜仁 教授

Advisor：Shun-Jen Cheng



in partial Fulfillment of the Requirements

for the Degree of

Master

in

Electrophysics

2012

HsinChu, Taiwan, Republic of China

中華民國一百零一年十月

# **Fine Structure Splitting and Optical Properties of Single Neutral Excitons in Quantum Dot Light Sources**

**Student :** Pei-Yi Lin

**Advisor :** Shun-Jen Cheng

**Department of Electrophysics**

National Chiao Tung University

## **Abstract**

This thesis theoretically studies the size effects of quantum dots (QDs) on the fine structure properties as well the optical polarization. Known as representative excellent quantum light sources, two semiconductor QDs, InAs/GaAs self-assembled QDs and hierarchical GaAs/AlGaAs QDs are considered. Excitonic structures of the QDs are computed numerically by combining the four-band Luttinger-Kohn  $k \cdot p$ 's model for valence hole and single-band model for conduction electron within the 3D-parabolic potential model of QD. Optical polarizations of the single excitons in the dots are calculated by using Fermi's Golden rule. Initial strain in InAs/GaAs self-assembled QDs induced by lattice mismatch is formulated as a function of size analytically and numerically calculated using finite-element software package, Comsol multiphysics®. Analytical results indicate that the energetic competition of the size-dependent short- and long-ranged e-h exchange interactions diminish the fine structure splitting of an elongated QD. Moreover, the electronic structures and optical polarization properties of GaAs bulk under stress control were studied theoretically, in which the corresponding microscopic Bloch wave functions were visualized under applied stress by using the Slater Orbital model.

# 量子點光源中精細結構匹裂與光學特性之研究

學生：林佩儀

指導教授：鄭舜仁 博士

國立交通大學

電子物理研究所碩士班

## 摘要

本論文主要以理論方法討論尺寸效應下量子點的精細匹裂(fine structure splitting)與光學異相性(optical anisotropic)。文中討論兩種具代表性的量子點光源: InAs/GaAs 自組式(self-assembled)量子點, 以及 hierchical GaAs/AlGaAs 量子點。文中使用單能帶以及四能帶  $k \cdot p$  模型並搭配三維簡協振子(3-D parabolic model)模型分別計算激子(exciton)系統的電子與電動結構。光學偏振部分以費米黃金定律(Fermi's Golden Rule)計算各方向之發光強度及異相性。文中討論的兩種量子點中, InAs/GaAs 自組式量子點因兩種材料晶格不匹配於量子點內部存在的應變效應可由解析方式得到量子點中心點的應變量; 此應變解析值亦可與套裝軟體 Comsol multiphysics<sup>®</sup> 比較。除四能帶模型的數值模擬以外, 文中亦以微擾方式簡化系統並得易分析的解析解。由解析解中可得量子點中的精細匹裂的消長乃由於長程作用力(long-range interaction)及短程作用力(short-range interaction)兩者的相互競爭引起。

除最基本的尺寸效應探討以外, 量子點的精細匹裂與光學異相性亦可由外加應力調控。文中於 GaAs 塊材外加單軸應力(uni-axial stress), 並探討塊材在應力下的能帶、光學偏振以及微觀尺度的 Bloch function 變化。對塊材在應力之下的變化有基本認知後, 我們未來工作更可將應力作用延伸至量子點。

## 致謝

碩士生涯首先要感謝的是鄭舜仁老師的指導，謝謝鄭老師在百忙之中還花了許多時間費心幫忙我修改論文。老師的多角化合作也讓我大開眼界，見識到許多頂尖團隊走在前端的工作。老師嚴謹的研究態度將讓我往後一再檢視自己的工作流程。同時也感謝台積電計畫支持將我的論文送予論文編修中心修改，編修結果實獲益良多。

謝謝我的父母及姊姊們總是在任何方面都給予永無止盡的支持，並總是擔心卻仍沒有懷疑地包容我所有任性的決定。感謝致融學長在我重拾書本、腦袋還一片空白之際伸出援手，你總是在我手足無措又煩躁時給予協助與鼓勵；即便領域不相同，仍是會試圖幫忙解惑，衷心祝福陳小黑接下來學術生涯順遂。謝謝我的好朋友思萱以及盈佳在新竹兩年生活的陪伴，有你們陪我去逛街跟唱歌才讓新竹這無聊的地方讓人不那麼抓狂。感謝張榮興學長的智慧話語，學長就像我的心靈導師一般。也謝謝室友冠緣在我初到新竹兵荒馬亂時幫忙找房子及一年的陪伴，還有佩君讓我見識到理工領域之外完全不同的世界。

感謝跟我密切合作的 Darcy 總是幫忙收拾殘局；大學長提供研究室安定的力量；珮紋學姐的貼心問候以及幫助；還有先前智豪、語宸、建智學長研究上無私的協助及傳授；以及智瑋、書睿、家祥的陪伴及所有協助。希望大家接下來研究室同仁以及學弟妹都可以學業順心、身體健康。

最後謝謝口委張文豪老師、林炯源老師及林聖迪老師的建議，讓我了解自己之後可能面臨的問題。

# Table of contents

Abstract.....	III
Table of contents.....	VI
Table of tables.....	X
Chapter 1 Introduction .....	1
1.1 Introduction .....	1
1.2 Motivation .....	2
1.3 Contents.....	4
Chapter 2 Fundamental Theory.....	5
2.1 Theory for Exciton .....	5
2.2 Strain effects.....	21
Chapter 3 Size Effects .....	36
3.1 Hierarchical GaAs QDs.....	38
3.2 InAs/GaAs self-assembled QDs.....	43
Chapter 4 Strain effects on semiconductor bulk .....	49
4.1 Fundamental bulk theory.....	49
4.2 Numerical results of bulk with applied stress .....	52
References .....	62
Appendix I Rotation Matrix .....	64
Appendix II Reference frame transformation of kinetic part.....	66
Appendix III Reference frame transformation of strain part.....	73
Appendix IV Strain modification by six-band model .....	77
Parameters .....	80



## Table of Figures

Table of contents .....	VI
<b>Table of tables</b> .....	<b>X</b>
Fig. 1.2.1 (a) InAs/GaAs self-assembled QDs has initial strain due to InAs and GaAs lattice mismatch. (b) Shape of InAs/GaAs self-assembled QDs. (c) hierarchical GaAs/AlGaAs QDs is strain free since the materials near by the QDs have similar lattice constant.....	2
Fig. 2.1.1 A diagram illustrates the hole potential and the relative position of <i>HH</i> - and <i>LH</i> - states and the <i>HH-LH</i> - splitting. ....	9
Fig. 2.1.2 The zero energy level locates at dark exciton state. The bright exciton was originally a two-fold degenerate level, but is separated due to the exchange interaction.....	10
Fig. 2.1.3 (a) Optical polarization polarization chart, and (b) the corresponding energy spectrum. ....	14
Fig. 2.1.4 A Gaussian function along <i>x</i> -direction. ....	18
Fig.2.1.5 Electron wave function along (a) <i>x</i> -direction, $L_x = 20$ nm, $A_x = 0.09$ , (b) <i>z</i> -direction, $L_z = 5$ nm, $A_z = 0.47$ .....	20
Fig. 2.2.1 shows a cubic shaped quantum dot and its corresponding length.....	22
Fig. 2.2.2 Strain quantities of symmetry cubic QDs (a) $\varepsilon_{xx}$ , $\varepsilon_{yy}$ , (b) $\varepsilon_{zz}$ , (c) $\varepsilon_{xx} + \varepsilon_{yy} - 2\varepsilon_{zz}$ , (d) $\varepsilon_{xx} + \varepsilon_{yy} + \varepsilon_{zz}$ from $L_x = 10 \sim 100$ nm, $L_z = 2$ nm .....	24
Fig. 2.2.3 Strain quantities of asymmetry quantum dots are equivalent. Asymmetrize $\xi = L_y / L_x = 0.85$ , $h = L_z = 2$ nm (a) $\varepsilon_{xx}$ , $\varepsilon_{yy}$ , (b) $\varepsilon_{zz}$ , (c)	

$\varepsilon_{xx} + \varepsilon_{yy} - 2\varepsilon_{zz}$  (d)  $\varepsilon_{xx} - \varepsilon_{yy}$  , (e)  $\varepsilon_{xx} + \varepsilon_{yy} + \varepsilon_{zz}$  from  $L_x = 10 \sim 100$  nm, ..... 26

Fig. 2.2.4 The displacement along the parallel direction and perpendicular direction relative to its original lattice length. .... 27

Fig. 2.2.5 (a) stresses in given coordinate system. (b) stress applied with an angle  $\phi_\sigma$  to the main reference coordinate. .... 34

Fig. 3.1 (a) The normal distribution that shows low energy state and polarization along x-direction. (b) The abnormal situation that shows low energy state emits along y-direction..... 37

Fig. 3.2 Energy difference from dark to bright exciton  $\Delta_{BD}$  of InAs and GaAs. .... 37

Fig. 3.1.1 (a)  $\rho_{HL}$  and  $\Delta_{HL}$  (b)  $\frac{\rho_{HL}}{\Delta_{HL}}$  (c)  $Pol_{\pi x, \pi y}$  with both numerical and analytical result. (d)  $E_g^{QD}$  (e)  $\Delta_{BD}$  (f)  $S_{\pi x, \pi y}$ ,  $\Delta_1$  and  $\Delta'_1$  of GaAs strain free QDs vary with size.  $l_z = 2$  nm and  $\xi' = l_y / l_x = 0.8$  ..... 39

Fig. 3.1.2 GaAs QDs without strain. PL polarization and energy spectrum of QDs vary with characteristic length of (a) 3nm (b) 3.25nm (c) 3.5nm (d) 3.75nm (e) 5nm (f) 6nm (g) 7nm (h) 8nm.  $l_z = 2$  nm and  $\xi' = l_y / l_x = 0.8$  ..... 40

Fig. 3.2.1 (a)  $\rho_{HL}$  and  $\Delta_{HL}$  (b)  $\frac{\rho_{HL}}{\Delta_{HL}}$  (c)  $Pol_{\pi x, \pi y}$  with both numerical and analytical result. (d)  $E_g^{QD}$  (e)  $\Delta_{BD}$  (f)  $S_{\pi x, \pi y}$ ,  $\Delta_1$  and  $\Delta'_1$  of InAs strain free QDs vary with size.  $l_z = 2$  nm and  $\xi' = l_y / l_x = 0.8$  ..... 43



Fig. 3.2.2 InAs/GaAs with initial strain. (a) strain tensors of  $\epsilon_{xx}$ ,  $\epsilon_{yy}$  and  $\epsilon_{zz}$ , (b)  $\Delta_1$ ,

(c)  $\rho_{HL}$ ,  $\rho_{HL}^k$  and  $\rho_{HL}^\epsilon$ , (d)  $\frac{\rho_{HL}^k}{\rho_{HL}}$  and  $\frac{\rho_{HL}^\epsilon}{\rho_{HL}}$ , (e)  $\Delta_{HL}$ ,  $\Delta_{HL}^k$  and  $\Delta_{HL}^\epsilon$ , (f)  $\frac{\Delta_{HL}^k}{\Delta_{HL}}$  and  $\frac{\Delta_{HL}^\epsilon}{\Delta_{HL}}$ , (g)  $\frac{\rho_{HL}}{\Delta_{HL}}$ , (h)  $Pol_{\pi x, \pi y}$ , (I)  $\Delta_{BD}$ , and  $\Delta_1$  (J)  $S_{\pi x, \pi y}$ ,  $\Delta_1$  and  $\Delta'$  against size with  $l_z = 2 \text{ nm}$  and  $\xi' = l_y / l_x = 0.8$  ..... 45

Fig. 3.2.3 Polar plots and PL spectra of InAs/GaAs QD varies with characteristic length of (a) 3.5nm, (b) 3.75nm, (c) 4nm, (d) 4.25nm, (e) 4.5nm (f) 5nm (g) 6nm (h) 7nm. .... 46

Fig. 4.1.1 An electron in the initial excited state spontaneously emit radiation, two states are probable for the emission process. .... 49

Fig. 4.2.1 GaAs bulk energy bands with stress (a) -2GPa (b) zero (c) 2GPa stress applied along [110]. .... 52

Fig. 4.2.2 PL polarization (first row) and energy spectrum (second row) of GaAs bulk with applied stress (a) -2GPa (b) zero (c) 2GPa (d) -2GPa (e) zero (f) 2GPa. Red lines denotes the low transition energy, blue line denotes the high transition. Stress applied along [110] ..... 53

Fig. 4.2.3 Microscopic Bloch function. First row are low energy states (a) -2GPa (b) zero (c) 2GPa. While second row are the Bloch function of the high energy states (d) -2GPa (e) zero (f) 2GPa. Stress applied along [110]. .... 54

Fig. 4.2.4 (a) The chart reveals the band-edge energies at  $\Gamma$ -point. (b) The chart reveals the low transition and high transition energies. (c) Band-edge energies of three bands at  $\Gamma$ -point. (d) Transition energies, the energy difference from the conduction band to the two hole-states. Stress applied

along [110] direction .....	55
Fig. 4.2.5 GaAs bulk energy bands with stress (a) -2GPa (b) zero (c) 2GPa. Stress applied along [100].....	56
Fig. 4.2.6 PL polarization (first row) and energy spectrum (second row)of GaAs bulk with stress (a) -2GPa (b) zero (c) 2GPa (d) -2GPa (e) zero (f) 2GPa. Red lines denotes the low transition energy one, blue denotes the high transition. Stress applied along [100] .....	57
Fig. 4.2.7 Microscopic Bloch function. First row are the high energy states (a) -2GPa (b) zero (c) 2GPa . While second row are the Bloch function for the low energy hole state(d) -2GPa (e) zero (f) 2GPa. Stress applied along [100] .....	57
Fig. 4.2.8 Stress applied along [100] (a) band-edge energies at $\Gamma$ -point of three bands.(b) Transition energies, the energy difference from the conduction band to the two hole-states. Stress applied along [100] direction. ....	58
Fig. 4.2.9 “Distortion of the electron cloud in response of an applied E-field.” (Hecht)[20] .....	58
Fig. IV.1 shows the LH-potential is underestimated in the 4-band model which leads to the overestimation of $\Delta_{HL}^e$ , therefore the 6 band model of strain part is used throughout this thesis. ....	77

## Table of tables

Table I. dipole matrix element ( $\vec{e} = \hat{x} \sin \theta \cos \phi + \hat{y} \sin \theta \sin \phi + \hat{z} \cos \theta$ )[19] .....	17
--	----

# Chapter 1 Introduction

## 1.1 Introduction

Following extensive study in recent decades, quantum optics has received renewed interest recently owing to its sensational applications. Quantum information has especially garnered considerable attention which can further extend to the areas such as of single-photon source, and quantum cryptography. The most important aspect of quantum optics is the use of quantum information in quantum computation and communication, quantum cryptography and single-photon source. Quantum information can replace the conventional computation signal 0 and 1 by entanglement states, information can also be presented by a linear combination of the two states rather than a long chain of 0 and 1, thus reducing the computational speed and storage space. Semiconductor quantum dot is especially noteworthy for its quantum confinement effect and atom-like energy level. Achieving the above applications depends on the ability to fabricate the quantum entanglement for spin excitons in quantum dots. The entanglement can be destroyed by the electron-hole exchange interaction and subsequent the fine structure splitting (FSS), which is induced by factors such as shape deformation, and build-in strain effect.

## 1.2 Motivation

Eliminating the fine structure splitting between the bright exciton states is of priority concern to successfully generate of entangled photon pair from a QD. This study investigates two quantum dots InAs/GaAs self-assembled QDs and GaAs/AlGaAs hierarchical QDs.

InAs/GaAs self-assembled QDs have a built-in initial strain due to InAs and GaAs lattice mismatching[1]. For hierarchical QDs, GaAs is grown on AlGaAs with a very close lattice constant and strain free in-dot[2].

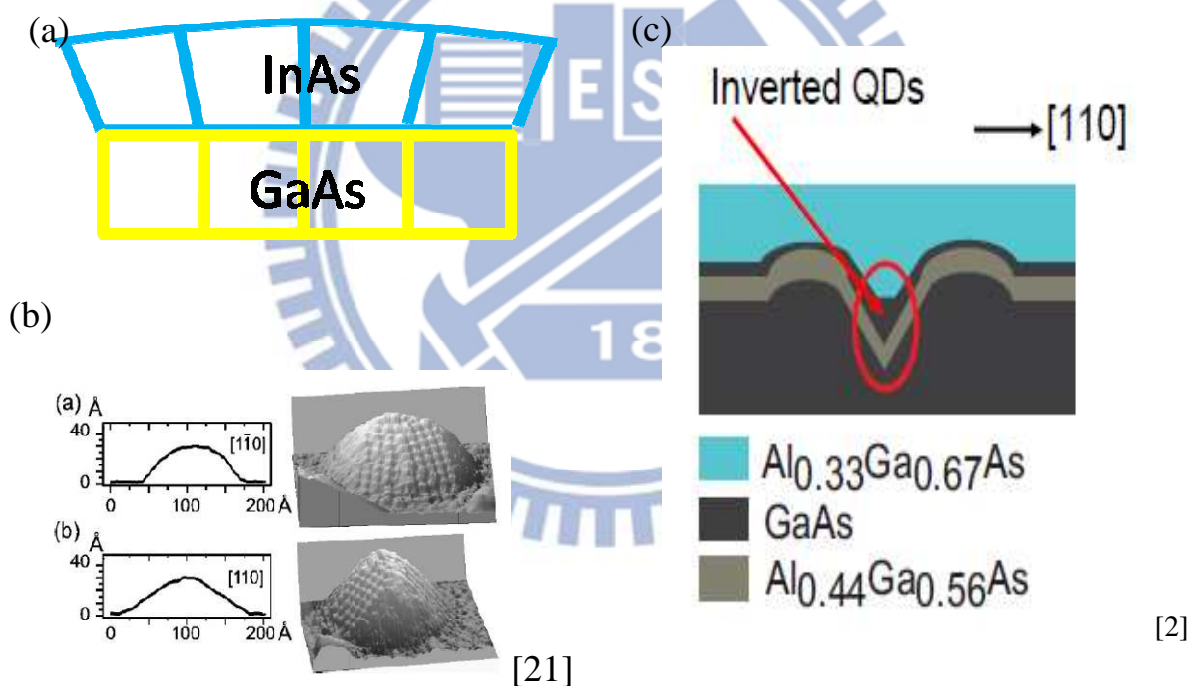


Fig. 1.2.1 (a) InAs/GaAs self-assembled QDs has initial strain due to InAs and GaAs lattice mismatch. (b) Shape of InAs/GaAs self-assembled QDs. (c) hierarchical GaAs/AlGaAs QDs is strain free since the materials near by the QDs have similar lattice constant.

Although the photon-pair emission is generated successfully and FSS can be

further eliminated by applying a magnetic field, electric field and external stress, a preliminary yet detailed understanding of geometrical configuration and materials is necessary. Analytical and numerical studies reveal the essential role of the optically active light-hole components of an exciton state in the fine structures and optical polarization properties of an elongated dot, which introduces additional short-range e-h exchange interactions to the exciton states and significantly changes the magnitude of fine structure splitting between bright exciton levels.

A previous work [6] presented a reduced Hamiltonian and simple analytical solution. By further simulating the exciton energy spectrum by a one-band four-band model with 3-D parabolic model, this study investigates the size effect of fine structure splitting as well as optical polarization. As is well known, optical polarization is induced by heavy- and light-hole coupling. The extent of heavy- and light-hole coupling is studied as well.

To eliminate the FSS value, this study also investigates how stress affects GaAs bulk. The quantity and direction of applied stress that works on the quantum dot cannot be measured or observed directly. However, stress that is induced by an electric field can be transformed by measuring the transition energies of bulk and observing the extended direction of polarizations, subsequently providing insight into exactly how stress is applied to quantum dots during experimentation.[2] Based on the microscopic Bloch function, exactly how the stress affects the distribution of electrons can be understood.

### 1.3 Contents

This thesis is organized as follows.

Chapter 2 introduces the fundamental theory of optical anisotropy and the fine structure of QD. Numerical computation of the excitonic structures of the dots is undertaken by combining the Luttinger-Kohn  $k \cdot p$  model for the valence hole and single-band model for conduction electron within the parabolic potential model of QD. Analytical and numerical results indicate the essential role of optically active light-hole components of an exciton state in the fine structures and optical polarization properties of an elongated dot, which introduces additional short-ranged e-h exchange interactions to the exciton states and transforms the magnitude of the fine structure splitting between bright exciton levels. This chapter also introduces strain theory.

Chapter 3 describes how FSS and Pol of GaAs/AlGaAs QDs and InAs/GaAs self-assembled QDs vary with size.

Chapter 4 summarizes the computation results of band structures, photoluminescence spectra, optical polarization and microscopic Bloch function of GaAs bulk subjected to uni-axial stresses.

Conclusions are finally drawn in Chapter 5, along with recommendations for future research.



## Chapter 2 Fundamental Theory

### 2.1 Theory for Exciton

#### Single exciton Hamiltonian

An exciton is formed from an electron in conduction band and an empty hole in valence band. The electron and hole wave functions are written as

$$\psi_{i_e, s_z}^e(\vec{r}) = g_{i_e}^e(\vec{r}) u_{s_z}^e(\vec{r}) \quad (2.1.1)$$

$$\psi_{i_h}^h(\vec{r}_h) = \sum_{j_z = \pm 3/2, \pm 1/2} g_{i_h, j_z}^h(\vec{r}) u_{j_z}^h(\vec{r}) \quad (2.1.2)$$

where  $u_{s_z}^e(\vec{r})$  and  $u_{j_z}^h(\vec{r})$  denote Bloch functions for describing the microscopic observation at  $\Gamma$ -point while  $g_{i_e, s_z}^e(\vec{r})$ , and  $g_{i_h, j_z}^h(\vec{r})$  present envelope functions that satisfy the Schrödinger equation.

The electronic structure in effective mass approximation is carried out by single-band model,

$$\left[ H^e + V_{QD}^e(\vec{r}_e) \right] g_{i_e, s_z}^e(\vec{r}_e) = E_{i_e}^e g_{i_e, s_z}^e(\vec{r}_e) \quad (2.1.3)$$

$$H^e = \frac{\hbar^2}{2m_e^* m_0} (k_x^2 + k_y^2 + k_z^2) + a_c (\epsilon_{xx} + \epsilon_{yy} + \epsilon_{zz}) [4] \quad (2.1.4)$$

where  $V_{QD}^e(\vec{r}_e)$  denotes the electron confinement potential.  $m^*$  represents electron effective mass.  $E_{i_e}^e$  refers to the eigenenergy of  $i_e$  the state.  $\epsilon_{ij}$  is the strain tensor, and  $a_c$  refers to a specific strain constant for conduction deformation potential.

The electronic structure of the valence hole is computed by four-band  $k \cdot p$  model. [4]

$$\begin{bmatrix} P+Q+V_{QD}^{HH} & -S & R & 0 \\ -S^\dagger & P-Q+V_{QD}^{LH} & 0 & R \\ R^\dagger & 0 & P-Q+V_{QD}^{LH} & S \\ 0 & R^\dagger & S^\dagger & P+Q+V_{QD}^{HH} \end{bmatrix} \begin{bmatrix} g_{ih,3/2}^h \\ g_{ih,1/2}^h \\ g_{ih,-1/2}^h \\ g_{ih,-3/2}^h \end{bmatrix} = E_{ih} \begin{bmatrix} g_{ih,3/2}^h \\ g_{ih,1/2}^h \\ g_{ih,-1/2}^h \\ g_{ih,-3/2}^h \end{bmatrix} \quad (2.1.5)$$

$$\begin{aligned} P &= P_k + P_\varepsilon & Q &= Q_k + Q_\varepsilon \\ R &= R_k + R_\varepsilon & S &= S_k + S_\varepsilon \end{aligned} \quad (2.1.6)$$

$$\begin{aligned} |u_{3/2}^h\rangle &= \left| \frac{3}{2}, \frac{3}{2} \right\rangle = -\frac{1}{\sqrt{2}} |(X+iY); \uparrow\rangle \\ |u_{1/2}^h\rangle &= \left| \frac{3}{2}, \frac{1}{2} \right\rangle = \frac{-1}{\sqrt{6}} |(X+iY); \downarrow\rangle + \frac{\sqrt{2}}{\sqrt{3}} |Z \uparrow\rangle \\ |u_{-1/2}^h\rangle &= \left| \frac{3}{2}, -\frac{1}{2} \right\rangle = \frac{1}{\sqrt{6}} |(X-iY); \uparrow\rangle + \frac{\sqrt{2}}{\sqrt{3}} |Z \downarrow\rangle \\ |u_{-3/2}^h\rangle &= \left| \frac{3}{2}, -\frac{3}{2} \right\rangle = \frac{1}{\sqrt{2}} |(X-iY); \downarrow\rangle \end{aligned} \quad (2.1.7)$$

$k_x$  along  $[110]$ ,  $k_y$  along  $[\bar{1}\bar{1}0]$ ,  $k_z$  along  $[001]$

$$\begin{aligned} P_k &= -\frac{\hbar^2 \gamma_1}{2m_0} \left( \frac{\partial^2}{\partial x^2} + \frac{\partial^2}{\partial y^2} + \frac{\partial^2}{\partial z^2} \right) & Q_k &= -\frac{\hbar^2 \gamma_2}{2m_0} \left( \frac{\partial^2}{\partial x^2} + \frac{\partial^2}{\partial y^2} - 2 \frac{\partial^2}{\partial z^2} \right) \\ R_k &= -\frac{\hbar^2}{2m_0} \left[ -\sqrt{3} \gamma_3 \left( \frac{\partial^2}{\partial x^2} - \frac{\partial^2}{\partial y^2} \right) + i 2 \sqrt{3} \gamma_2 \frac{\partial^2}{\partial x \partial y} \right] \\ S_k &= -\frac{\hbar^2 \gamma_3}{m_0} \sqrt{3} \left( \frac{\partial}{\partial x} - i \frac{\partial}{\partial y} \right) \frac{\partial}{\partial z} \end{aligned} \quad (2.1.8)$$

$\varepsilon_{xx}$  along  $[110]$ ,  $\varepsilon_{yy}$  along  $[\bar{1}\bar{1}0]$ ,  $\varepsilon_{zz}$  along  $[001]$

$$\begin{aligned} P_\varepsilon &= -a_v (\varepsilon_{xx} + \varepsilon_{yy} + \varepsilon_{zz}) & Q_\varepsilon &= -\frac{b}{2} (\varepsilon_{xx} + \varepsilon_{yy} - 2\varepsilon_{zz}) \\ R_\varepsilon &= \frac{d}{2} (\varepsilon_{xx} - \varepsilon_{yy}) - i \sqrt{3} b \varepsilon_{xy} & S_\varepsilon &= -d (\varepsilon_{xy} - i \varepsilon_{yz}) \end{aligned} \quad (2.1.9)$$

$\gamma_1$ ,  $\gamma_2$  and  $\gamma_3$  denote Luttinger-Kohn  $k \cdot p$  parameters, and  $a_v$ ,  $b$ ,  $d$  represent strain constants for conduction deformation potential.

Appendix II lists the Hamiltonian elements.

### Exchange interaction for multi-bands theory

The whole single exciton Hamiltonian in a quantum dot is

$$H_X = H_e(\hat{p}_e, \vec{r}_e) + H_h(\hat{p}_h, \vec{r}_h) - V_{eh}(\vec{r}_e, \vec{r}_h) \quad (2.1.10)$$

$H_e(\hat{p}_e, \vec{r}_e)$  ( $H_h(\hat{p}_h, \vec{r}_h)$ ) denotes electron(hole) Hamiltonian, and

$V_{eh}(\vec{r}_e, \vec{r}_h) = \frac{e^2}{4\pi\epsilon_0\kappa|\vec{r}_e - \vec{r}_h|}$  represents the electron-hole interaction. Notably the

energy spectrum can be obtained by solving the Schrödinger equation

$$H_X|\Psi_n^X\rangle = E_n^X|\Psi_n^X\rangle \quad (2.1.11)$$

An electron  $|i_e\rangle$  and a hole state  $|i_h\rangle$  form an exciton  $|i_e\rangle|i_h\rangle$ , in which the exciton state is expressed as

$$|\Psi_n^X\rangle = \sum_{\{i_h, i_e\}} C_{i_h, i_e} h_{i_h}^\dagger c_{i_e}^\dagger |vac\rangle \quad (2.1.12)$$

where  $C_{i_h, i_e}$  are coefficients to be determined and  $i_e, i_h$  denote electron and hole orbitals. The Hamiltonian can be further written as

$$\begin{aligned} H_X = & \sum_{i_e, s_z} E_{i_e}^e c_{i_e}^\dagger c_{i_e} + \sum_{j_h, j_z} E_{j_h}^h h_{j_h}^\dagger h_{j_h} \\ & + \sum_{i_e, j_h, k_h, l_e} V_{i_e, j_h, k_h, l_e}^{eh} c_{i_e, s_z}^\dagger h_{j_h, j_z}^\dagger h_{k_h, j_z} c_{l_e, s_z} - \sum_{i_e, j_h, k_h, l_e} V_{i_e, j_h, k_h, l_e}^{ehxc} c_{i_e, s_z}^\dagger h_{j_h, j_z}^\dagger h_{k_h, j_z} c_{l_e, s_z}, \end{aligned} \quad (2.1.13)$$

The composite indexes  $i_e(j_h)$  denotes the electron (valence hole) orbitals,  $s_z(j_z)$  denotes the electron (hole) orbitals.  $c_{i_e, s_z}^\dagger$  and  $c_{i_e, s_z}$  ( $h_{j_h, j_z}^\dagger$  and  $h_{j_h, j_z}$ ) are the electron (hole) creation and annihilation operators.

$V_{i_e, j_h, k_h, l_e}^{eh}$  and  $V_{i_e, j_h, k_h, l_e}^{ehxc}$  are *electron-hole Coulomb interaction* and *electron hole exchange interaction* where

$$V_{i_e, j_h, k_h, l_e}^{eh} \equiv \iint d^3r_e d^3r_h \psi_{i_e}^{e*}(\vec{r}_e) \psi_{j_h}^{h*}(\vec{r}_h) \frac{e^2}{4\pi\epsilon_0\epsilon_b|\vec{r}_e - \vec{r}_h|} \psi_{k_h}^{h*}(\vec{r}_h) \psi_{l_e}^{e*}(\vec{r}_e) \quad (2.1.14)$$

$$V_{i_e, j_h, k_h, l_e}^{eh, xc} \equiv \iint d^3r_1 d^3r_2 \psi_{i_e}^{e*}(\vec{r}_2) \psi_{j_h}^h(\vec{r}_2) \frac{e^2}{4\pi\epsilon_0\epsilon_b|\vec{r}_e - \vec{r}_h|} \psi_{k_h}^{h*}(\vec{r}_1) \psi_{l_e}^e(\vec{r}_1) \quad (2.1.15)$$

## Model analysis

Eigenstates of 4-band  $k \cdot p$  Hamiltonian without HH-LH coupling are taken as the basis for further expanding the envelope function  $g_{i_h, j_z}^h(\vec{r})$ . Where  $f_i^{HH/LH}(\vec{r}_h)$  are defined to be the basis to expand the HH- or LH- envelope function as

$$\begin{aligned} g_{i_h, \pm 3/2}^h(\vec{r}_h) &= \sum_{i=1,2,3\dots} a_i^{\{i_h; \pm 3/2\}} f_i^{HH}(\vec{r}_h) \\ g_{i_h, \pm 1/2}^h(\vec{r}_h) &= \sum_{i=1,2,3\dots} a_i^{\{i_h; \pm 1/2\}} f_i^{LH}(\vec{r}_h) \end{aligned} \quad (2.1.16)$$

To obtain a simple form, only the first term ( $i=1$ ) is taken. Thus  $f_1^{HH/LH}(\vec{r}_h) = f_{HH/LH}$  and  $f_1^e(\vec{r}_h) = f_e$ . Moreover, to rearrange the order of the basis of Hamiltonian in Eq. (2.1.5). The reduced basis of single exciton  $|i_e\rangle|i_h\rangle$  becomes

$$\{|s_z\rangle|j_z\rangle\} = \{|f_e u_{-1/2}^e\rangle|f_{HH} u_{+3/2}^h\rangle, |f_e u_{+1/2}^e\rangle|f_{HH} u_{-3/2}^h\rangle, |f_e u_{+1/2}^e\rangle|f_{LH} u_{+1/2}^h\rangle, |f_e u_{-1/2}^e\rangle|f_{LH} u_{-1/2}^h\rangle\} \quad (2.1.17)$$

and the exciton Hamiltonian[13-15] can be expressed as

$$\begin{aligned} H_X \approx E_X^{HH,(0)} I_{4 \times 4} + & \begin{pmatrix} 0 & 0 & 0 & \rho_{HL} \exp(-i\phi_{HL}) \\ 0 & 0 & \rho_{HL} \exp(-i\phi_{HL}) & 0 \\ 0 & \rho_{HL} \exp(-i\phi_{HL}) & \Delta_{HL} & 0 \\ \rho_{HL} \exp(-i\phi_{HL}) & 0 & 0 & \Delta_{HL} \end{pmatrix} \\ + & \begin{pmatrix} 2(\delta_0 + \Delta_0) & -\Delta_1 & -\frac{2}{\sqrt{3}}(\delta_0 + \Delta_0) & \frac{1}{\sqrt{3}}\Delta_1 \\ -\Delta_1 & 2(\delta_0 + \Delta_0) & \frac{1}{\sqrt{3}}\Delta_1 & -\frac{2}{\sqrt{3}}(\delta_0 + \Delta_0) \\ -\frac{2}{\sqrt{3}}(\delta_0 + \Delta_0) & \frac{1}{\sqrt{3}}\Delta_1 & \frac{2}{3}(\delta_0 + \Delta_0) & -\frac{1}{\sqrt{3}}\Delta_1 \\ \frac{1}{\sqrt{3}}\Delta_1 & -\frac{2}{\sqrt{3}}(\delta_0 + \Delta_0) & -\frac{1}{\sqrt{3}}\Delta_1 & \frac{2}{3}(\delta_0 + \Delta_0) \end{pmatrix} \end{aligned} \quad (2.1.18)$$

Where

$$E_X^{HH,(0)} \equiv \langle f_e | \langle f_{HH} | H_e + (P + Q + V_{QD}^{HH}) - V_{eh} | f_e \rangle | f_{HH} \rangle \quad (2.1.19)$$

$$E_X^{LH,(0)} \equiv \langle f_e | \langle f_{LH} | H_e + (P - Q + V_{QD}^{LH}) - V_{eh} | f_e \rangle | f_{LH} \rangle \quad (2.1.20)$$

$\rho_{HL}$  leads to heavy- and light-hole coupling.

$$\begin{aligned} \rho_{HL} \exp(-i\phi_{HL}) &\equiv \tilde{\rho}_{HL} \\ &\equiv \langle f_e | \langle f_{HH} | (R_k + R_\varepsilon) | f_e \rangle | f_{LH} \rangle \end{aligned} \quad (2.1.21)$$

$\Delta_{HL}$  denotes the energy separation of heavy hole and light hole

$$\begin{aligned} \Delta_{HL} &\equiv E_X^{LH,(0)} - E_X^{HH,(0)} \\ &= \langle f_{LH} | (P - Q + V_{QD}^{LH}) | f_{LH} \rangle - \langle f_{HH} | (P + Q + V_{QD}^{HH}) | f_{LH} \rangle \\ &= -2 \langle f_{HH} | Q - V_{QD}^{LH} - V_{QD}^{LH} | f_{LH} \rangle \end{aligned} \quad (2.1.22)$$

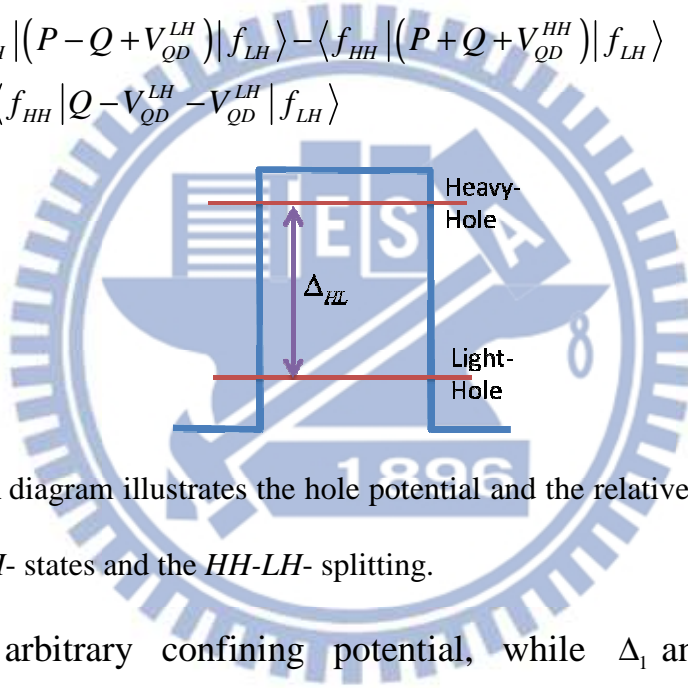


Fig. 2.1.1 A diagram illustrates the hole potential and the relative position of  $HH$ - and  $LH$ - states and the  $HH$ - $LH$ - splitting.

$V_{QD}$  represents arbitrary confining potential, while  $\Delta_1$  and  $\Delta_0$  denote the long-range part of e-h exchange interaction.

$$\begin{aligned} \Delta_1 &\approx \sum_{i,j=1(i \neq j)}^{N_{cell}} \int_{\eta_i \in WS(R_i)} \int_{\eta_j \in WS(R_j)} d\vec{r}_1 d\vec{r}_2 \\ &\left\{ f_e^\dagger(\vec{r}_2) u_{-1/2}^{e\dagger}(\vec{r}_2) f_{HH}(\vec{r}_2) u_{+3/2}^h(\vec{r}_2) \frac{e^2}{4\pi\epsilon} \frac{1}{|\vec{r}_1 - \vec{r}_2|} f_{LH}^\dagger(\vec{r}_1) u_{+1/2}^{e\dagger}(\vec{r}_1) f_e(\vec{r}_1) u_{-1/2}^e(\vec{r}_1) \right\} [16] \end{aligned} \quad (2.1.23)$$

$$\begin{aligned} \Delta_0 &\approx \sum_{i,j=1(i \neq j)}^{N_{cell}} \int_{\eta_i \in WS(R_i)} \int_{\eta_j \in WS(R_j)} d\vec{r}_1 d\vec{r}_2 \\ &\left\{ f_e^\dagger(\vec{r}_2) u_{-1/2}^{e\dagger}(\vec{r}_2) f_{HH}(\vec{r}_2) u_{+3/2}^h(\vec{r}_2) \frac{e^2}{4\pi\epsilon} \frac{1}{|\vec{r}_1 - \vec{r}_2|} f_{HH}^\dagger(\vec{r}_1) u_{+3/2}^{e\dagger}(\vec{r}_1) f_e(\vec{r}_1) u_{-1/2}^e(\vec{r}_1) \right\} [16] \end{aligned} \quad (2.1.24)$$

$$\delta_0 + \Delta_0 \equiv \Delta_{BD} \quad (2.1.25)$$

$\Delta_{BD}$  refers to the bright exciton and dark exciton levels (BX-DX) splitting, which is induced mainly by long-range interaction.

$\delta_0$  denotes the short-range portion of the e-h exchange interaction.

$$\delta_0 \approx \sum_{i=1} \int_{\vec{r}_1 \in WS(R_i)} \int_{\vec{r}_2 \in WS(R_j)} d\vec{r}_1 d\vec{r}_2 \left\{ f_e^\dagger(\vec{r}_2) u_{-1/2}^{e\dagger}(\vec{r}_2) f_{HH}(\vec{r}_2) u_{+3/2}^h(\vec{r}_2) \frac{e^2}{4\pi\epsilon} \frac{1}{|\vec{r}_1 - \vec{r}_2|} f_{HH}^\dagger(\vec{r}_1) u_{+3/2}^{e\dagger}(\vec{r}_1) f_e(\vec{r}_1) u_{-1/2}^e(\vec{r}_1) \right\}^{[16]} \quad (2.1.26)$$

$R_i$  and  $R_j$  represent positions of the WS cells.

The eigenenergies are obtained by diagonalizing the matrix, and the separation of the two lowest eigenvalues is defined as  $E_n^x$  and  $E_n^y$ , which correspond to  $E_{\pi x}$  or  $E_{\pi y}$ , as introduced later. The zero energy level of the Hamiltonian is positioned as the dark exciton state, as shown below.

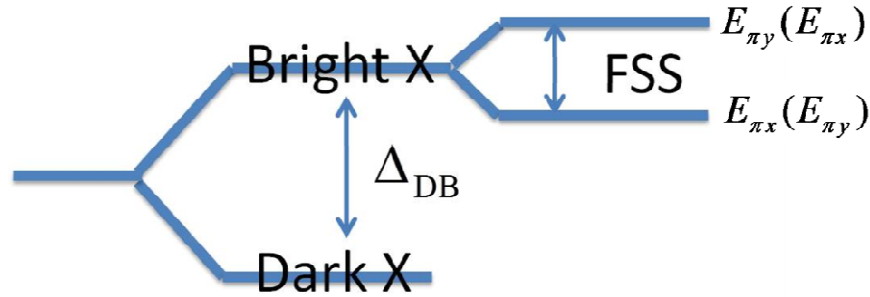


Fig. 2.1.2 The zero energy level locates at dark exciton state. The bright exciton was originally a two-fold degenerate level, but is separated due to the exchange interaction.

### Asymmetric 3-D parabolic model

The confining potential of a quantum dot is described using asymmetric 3-D



parabolic model, and is written into three parts as

$$V_{QD}^e = \frac{1}{2} m_e \omega_x^{e2} x^2 + \frac{1}{2} m_e \omega_y^{e2} y^2 + \frac{1}{2} m_e \omega_z^{e2} z^2 \quad (2.1.27)$$

$$V_{QD}^{HH} = \frac{1}{2} m_{HH,\parallel} \omega_x^{HH2} x^2 + \frac{1}{2} m_{HH,\parallel} \omega_y^{HH2} y^2 + \frac{1}{2} m_{HH,\perp} \omega_z^{HH2} z^2 \quad (2.1.28)$$

$$V_{QD}^{LH} = \frac{1}{2} m_{LH,\parallel} \omega_x^{LH2} x^2 + \frac{1}{2} m_{LH,\parallel} \omega_y^{LH2} y^2 + \frac{1}{2} m_{LH,\perp} \omega_z^{LH2} z^2 \quad (2.1.29)$$

Where the effective masses are

$$\begin{aligned} m_{HH,\parallel} &= \frac{m_0}{\gamma_1 + \gamma_2} & m_{HH,\perp} &= \frac{m_0}{\gamma_1 - 2\gamma_2} \\ m_{LH,\parallel} &= \frac{m_0}{\gamma_1 - \gamma_2} & m_{LH,\perp} &= \frac{m_0}{\gamma_1 + 2\gamma_2} \end{aligned} \quad (2.1.30)$$

Eigenstates  $f_i^e(\vec{r}_e) / f_i^{HH/LH}(\vec{r}_h)$  of Hamiltonian (without HH-LH coupling) are denotes as the envelope function. The envelope functions of the electron and hole orbitals are thus

$$f_e(\vec{r}_e) = \sqrt{\frac{1}{\pi^{3/2} l_x^e l_y^e l_z^e}} \exp \left[ -\frac{1}{2} \left( \left( \frac{x}{l_x^e} \right)^2 + \left( \frac{y}{l_y^e} \right)^2 + \left( \frac{z}{l_z^e} \right)^2 \right) \right] \quad (2.1.31)$$

$$f_{HH}(\vec{r}_h) = \sqrt{\frac{1}{\pi^{3/2} l_x^{HH} l_y^{HH} l_z^{HH}}} \exp \left[ -\frac{1}{2} \left( \left( \frac{x}{l_x^{HH}} \right)^2 + \left( \frac{y}{l_y^{HH}} \right)^2 + \left( \frac{z}{l_z^{HH}} \right)^2 \right) \right] \quad (2.1.32)$$

$$f_{LH}(\vec{r}_h) = \sqrt{\frac{1}{\pi^{3/2} l_x^{LH} l_y^{LH} l_z^{LH}}} \exp \left[ -\frac{1}{2} \left( \left( \frac{x}{l_x^{LH}} \right)^2 + \left( \frac{y}{l_y^{LH}} \right)^2 + \left( \frac{z}{l_z^{LH}} \right)^2 \right) \right] \quad (2.1.33)$$

where

$$\begin{aligned} l_\alpha^e &= \sqrt{\frac{\hbar}{m_e \omega_\alpha^e}} & l_\alpha^{HH} &= \sqrt{\frac{\hbar}{m_{HH,\alpha} \omega_\alpha^{HH}}} & l_\alpha^{LH} &= \sqrt{\frac{\hbar}{m_{LH,\alpha} \omega_\alpha^{LH}}} \\ l_\alpha &\equiv \sqrt{2} \langle \alpha^2 \rangle^{1/2} \quad (\alpha = x, y, z) \end{aligned} \quad (2.1.34)$$

are the characteristic length as well as the wave function extended.

Assume that  $l_{\alpha}^e = l_{\alpha}^{HH} = l_{\alpha}^{LH} \equiv l_{\alpha}$  and  $\xi' = \frac{l_y}{l_x}$

### QDs with electron-hole exchange interaction

With the wave function of 3D parabolic potential as the basis, the elements of Hamiltonian in Eqs. (2.1.14) and (2.1.15) thus become

$$\begin{aligned}\tilde{\rho}_{HL} &= \frac{\hbar^2 \gamma_3}{4m_0} \frac{1}{l_y^2} (1 - \xi'^2) - \frac{|d|}{2} (\varepsilon_{xx} - \varepsilon_{yy}) + i\sqrt{3}|b|\varepsilon_{xy} \\ &= \rho_{HL}^k + \rho_{HL}^{\varepsilon}\end{aligned}\quad (2.1.35)$$

$$\rho_{HL}^k = \frac{\hbar^2 \gamma_3}{4m_0} \frac{1}{l_y^2} (1 - \xi'^2) \quad (2.1.36)$$

$$\rho_{HL}^{\varepsilon} = -\frac{|d|}{2} (\varepsilon_{xx} - \varepsilon_{yy}) + i\sqrt{3}|b|\varepsilon_{xy} \quad (2.1.37)$$

$$\Delta_{HL} = \frac{\hbar^2 \gamma_2}{m_0} \left( \frac{1}{l_z^2} - \frac{1}{2l_x^2} - \frac{1}{2l_y^2} \right) - |b|(\varepsilon_{xx} + \varepsilon_{yy} - 2\varepsilon_{zz}) \quad (2.1.38)$$

$$= \Delta_{HL}^k + \Delta_{HL}^{\varepsilon} \quad (2.1.39)$$

$$\Delta_{HL}^k = \frac{\hbar^2 \gamma_2}{m_0} \left( \frac{1}{l_z^2} - \frac{1}{2l_x^2} - \frac{1}{2l_y^2} \right) \quad (2.1.40)$$

$$\Delta_{HL}^{\varepsilon} = -|b|(\varepsilon_{xx} + \varepsilon_{yy} - 2\varepsilon_{zz}) \quad (2.1.41)$$

Notable, according to the thesis of Chang[18], the quantity of *HH- LH-* splitting in a four-band model is over estimated, while the strain effect is involved. Therefore, the *HH- LH-* splitting that effected by strain of *six-band model* is employed in our numerical calculation. The geometry dependence part(*k* part) remains using the 4-band model.

For the *six-band* model,  $\Delta_{HL}^k$  remains Eq. (2.1.40) but

$$\Delta_{HL}^{\varepsilon} = -\frac{1}{2}(3Q_{\varepsilon} - \Delta_{so} + \sqrt{\Delta_{so}^2 + 2\Delta_{so}Q_{\varepsilon} + 9Q_{\varepsilon}^2}) \quad (2.1.42)$$

$$\Delta_1 \approx \frac{1}{4\pi\epsilon_d} \frac{3\sqrt{\pi}e^2\hbar^2 E_p}{16\sqrt{2}m_0 E_g^{QD2}} \frac{(1-\xi')}{\xi^{2'}} \frac{1}{l_x^3} e^{\left(\frac{3\sqrt{\pi}l_z}{4l_y}\right)^2} \operatorname{erfc}\left(\frac{3\sqrt{\pi}l_z}{4l_y}\right) \quad (2.1.43)$$

where  $\epsilon_d$ ,  $E_p$ ,  $E_g^{QD}$  denote static dielectric constant, optical matrix parameter and energy gap of QD. The energy gap of QD is determined by

$$E_g^{QD} = E_g + E_e + E_{HH} \quad (2.1.44)$$

where  $E_g$  is simply the bulk energy gap, and  $E_e$  and  $E_{HH}$  represent the ground state energy with respect to the electron and heavy-hole orbital envelope function.

$$E_e = E_{HH} = \frac{\hbar^2}{2m_e} (l_x^{-2} + l_y^{-2} + l_z^{-2}) \quad (2.1.45)$$

$$\begin{aligned} \delta_0 + \Delta_0 \equiv \Delta_{BD} &\approx \Delta_{eh,bulk}^{xc} \times (\pi a_B^*)^3 \int d^3r |f_e(\vec{r}) f_{HH}(\vec{r})|^2 \\ &= \frac{a_B^{*3} \Delta_{eh,bulk}^{xc}}{\sqrt{8\pi} l_x l_y l_z} \end{aligned} \quad (2.1.46)$$

[17]

with the condition  $l_\alpha^e = l_\alpha^{HH} = l_\alpha^{LH} \equiv l_\alpha$ , ( $\alpha=x, y, z$ ).

$a_B^*$  is refer to bulk exciton bohr radius and  $\Delta_{eh,bulk}^{xc}$  denotes bulk electron-hole exchange energy. Moreover, the energy is obtained by Hamiltonian matrix diagonalization.

### Simplified exciton two-level system

A simpler formula is derived to analyze and observe the basic physical picture by reducing the  $4 \times 4$  to  $2 \times 2$  one by using the Löwden perturbation method.

$$H_X \approx E_X^{HH,(0)} I_{2 \times 2} + \begin{pmatrix} \Delta_{BD} - \frac{|\tilde{\rho}_{HL}|^2}{\Delta_{HL}} & \tilde{\Delta}_{eff} \\ \tilde{\Delta}_{eff} & \Delta_{BD} - \frac{|\rho_{HL}|^2}{\Delta_{HL}} \end{pmatrix} \quad (2.1.47)$$

The basis now are the two bright states  $|f_e u_{-1/2}^e\rangle |f_{HH} u_{+3/2}^h\rangle, |f_e u_{+1/2}^e\rangle |f_{HH} u_{-3/2}^h\rangle$

The eigen energies are

$$E_{X;\pm} = (E_X^{HH,(0)} + (\Delta_{BD} - \frac{|\tilde{\rho}_{HL}|^2}{\Delta_{HL}})) \pm \Delta_{eff} \quad (2.1.48)$$

Subsequently leading to the splitting between two bright states which is known as *fine structure splitting* ( $S_{\pi_x, \pi_y}$ ).

$$\begin{aligned} \tilde{\Delta}_{eff} &\equiv \Delta_{eff} e^{-i\theta_{eff}} \\ &= -\Delta_1 + \frac{2}{\sqrt{3}} \frac{\tilde{\rho}_{HL}}{\Delta_{HL}} \Delta_{BD} \\ &= -\Delta_1 + \Delta' + i\Delta'' \end{aligned} \quad (2.1.49)$$

$$\Delta' = \frac{2}{\sqrt{3}} \frac{\Re \tilde{\rho}_{HL}}{\Delta_{HL}} \Delta_{BD} \quad (2.1.50)$$

$$\Delta'' = \frac{2}{\sqrt{3}} \frac{\Im \tilde{\rho}_{HL}}{\Delta_{HL}} \Delta_{BD} \quad (2.1.51)$$

$$S_{\pi_x, \pi_y} = 2(-\Delta_1 + \Delta') \equiv E_{\pi_x} - E_{\pi_y} \quad (2.1.52)$$

while corresponds to the polarization along  $\pi_x$  and  $\pi_y$ .

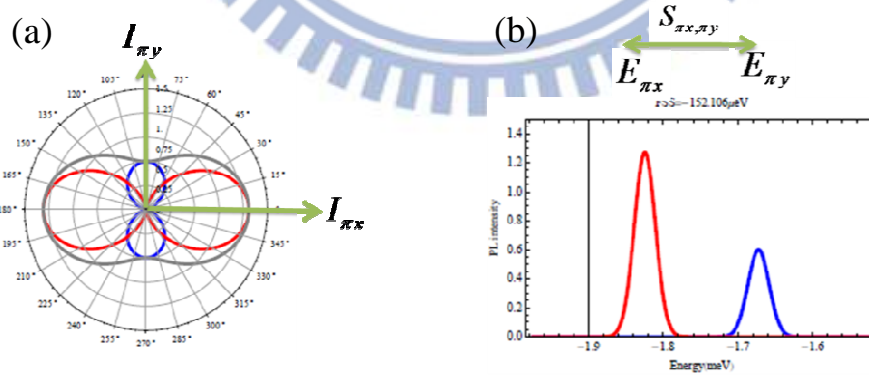


Fig. 2.1.3 (a) Optical polarization chart, and (b) the corresponding energy spectrum.

For the initial shear strain  $\varepsilon_{xy} = 0$ , this thesis considers only the  $-\Delta_1 + \Delta'$  portion, which illustrates the splitting of the competition among the two components. The greater equality the two components implies a smaller splitting. Once the size is determined, the long-range term,  $\Delta_1$  is also derived. However, the  $\Delta'$  term can be further tuned via strain effect to achieve small or even zero splitting.

### Optical polarization of single exciton in QDs

An electron is excited to conduction band, creating a hole in valence band; the electron then recombines with a hole and emits light to release energy. This process is called *spontaneous emission*. For the PL polarization emission spectrum, the intensity in each angle is manipulated using Fermi's Golden rule.[19]

$$I_n(\vec{e}; \omega) \propto W_{fi} \propto \left| \langle 0 | P_{\vec{e}}^- | \psi_n^x \rangle \right|^2 \delta(E_n^x - \hbar\omega) \quad (2.1.53)$$

$|\psi_n^x\rangle$  denotes the initial state,  $\langle 0 |$  represents the final state as well the vacuum state; and  $P_{\vec{e}}^-$  is refer to the polarization operator which can be performed as

$$P_{\vec{e}}^- = \sum_{i_h, i_e} D_{i_h, i_e}(\vec{e}) h_{i_h} c_{i_e} \quad (2.1.54)$$

$$\begin{aligned} D_{i_v, i_c}(\vec{e}) &\equiv \langle \psi_{i_h}^h | \hat{e} \cdot \hat{p} | \psi_{i_e}^e \rangle \\ &\approx \sum_{j_z} \sum_{s_z} \langle g_{i_h, j_z}^h | g_{i_e, s_z}^e \rangle \langle u_{j_h}^h | \hat{e} \cdot \hat{p} | u_{s_e}^e \rangle \\ &= \sum_{j_z} \sum_{s_z} \langle g_{i_h, j_z}^h | g_{i_e, s_z}^e \rangle A_{j_z, s_z}(\vec{e}) \end{aligned} \quad (2.1.55)$$

$D_{i_v, i_c}(\vec{e})$  represents dipole matrix element,  $h_{i_h}$ ,  $c_{i_e}$  are hole and electron annihilation operators.

Equations (2.1.1) and (2.1.2) introduce  $\langle \psi_{i_h}^h |$  and  $|\psi_{i_e}^e \rangle$ .

$$A_{J_z, S_z}(\vec{e}) \equiv \langle u_{j_z}^h | [\hat{e} \bullet \hat{p}] | u_{s_z}^e \rangle \quad (2.1.56)$$

Based on (2.1.16) to (2.1.18), the emission intensity is proportional to the dipole matrix element, the dipole matrix element

$$I_n(\vec{e}; \omega) \propto D_{i_v, i_c}^2(\vec{e}) \quad (2.1.57)$$

where

$$p_{cv}(\vec{0}) = \frac{i}{\hbar} \sqrt{\frac{m_0 E_p}{2}} \quad (2.1.58)$$

$E_p$  denotes the optical matrix element.

Further use the Lödwen perturbation theory, the two lowest *HH-LH*-mixed wavefunctions are written as

$$|\psi_{n=1}^X \rangle' = |f_e u_{-1/2}^e \rangle |f_{HH} u_{+3/2}^h \rangle - \frac{\tilde{\rho}_{HL}}{\Delta_{HL}} |f_e u_{-1/2}^e \rangle |f_{LH} u_{-1/2}^h \rangle \quad (2.1.59)$$

$$|\psi_{n=2}^X \rangle' = |f_e u_{+1/2}^e \rangle |f_{HH} u_{-3/2}^h \rangle - \frac{\tilde{\rho}_{HL}}{\Delta_{HL}} |f_e u_{+1/2}^e \rangle |f_{LH} u_{+1/2}^h \rangle \quad (2.1.60)$$



Table I. dipole matrix element ( $\vec{e} = \hat{x} \sin \theta \cos \phi + \hat{y} \sin \theta \sin \phi + \hat{z} \cos \theta$ )[18]

$J_z$	$S_z$	$A_{J_z, S_z}(\vec{e})$
$\frac{3}{2}$	$\frac{1}{2}$	$A_{3/2, 1/2}(\vec{e}) = \frac{1}{\sqrt{2}} p_{cv}(\vec{0}) \sin \theta e^{-i\phi}$
$\frac{1}{2}$	$\frac{1}{2}$	$A_{1/2, 1/2}(\vec{e}) = -\sqrt{\frac{2}{3}} p_{cv}(\vec{0}) \cos \theta$
$-\frac{1}{2}$	$\frac{1}{2}$	$A_{-1/2, 1/2}(\vec{e}) = \frac{-1}{\sqrt{6}} p_{cv}(\vec{0}) \sin \theta e^{i\phi}$
$-\frac{3}{2}$	$\frac{1}{2}$	$A_{-3/2, 1/2}(\vec{e}) = 0$
$\frac{3}{2}$	$-\frac{1}{2}$	$A_{3/2, -1/2}(\vec{e}) = 0$
$\frac{1}{2}$	$-\frac{1}{2}$	$A_{1/2, -1/2}(\vec{e}) = \frac{1}{\sqrt{6}} p_{cv}(\vec{0}) \sin \theta e^{-i\phi}$
$-\frac{1}{2}$	$-\frac{1}{2}$	$A_{-1/2, -1/2}(\vec{e}) = -\sqrt{\frac{2}{3}} p_{cv}(\vec{0}) \cos \theta$
$-\frac{3}{2}$	$-\frac{1}{2}$	$A_{-3/2, -1/2}(\vec{e}) = \frac{-1}{\sqrt{2}} p_{cv}(\vec{0}) \sin \theta e^{i\phi}$

By returning the functions back to Eq. (2.1.50) and using Table I, the polarization is obtained as

$$I_{\pi x} = I_{n=1}(\theta=0) + I_{n=2}(\theta=0) \quad (2.1. 61)$$

$$I_{\pi y} = I_{n=1}(\theta=\pi/2) + I_{n=2}(\theta=\pi/2) \quad (2.1. 62)$$

$$Pol_{\pi x, \pi y} \equiv \frac{I_{\pi x} - I_{\pi y}}{I_{\pi x} + I_{\pi y}} = \frac{2\gamma}{1 + \gamma^2} \quad [6] \quad (2.1. 63)$$

where  $\gamma \equiv \frac{\rho_{HL}}{\sqrt{3}\Delta_{HL}}$ , and with the condition  $\Delta_{HL} \gg \tilde{\rho}_{HL}$ , Eq. (2.1.59) becomes

$$Pol_{\pi x, \pi y} = 2\gamma = \frac{2\rho_{HL}}{\sqrt{3}\Delta_{HL}} \quad [6] \quad (2.1. 64)$$

For another definition  $Pol_{+,-}$  and  $\Delta_{Fss}$

	$\Delta_{Fss} = E_{X;+} - E_{X;-}$	$Pol_{+,-} = \frac{I_+ - I_-}{I_+ + I_-}$	(2.1. 65)
--	------------------------------------	---	-----------

if  $-\Delta_1 + \Delta' > 0$

	$S_{\pi x, \pi y} = \Delta_{Fss}$	$Pol_{\pi x, \pi y} = Pol_{+,-}$	(2.1. 66)
--	-----------------------------------	----------------------------------	-----------

if  $-\Delta_1 + \Delta' < 0$

	$S_{\pi x, \pi y} = -\Delta_{Fss}$	$Pol_{\pi x, \pi y} = -Pol_{+,-}$	(2.1. 67)
--	------------------------------------	-----------------------------------	-----------

Note that  $\Delta_{Fss}$  is always positive.

### Characteristic length

A wave function described by the Gaussian function in x-direction can be expressed as

$$f(x) = \left( \frac{1}{l_x^2 \pi} \right)^{1/4} e^{-\frac{x^2}{2l_x^2}} \quad (2.1. 68)$$

and also sketched as

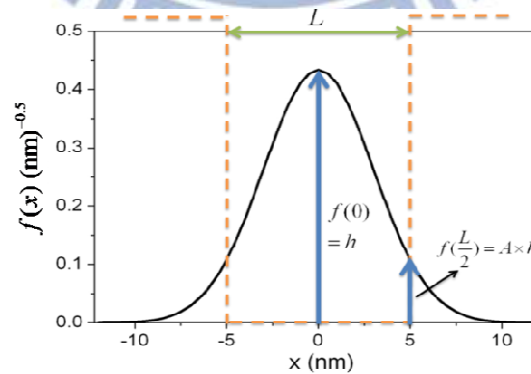


Fig. 2.1.4 A Gaussian function along x-direction.

Assume that the wave function is reduced to A percent of the peak ( $h$ ) at boundary  $L/2$ . The height at  $L/2$  can be expressed as

$$f\left(\frac{L}{2}\right) = A \times f(0) \quad (2.1.69)$$

Therefore,

$$f(0) = \left(\frac{1}{l_x^2 \pi}\right)^{1/4} = h \quad (2.1.70)$$

$$f\left(\frac{L}{2}\right) = \left(\frac{1}{l_x^2 \pi}\right)^{1/4} e^{-\frac{\left(\frac{L}{2}\right)^2}{2l_x^2}} = A \times h = A \times \left(\frac{1}{l_x^2 \pi}\right)^{1/4} \quad (2.1.71)$$

from Eq. (2.3.2.4), we obtain the relation between the geometric length and its characteristic length can be obtained via the ratio  $A$

$$\frac{L_x^2}{8l_x^2} = \ln\left(\frac{1}{A}\right) \quad (2.1.72)$$

or

$$L_x = l_x \sqrt{8 \ln\left(\frac{1}{A}\right)} \quad (2.1.73)$$

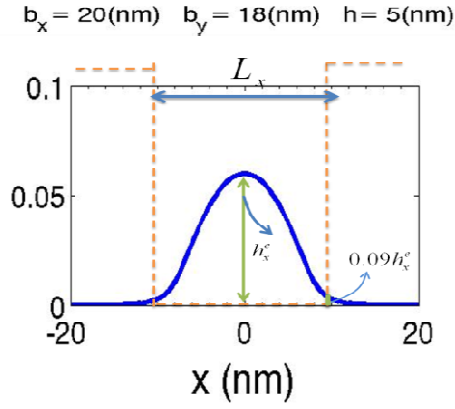
$$l_x = \frac{L_x}{\sqrt{8 \ln\left(\frac{1}{A}\right)}} \quad (2.1.74)$$

as in the case for other directions.

Consider a case of InAs/GaAs cubic shaped quantum dot.

A  $L_x = 20(\text{nm})$ ,  $L_y = 18(\text{nm})$  and  $L_z = 5(\text{nm})$  InAs/GaAs *cubic* quantum dot wave functions are obtained by one-band (six-band) for electron (hole) finite difference numerical method which was programmed in the thesis of Ku[12]. The initial strains are considered. The strain distributions in and out of dots are computed by using finite element software package *Comsol multiphysics*® .

(a)



(b)

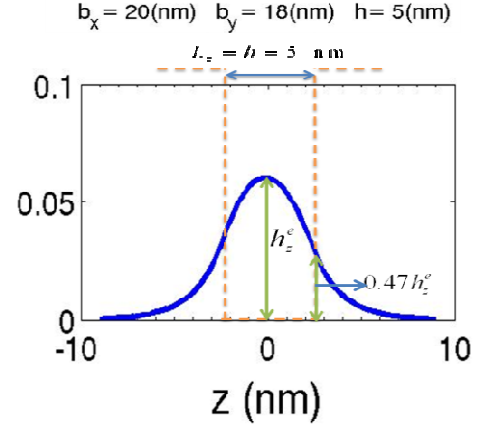


Fig.2.1.5 Electron wave function along (a)  $x$ -direction,

$L_x = 20 \text{ nm}$ ,  $A_x = 0.09$ , (b)  $z$ -direction,  $L_z = 5 \text{ nm}$ ,  $A_z = 0.47$ .

According to Eq. (2.1.68),  $l_x^e = 4.56 (\text{nm})$  and  $l_y^e = \xi \times 4.56 (\text{nm})$   $l_z^e = 2.03 (\text{nm})$ .

Or  $L_x = 4.39 l_x^e$ ,  $L_y = 4.39 l_x^e \times \xi$ ,  $L_z = 2.5 l_z^e$

## 2.2 Strain effects

### Initial strain in InAs/GaAs self-assembled QDs

InAs/GaAs self-assembled QDs have built-in strains due to the lattice mismatching of the two materials InAs and GaAs, this effect induces initial strains. Here, this induced strain is treated as an initial strain in the analysis[8]. The in-plane mismatch is defined as

$$\varepsilon_0 = \frac{a_{\text{GaAs}} - a_{\text{InAs}}}{a_{\text{InAs}}} = \varepsilon_{xx} = \varepsilon_{yy} = -6.69\% \quad (2.2.1)$$

$$\varepsilon_{zz} = -\frac{2c_{12}}{c_{11}} \varepsilon_0 = 7.27\% \quad (2.2.2)$$

$a_{\text{InAs}} = 6.055 \text{ \AA}$  (  $a_{\text{GaAs}} = 5.65 \text{ \AA}$  ) denotes the lattice constant of InAs(GaAs).  $\varepsilon_0$  represents the lattice mismatching percentage. The negative sign refers to the compression in the  $x$  and  $y$  directions, in which the compression of  $xy$ -plane results the tension in  $z$ -direction.

This case involves a very large and thin plate, explaining why a general formalism that changes with size is derived here. References [10] and [11] provide the general formulae. Prof. Cheng derived the following application analysis formulae. Notably, the strain elements are precisely at the *center* of cubic shaped quantum dots of *isotropic material*. For an isotropic crystal, the elastic matrix  $c_{ij}^{\text{iso}}$  is set to be:

$$\mathbf{c}_{ij}^{\text{iso}} = \begin{bmatrix} c_{11} & c_{12} & c_{12} & 0 & 0 & 0 \\ c_{12} & c_{11} & c_{12} & 0 & 0 & 0 \\ c_{12} & c_{12} & c_{11} & 0 & 0 & 0 \\ 0 & 0 & 0 & c_{44}^{\text{iso}} & 0 & 0 \\ 0 & 0 & 0 & 0 & c_{44}^{\text{iso}} & 0 \\ 0 & 0 & 0 & 0 & 0 & c_{44}^{\text{iso}} \end{bmatrix} \quad [7] \quad (2.2.3)$$

$$c_{44}^{\text{iso}} = \frac{1}{2}(c_{11} - c_{12}) \quad (2.2.4)$$

## Analytical solution for initial strain

### Symmetry dots

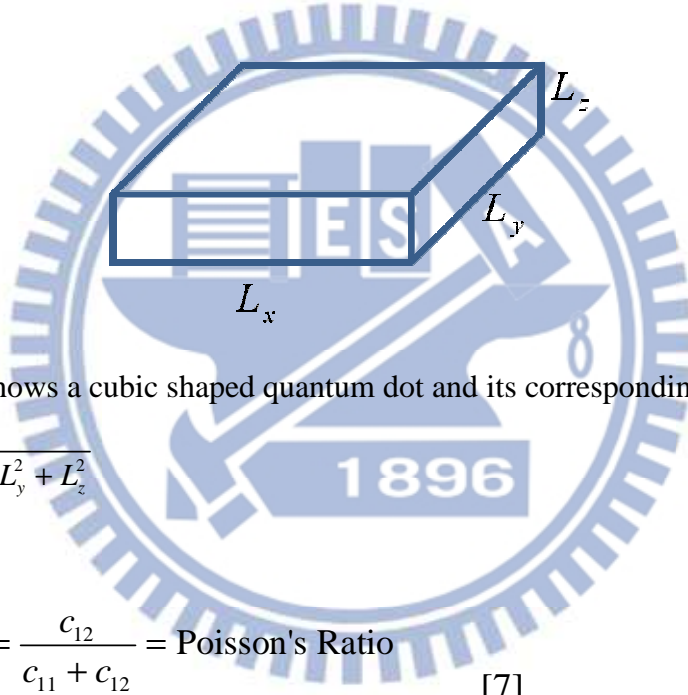


Fig. 2.2.1 shows a cubic shaped quantum dot and its corresponding length.

$$L_0 = \sqrt{L_x^2 + L_y^2 + L_z^2} \quad (2.2.5)$$

$$\nu = -\frac{s_{12}}{s_{11}} = \frac{c_{12}}{c_{11} + c_{12}} = \text{Poisson's Ratio} \quad [7] \quad (2.2.6)$$

$$\Lambda = \frac{\varepsilon_0(1+\nu)}{\pi(1-\nu)} \quad (2.2.7)$$

$$\varepsilon_{xx}(0,0,0) = 8\Lambda \arctan\left[\frac{L_y L_z}{L_x L_0}\right] - \varepsilon_0 \quad (2.2.8)$$

$$\varepsilon_{yy}(0,0,0) = 8\Lambda \arctan\left[\frac{L_x L_z}{L_y L_0}\right] - \varepsilon_0 \quad (2.2.9)$$

$$\varepsilon_{zz}(0,0,0) = 8\Lambda \arctan\left[\frac{L_x L_y}{L_z L_0}\right] - \varepsilon_0 \quad (2.2.10)$$

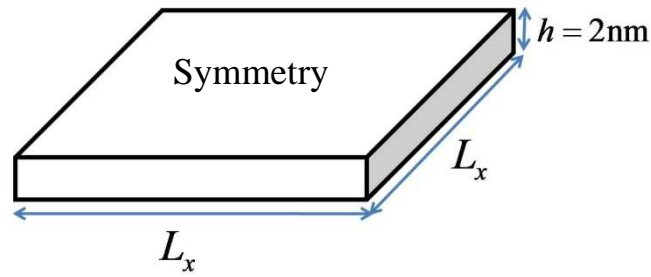


$$\varepsilon_{xy}(0,0,0) = \varepsilon_{xz}(0,0,0) = \varepsilon_{yz}(0,0,0) \quad (2.2.11)$$

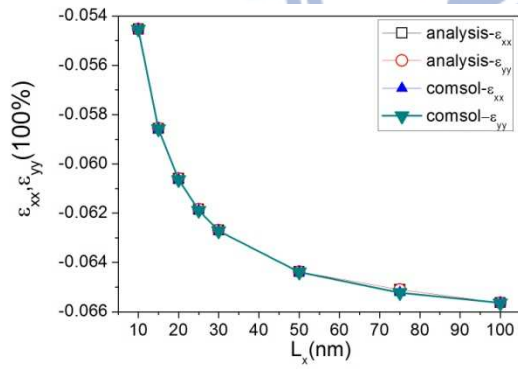
The following section summarizes those results and compare them with the results of the finite element software package *Comsol multiphysics*.

### Software comsol manipulation of the initial strain in self-assembled InAs/GaAs cubic shaped quantum dot

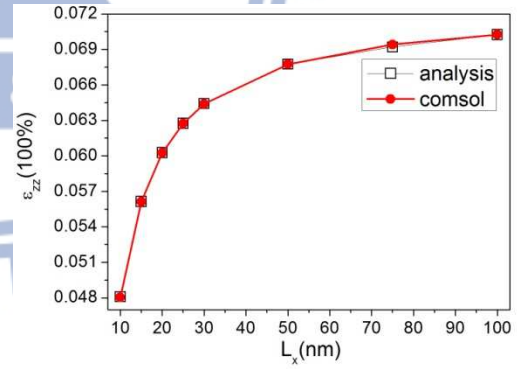
Symmetry cubic QDs



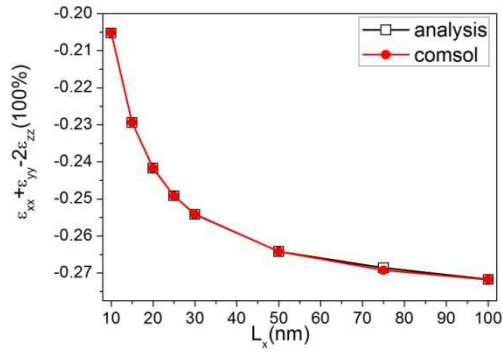
(a)



(b)



(c)



(d)

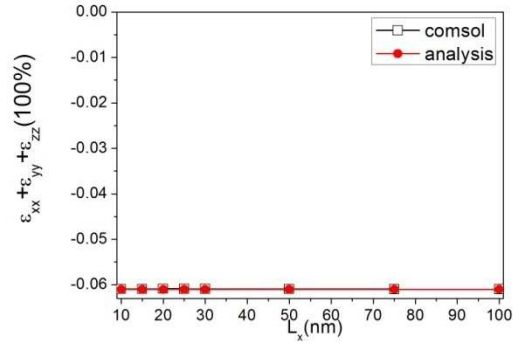
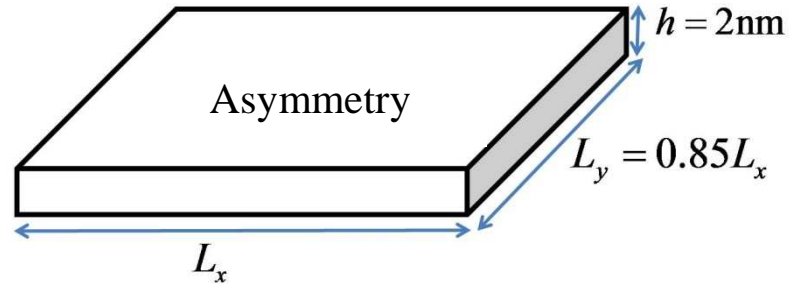


Fig. 2.2.2 Strain quantities of symmetry cubic QDs (a)  $\epsilon_{xx}$ ,  $\epsilon_{yy}$ , (b)  $\epsilon_{zz}$ , (c)

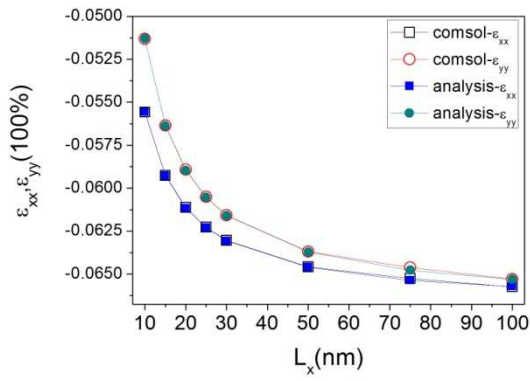
$\epsilon_{xx} + \epsilon_{yy} - 2\epsilon_{zz}$ , (d)  $\epsilon_{xx} + \epsilon_{yy} + \epsilon_{zz}$  from  $L_x = 10 \sim 100$  nm,  $L_z = 2$  nm.

When the plate is extremely large as  $L_x = L_y = 100$  nm,  $\epsilon_{xx}$  and  $\epsilon_{yy}$  approach  $\epsilon_0 = -6.69\%$ ,  $\epsilon_{zz}$  is close to  $7.27\%$ . For a symmetry QD,  $\epsilon_{xx} = \epsilon_{yy}$ . Shear strain tensors are zero in the simulation of *comsol*, which consists of the analytical solution. As is well known, the reason that  $|\epsilon_{xx}| > |\epsilon_{yy}|$  is very similar to that for rubber bands, in which longer the bands, more easier to extended the bands. Therefore, the strain tensors decrease as the cubits become diminish in size.

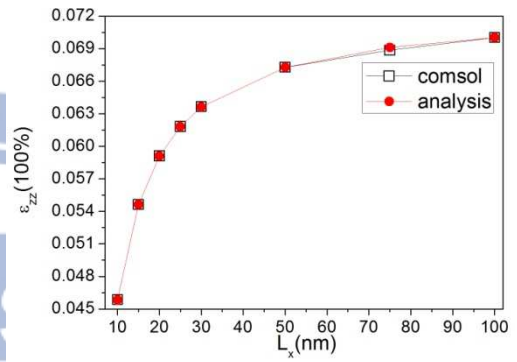
## Asymmetric cubic QDs



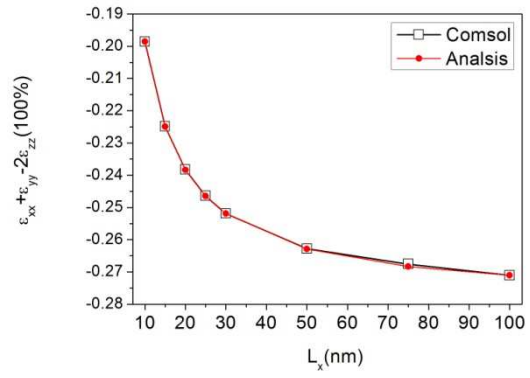
(a)



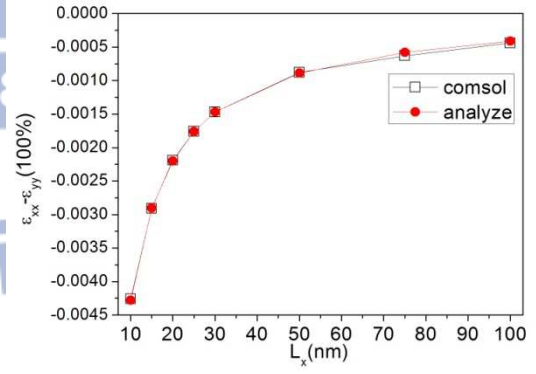
(b)



(c)



(d)



(e)

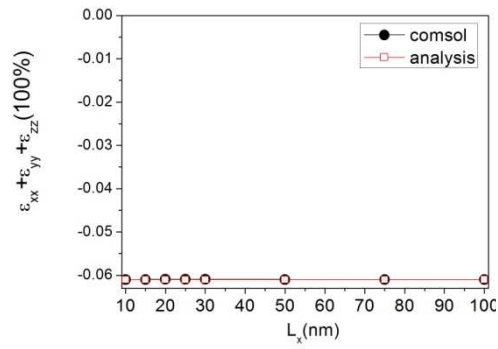


Fig. 2.2.3 Strain quantities of asymmetry quantum dots are equivalent.

Asymmetrize  $\xi = L_y / L_x = 0.85$  ,  $h = L_z = 2$  nm (a)  $\epsilon_{xx}$ ,  $\epsilon_{yy}$ , (b)  $\epsilon_{zz}$  , (c)

$\epsilon_{xx} + \epsilon_{yy} - 2\epsilon_{zz}$  (d)  $\epsilon_{xx} - \epsilon_{yy}$  , (e)  $\epsilon_{xx} + \epsilon_{yy} + \epsilon_{zz}$  from  $L_x = 10 \sim 100$  nm.

Obviously,  $\epsilon_{xx}$  and  $\epsilon_{yy}$  are unequal in Fig. 2.2.3 (a). Since  $L_x$  is longer than  $L_y$ , like rubber bands, the longer side is easily extended; thus, the length variation in  $x$ -direction is greater than that in  $y$ -direction. Still, the shear strain tensors are zero as in the symmetric case.

The strain quantities related to Hamiltonian are introduced as follows.

$$Q_\epsilon = -\frac{b}{2}(\epsilon_{xx} + \epsilon_{yy} - 2\epsilon_{zz})$$

$$R_\epsilon = \frac{d}{2}(\epsilon_{xx} - \epsilon_{yy}) - i\sqrt{3}b\epsilon_{xy}$$

$$P_\epsilon = a_v(\epsilon_{xx} + \epsilon_{yy} + \epsilon_{zz})$$

### Applied stress induced strain

A force acts on a body might cause a displacement in shape. Stress resembles force, and the displacement resembles strain. However, in this study, strain is not a specific length of displacement but the ratio of displacement compared with the original length.

### Definition of strain

Origin point  $O$  is fixed in the end of string, and a point  $P$  moves on the string that moves at a distance  $u$  to  $P'$ ,  $OP = x$  and  $OP' = x + u$ .

Consider two close points  $P$  and  $Q_i$ , in which distance between  $P$  and  $Q_i$  denoted as  $\Delta x_i = PQ_i$  ( $\Delta x_1 = PQ_1$ ,  $\Delta x_2 = PQ_2$  ...). After deformation,

$$\begin{aligned} P &\rightarrow P' \\ Q_i &\rightarrow Q'_i \end{aligned} \quad (2.2.12)$$

Next,  $PQ_1 \rightarrow P'Q'_1$ ,  $PQ_2 \rightarrow P'Q'_2$ , such that  $PQ_i \rightarrow P'Q'_i$ .  $P'Q'_i$  represents the sum of two vectors  $\Delta x_i + \Delta u_i$ .

The normal strain tensor is given by

$$e_{11} = \frac{\Delta u_1}{\Delta x_1} \quad (2.2.13)$$

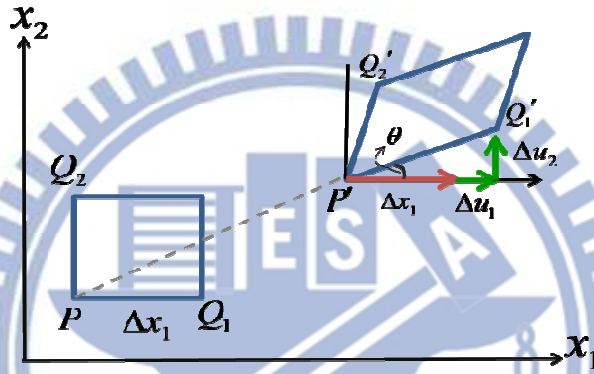


Fig. 2.2.4 The displacement along the parallel direction and perpendicular direction relative to its original lattice length.

For the angle

$$\tan \theta = \frac{\Delta u_2}{\Delta x_1 + \Delta u_1} \quad (2.2.14)$$

Since we restrict the discussion to small displacements,  $\Delta x_1$  is much greater than the displacements  $\Delta u_1$  and  $\Delta u_2$  ( $\Delta x_1 \gg \Delta u_1, \Delta u_2$ ) thus the angle  $\theta$  is small as well. Thus, the Eq.(2.1.5) is

$$\theta = \frac{\Delta u_2}{\Delta x_1} = e_{21} \quad (2.2.15)$$

Similarly

$$e_{ii} = \frac{\Delta u_i}{\Delta x_i} \quad (2.2.16)$$

and

$$e_{ij} = \frac{\Delta u_i}{\Delta x_j} = \theta \quad (2.2.17)$$

Next, the symmetrical part of  $e_{ij}$  is further defined as  $\mathcal{E}_{ij}$ . That is,

$$\mathcal{E}_{ii} = e_{ii} \quad (2.2.18)$$

and

$$\mathcal{E}_{ij} = \frac{1}{2}(e_{ij} + e_{ji}) \quad (i, j = 1, 2) \quad (2.2.19)$$

$\mathcal{E}_{ii}$  is purely the displacement in length and so called normal strain,  $\mathcal{E}_{ij}$  is the shear strain and as well the change in angle. The definition of three-dimensional strain resembles the two-dimensional strain. The strain tensor can be presented as:

$$e_{ij} = \frac{\Delta u_i}{\Delta x_j} \quad (i, j = 1, 2, 3) \quad (2.2.20)$$

Similar to the symmetrical property in two-dimensional form, the stress tensor of the *symmetrical part* of  $e_{ij}$  is represented as  $\mathcal{E}_{ij}$ .

$$\mathcal{E}_{ij} = \frac{1}{2}(e_{ij} + e_{ji}) \quad (i, j = 1, 2, 3) \quad (2.2.21)$$

For the symmetrical strain tensor,

$$\mathcal{E}_{ij} = \mathcal{E}_{ji} \quad (2.2.22)$$

**Hooke's Law** states that

$$\sigma = c\mathcal{E} \quad (2.2.23)$$

$$\mathcal{E} = s\sigma \quad (2.2.24)$$

$s$  represents the elastic compliance constant. The compliance is related to the elastic stiffness constant,  $c$ .  $c$  is known as Young's Modulus. Also, stress  $\sigma$  is applied homogeneously to a crystal results a strain  $\epsilon$  respectively. The relationship between stress and strain in tensor form is given by

$$\epsilon_{ij} = s_{ijkl} \sigma_{kl} \quad (i, j, k, l = 1, 2, 3) \quad (2.2.25)$$

the Einstein notation is used here.

### Stress induced strain in any reference frame

Hooke's law can be written in tensor form as

$$\epsilon_{ij} = s_{ijkl} \sigma_{kl} \quad (2.2.26)$$

The strain tensor is expanded as

$$\begin{aligned} \epsilon_{11} &= s_{1111} \sigma_{11} + s_{1112} \sigma_{12} + s_{1113} \sigma_{13} + \\ &\quad s_{1121} \sigma_{21} + s_{1122} \sigma_{22} + s_{1123} \sigma_{23} + \\ &\quad s_{1131} \sigma_{31} + s_{1132} \sigma_{32} + s_{1133} \sigma_{33} \\ \epsilon_{23} &= s_{2311} \sigma_{11} + s_{2312} \sigma_{12} + s_{2313} \sigma_{13} + \\ &\quad s_{2321} \sigma_{21} + s_{2322} \sigma_{22} + s_{2323} \sigma_{23} + \\ &\quad s_{2331} \sigma_{31} + s_{2332} \sigma_{32} + s_{2333} \sigma_{33} \\ &\quad \vdots \end{aligned} \quad (2.2.27)$$

Tensor into matrix form is followed by the notation rule.

	$xx$	$yy$	$zz$	$yz,zy$	$zx,xz$	$xy,yx$
tensor notation (ij)	11	22	33	23,32	31,13	12,21
matrix notation (m)	1	2	3	4	5	6



For strain, from tensor notation to matrix notation

$$\varepsilon_{ij} = \varepsilon_m \quad \text{when } i = j$$

$$\varepsilon_{ij} = \frac{1}{2} \varepsilon_m \quad \text{when } i \neq j$$

From tensor notation to matrix notation

$$s_{ijkl} = s_{mn} \quad \text{when m and n are 1, 2, 3}$$

$$s_{ijkl} = \frac{1}{2} s_{mn} \quad \text{when either m and n are 4,5 or 6}$$

$$s_{ijkl} = \frac{1}{4} s_{mn} \quad \text{when both m and n are 4, 5, or 6}$$

For stress

$$\sigma_{ij} = \sigma_m \quad \text{for any i and j}$$

The stress induced strain thus becomes

$$\begin{aligned} \varepsilon_1 &= s_{11}\sigma_1 + \frac{1}{2}s_{16}\sigma_6 + \frac{1}{2}s_{15}\sigma_5 + \\ &\quad \frac{1}{2}s_{16}\sigma_6 + s_{12}\sigma_2 + \frac{1}{2}s_{14}\sigma_4 + \\ &\quad \frac{1}{2}s_{15}\sigma_5 + \frac{1}{2}s_{14}\sigma_4 + s_{13}\sigma_3 \\ \frac{1}{2}\varepsilon_4 &= s_{41}\sigma_1 + \frac{1}{4}s_{46}\sigma_6 + \frac{1}{4}s_{45}\sigma_5 + \\ &\quad \frac{1}{4}s_{46}\sigma_6 + \frac{1}{2}s_{42}\sigma_2 + \frac{1}{4}s_{44}\sigma_4 + \\ &\quad \frac{1}{4}s_{45}\sigma_5 + \frac{1}{4}s_{44}\sigma_4 + \frac{1}{2}s_{43}\sigma_3 \end{aligned} \tag{2.2.28}$$

$$\varepsilon_1 = s_{11}\sigma_1 + s_{12}\sigma_2 + s_{13}\sigma_3$$

$$\frac{1}{2}\varepsilon_4 = \frac{1}{4}s_{44}\sigma_4 + \frac{1}{4}s_{44}\sigma_4 = \frac{1}{2}s_{44}\sigma_4 \tag{2.2.29}$$

⋮

Furthermore, the matrix notation is transformed into Cartesian notation.

$$\begin{bmatrix} \epsilon_1 \\ \epsilon_2 \\ \epsilon_3 \\ \epsilon_4 \\ \epsilon_5 \\ \epsilon_6 \end{bmatrix} = \begin{bmatrix} \epsilon_{xx} \\ \epsilon_{yy} \\ \epsilon_{zz} \\ 2\epsilon_{yz} \\ 2\epsilon_{xz} \\ 2\epsilon_{xy} \end{bmatrix} = \begin{bmatrix} s_{11} & s_{12} & s_{13} & s_{14} & s_{15} & s_{16} \\ s_{21} & s_{22} & s_{23} & s_{24} & s_{25} & s_{26} \\ s_{31} & s_{32} & s_{33} & s_{34} & s_{35} & s_{36} \\ s_{41} & s_{42} & s_{43} & s_{44} & s_{45} & s_{46} \\ s_{51} & s_{52} & s_{53} & s_{54} & s_{55} & s_{56} \\ s_{61} & s_{62} & s_{63} & s_{64} & s_{65} & s_{66} \end{bmatrix} \begin{bmatrix} \sigma_{xx} \\ \sigma_{yy} \\ \sigma_{zz} \\ \sigma_{yz} \\ \sigma_{xz} \\ \sigma_{xy} \end{bmatrix} \quad (2.2.30)$$

For the cubic crystal in which the main axis is along [100], the compliance can be obtained from the elastic stiffness constant,  $c$ . [7]

The compliance matrix is precisely for *cubic crystal* along [100][7]:

$$\begin{aligned} s_{11}^{[100]} &= s_{22}^{[100]} = s_{33}^{[100]} = \frac{c_{11} + c_{12}}{c_{11}^2 + c_{11}c_{12} - 2c_{12}^2} \\ s_{12}^{[100]} &= s_{21}^{[100]} = s_{13}^{[100]} = s_{31}^{[100]} = \frac{-c_{12}}{c_{11}^2 + c_{11}c_{12} - 2c_{12}^2} \\ s_{44}^{[100]} &= s_{55}^{[100]} = s_{66}^{[100]} = \frac{1}{c_{44}} \\ \text{else} &= 0 \end{aligned} \quad (2.2.31)$$

$$s_{ij}^{[100]} = \begin{bmatrix} s_{11}^{[100]} & s_{12}^{[100]} & s_{12}^{[100]} & 0 & 0 & 0 \\ s_{12}^{[100]} & s_{11}^{[100]} & s_{12}^{[100]} & 0 & 0 & 0 \\ s_{12}^{[100]} & s_{12}^{[100]} & s_{11}^{[100]} & 0 & 0 & 0 \\ 0 & 0 & 0 & s_{44}^{[100]} & 0 & 0 \\ 0 & 0 & 0 & 0 & s_{44}^{[100]} & 0 \\ 0 & 0 & 0 & 0 & 0 & s_{44}^{[100]} \end{bmatrix} \quad (2.2.32)$$

While for the main reference frame along [110]-direction, the compliance becomes

$$\begin{aligned}
s_{11}^{[110]} &= \frac{1}{2} \left( s_{11}^{[100]} + s_{12}^{[100]} + \frac{1}{2} s_{44}^{[100]} \right) & s_{13}^{[110]} &= s_{23}^{[110]} = s_{32}^{[110]} = s_{31}^{[110]} = s_{13}^{[100]} \\
s_{12}^{[110]} &= \frac{1}{2} \left( s_{11}^{[100]} + s_{12}^{[100]} - \frac{1}{2} s_{44}^{[100]} \right) & s_{33}^{[110]} &= s_{33}^{[100]} = s_{11}^{[100]} \\
s_{66}^{[110]} &= 2(s_{11}^{[100]} - s_{12}^{[100]}) & s_{44}^{[110]} &= s_{55}^{[110]} = s_{44}^{[100]} \\
\text{else} &= 0 \\
\text{note that } s_{ij} &= s_{ji}
\end{aligned} \tag{2.2.33}$$

As a result

$$s_{ij}^{[110]} = \begin{bmatrix} \frac{1}{2} \left( s_{11}^{[100]} + s_{12}^{[100]} + \frac{1}{2} s_{44}^{[100]} \right) & \frac{1}{2} \left( s_{11}^{[100]} + s_{12}^{[100]} - \frac{1}{2} s_{44}^{[100]} \right) & s_{12}^{[100]} & 0 & 0 & 0 \\ \frac{1}{2} \left( s_{11}^{[100]} + s_{12}^{[100]} - \frac{1}{2} s_{44}^{[100]} \right) & \frac{1}{2} \left( s_{11}^{[100]} + s_{12}^{[100]} + \frac{1}{2} s_{44}^{[100]} \right) & s_{12}^{[100]} & 0 & 0 & 0 \\ s_{12}^{[100]} & s_{12}^{[100]} & s_{11}^{[100]} & 0 & 0 & 0 \\ 0 & 0 & 0 & s_{44}^{[100]} & 0 & 0 \\ 0 & 0 & 0 & 0 & s_{44}^{[100]} & 0 \\ 0 & 0 & 0 & 0 & 0 & 2(s_{11}^{[100]} - s_{12}^{[100]}) \end{bmatrix} \tag{2.2.34}$$

### Stress Transformation

Although the stress in Eqs. (2.2.30) is referenced on the main reference frame, stress may occasionally occur that misaligns the main axes.

For a second-rank stress tensor that works misaligned with the main axes, the stress is transformed by two transformation matrixes and the vector component in the main reference frame is obtained. Here, the double-prime label represents the frame of applied stress, and the raw label states its component in the reference frame.[7]

$$\sigma_{mn} = a_{om} a_{pn} \sigma''_{op} \tag{2.2.35}$$

The angles are redefined here, in which the stress is assumed to be misaligned with the main axes with an angle  $\phi_\sigma$  to  $x$ , Appendix I describes the choice and settlement of the rotation matrix.

$$a_{om} = \begin{bmatrix} \cos \phi_\sigma & \sin \phi_\sigma & 0 \\ -\sin \phi_\sigma & \cos \phi_\sigma & 0 \\ 0 & 0 & 1 \end{bmatrix} \quad (2.2.36)$$

For stress applied on the *xy-plane*,  $\theta_\sigma = 0$ ,

$$\begin{aligned} a_{11} &= \cos \phi_\sigma \\ a_{12} &= \sin \phi_\sigma \\ &\vdots \\ a_{33} &= 1 \end{aligned} \quad (2.2.37)$$

*Ex :*

$$\begin{aligned} \sigma_{11} &= \sum_{o,p=1}^3 a_{o1} a_{p1} \sigma''_{op} \\ &= a_{11} a_{11} \sigma''_{11} + a_{11} a_{21} \sigma''_{12} + a_{11} a_{31} \sigma''_{13} + \\ &\quad a_{21} a_{11} \sigma''_{21} + a_{21} a_{21} \sigma''_{22} + a_{21} a_{31} \sigma''_{23} + \\ &\quad a_{31} a_{11} \sigma''_{31} + a_{31} a_{21} \sigma''_{32} + a_{31} a_{31} \sigma''_{33} \\ \sigma_{12} &= \sum_{o,p=1}^3 a_{o1} a_{p2} \sigma''_{op} \\ &\vdots \\ &\text{and so on} \end{aligned} \quad (2.2.38)$$

For a set of bi-axial stresses  $\sigma''_{11}$  and  $\sigma''_{22}$  that lie on the *xy-plane* and perpendicular to each other:

$$\begin{aligned} \text{Ex : } \sigma_{11} &= a_{o1} a_{p1} \sigma''_{op} \\ &= a_{11} a_{11} \sigma''_{11} + a_{21} a_{21} \sigma''_{22} \\ &= \cos^2 \phi_\sigma \times \sigma''_{11} + \sin^2 \phi_\sigma \times \sigma''_{22} \\ &\vdots \end{aligned} \quad (2.2.39)$$

With the same method, all of the stress tensor elements are obtained. Finally, the stress becomes:

$$\begin{aligned}
\sigma_1 &= \cos^2 \phi_\sigma \times \sigma_1'' + \sin^2 \phi_\sigma \times \sigma_2'' \\
\sigma_2 &= \sin^2 \phi_\sigma \times \sigma_1'' + \cos^2 \phi_\sigma \times \sigma_2'' \\
&\vdots \\
\sigma_6 &= \sin \phi_\sigma \cos \phi_\sigma \times \sigma_1'' - \sin \phi_\sigma \cos \phi_\sigma \times \sigma_2''
\end{aligned} \tag{2.2.40}$$

The stress components in the reference frame can be obtained via the second-rank tensor method and represented as

$$\begin{bmatrix} \sigma_1 \\ \sigma_2 \\ \sigma_3 \\ \sigma_4 \\ \sigma_5 \\ \sigma_6 \end{bmatrix} = \begin{bmatrix} \cos^2 \phi_\sigma \\ \sin^2 \phi_\sigma \\ 0 \\ 0 \\ 0 \\ \sin \phi_\sigma \cos \phi_\sigma \end{bmatrix} \times \sigma_1'' + \begin{bmatrix} \sin^2 \phi_\sigma \\ \cos^2 \phi_\sigma \\ 0 \\ 0 \\ 0 \\ -\sin \phi_\sigma \cos \phi_\sigma \end{bmatrix} \times \sigma_2'' \tag{2.2.41}$$

This equation is universally used for stress that is misaligned with the main axes with an angle  $\phi_\sigma$  to the reference frame  $x$ .

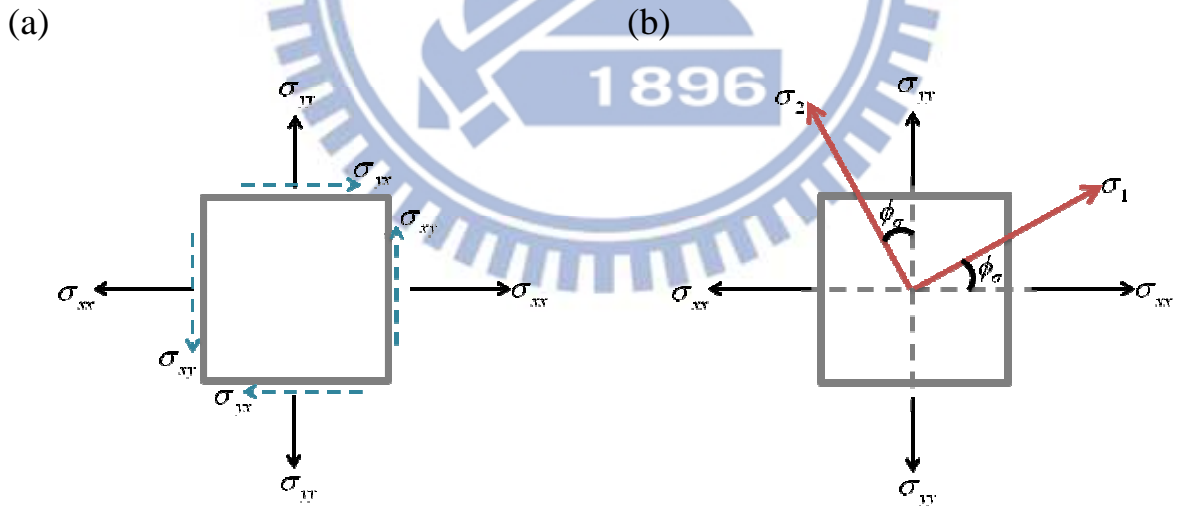


Fig. 2.2.5 (a) stresses in given coordinate system. (b) stress applied with an angle  $\phi_\sigma$  to the main reference coordinate.

For the following usage, the matrix notations are presented as the Cartesian notation, subsequently allowing for additional discussion via direct observation.

$$\begin{bmatrix} \sigma_{xx} \\ \sigma_{yy} \\ \sigma_{zz} \\ \sigma_{xz} \\ \sigma_{yz} \\ \sigma_{xy} \end{bmatrix} = \begin{bmatrix} \cos^2 \phi_\sigma \\ \sin^2 \phi_\sigma \\ 0 \\ 0 \\ 0 \\ \sin \phi_\sigma \cos \phi_\sigma \end{bmatrix} \times \sigma_1 + \begin{bmatrix} \sin^2 \phi_\sigma \\ \cos^2 \phi_\sigma \\ 0 \\ 0 \\ 0 \\ -\sin \phi_\sigma \cos \phi_\sigma \end{bmatrix} \times \sigma_2 \quad (2.2.42)$$

Also, insert Eq. (2.2.42) into Eq. (2.2.30).

The *strain* induced by a set of *bi-axial stress* and applied with an angle  $\phi_\sigma$  to  $x$  and  $y$  axes for any reference frame is shown below:

$$\begin{bmatrix} \epsilon_{xx} \\ \epsilon_{yy} \\ \epsilon_{zz} \\ 2\epsilon_{yz} \\ 2\epsilon_{zx} \\ 2\epsilon_{xy} \end{bmatrix} = \begin{bmatrix} s_{11} \cos^2 \phi_\sigma + s_{12} \sin^2 \phi_\sigma \\ s_{12} \cos^2 \phi_\sigma + s_{11} \sin^2 \phi_\sigma \\ s_{13} \\ 0 \\ 0 \\ s_{66} \times (\sin \phi_\sigma \cos \phi_\sigma) \end{bmatrix} \times \sigma_1 + \begin{bmatrix} s_{11} \sin^2 \phi_\sigma + s_{12} \cos^2 \phi_\sigma \\ s_{12} \sin^2 \phi_\sigma + s_{11} \cos^2 \phi_\sigma \\ s_{13} \\ 0 \\ 0 \\ -s_{66} \sin \phi_\sigma \cos \phi_\sigma \end{bmatrix} \times \sigma_2 \quad (2.2.43)$$

Thus, for the main reference frame along  $[110]$ , the stress induced strain can be written as

$$\begin{bmatrix} \epsilon_{xx} \\ \epsilon_{yy} \\ \epsilon_{zz} \\ 2\epsilon_{yz} \\ 2\epsilon_{zx} \\ 2\epsilon_{xy} \end{bmatrix} = \begin{bmatrix} s_{11}^{[110]} \cos^2 \phi_\sigma + s_{12}^{[110]} \sin^2 \phi_\sigma \\ s_{12}^{[110]} \cos^2 \phi_\sigma + s_{11}^{[110]} \sin^2 \phi_\sigma \\ s_{13}^{[110]} \\ 0 \\ 0 \\ s_{66}^{[110]} \times (\sin \phi_\sigma \cos \phi_\sigma) \end{bmatrix} \times \sigma_1 + \begin{bmatrix} s_{11}^{[110]} \sin^2 \phi_\sigma + s_{12}^{[110]} \cos^2 \phi_\sigma \\ s_{12}^{[110]} \sin^2 \phi_\sigma + s_{11}^{[110]} \cos^2 \phi_\sigma \\ s_{13}^{[110]} \\ 0 \\ 0 \\ -s_{66}^{[110]} \sin \phi_\sigma \cos \phi_\sigma \end{bmatrix} \times \sigma_2 \quad (2.2.44)$$

## Chapter 3 Size Effects

Based on the above theory and equations, the Hamiltonian for exciton can be constructed; the fine structure splitting and degree of linear polarization in QDs can be determined as well. All of the elements in Hamiltonian are determined by the shape of QDs, parameters of material and, finally, the strain effect.

Due to the summation and cancellation of dipole-dipole interaction in  $x$  and  $y$  direction, the state of low energy used to emit along  $x$ -direction, while the high energy state emits along  $y$ -direction as shown in the figure below in which the  $S_{\pi x, \pi y} < 0$ . However, the abnormal phenomenon is observed in InAs/GaAs QDs ( $S_{\pi x, \pi y} > 0$ ), the following is the discussion of this observation. As the optical polarization, the total polarization of high and low energy states is along  $x$ -direction which corresponds to the elongation of QDs.

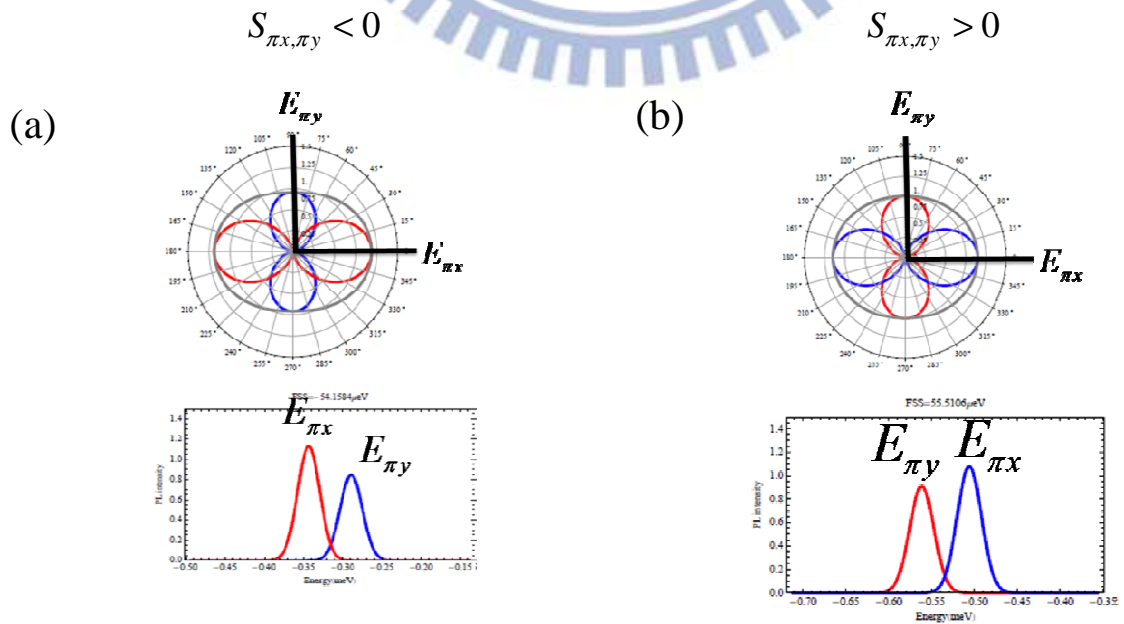




Fig. 3.1 (a) The normal distribution that shows low energy state and polarization along x-direction. (b) The abnormal situation that shows low energy state emits along y-direction.

Most of the physical quantities like  $HH$ -  $LH$ - coupling term  $\rho_{HL}$ ,  $HH$ -  $LH$ - energy separation  $\Delta_{HL}$  and long-range interaction  $\Delta_l$  closely resemble each other in terms of the two materials InAs/GaAs and GaAs/AlGaAs. Notably, two materials most obviously differ in the term of  $\Delta_{BD}$ , the energy separation between bright and dark exciton based on Eq. (2.1.46)

$$\Delta_{BD} \propto \Delta_{eh,bulk}^{xc} \times \frac{a_B^{*3}}{\xi} l_x^{-2} l_z^{-1}$$

The Bohr radius of InAs is 34nm, while that of GaAs is 11nm. The energy from dark to bright exciton is directly proportional to the third power of Bohr radius, subsequently leading to a very large adjustment of the energy from dark to bright exciton of InAs.

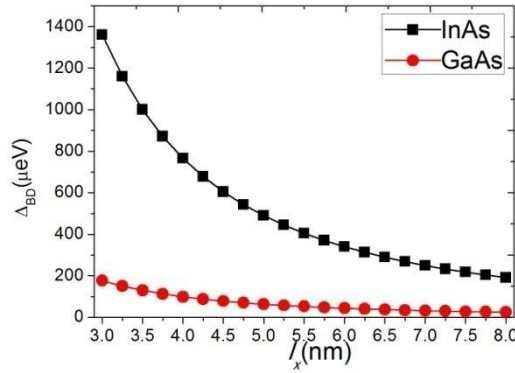


Fig. 3.2 Energy difference from dark to bright exciton  $\Delta_{BD}$  of InAs and GaAs.

The very large  $\Delta_{BD}$  promotes the low energy state,  $\pi_x$  higher and eventually

leads to the  $\pi_y$  state.

The band gap of bulk InAs is 0.413eV, and 1.518eV. One is very wide and the other is narrow. Effective mass of each material can be determined based on the energy gap, and the Bohr radius is further related to the effective mass.

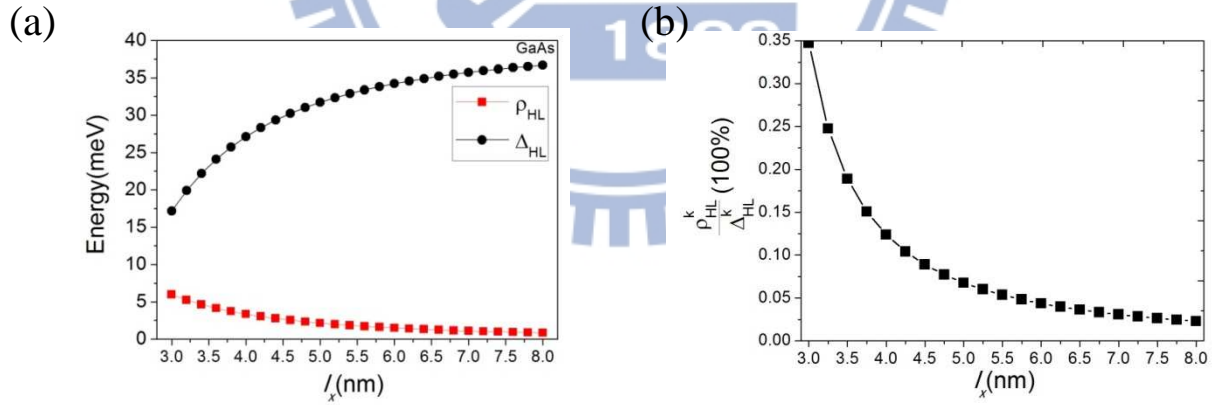
$$m_e^* = \frac{m_0}{1 + E_p / E_g}$$

$$a_B^* = a_B \times \frac{\epsilon_b}{m_e^*}$$

Consequently, the Bohr radius of InAs is 34nm and while that of GaAs is 11nm.

### 3.1 Hierarchical GaAs QDs

Hierarchical GaAs QDs are stress free QDs. Only the size effects on GaAs QDs are considered here. The numerical results of FSS are obtained by diagonalizing the Hamiltonian in Eq. (2.1.18).



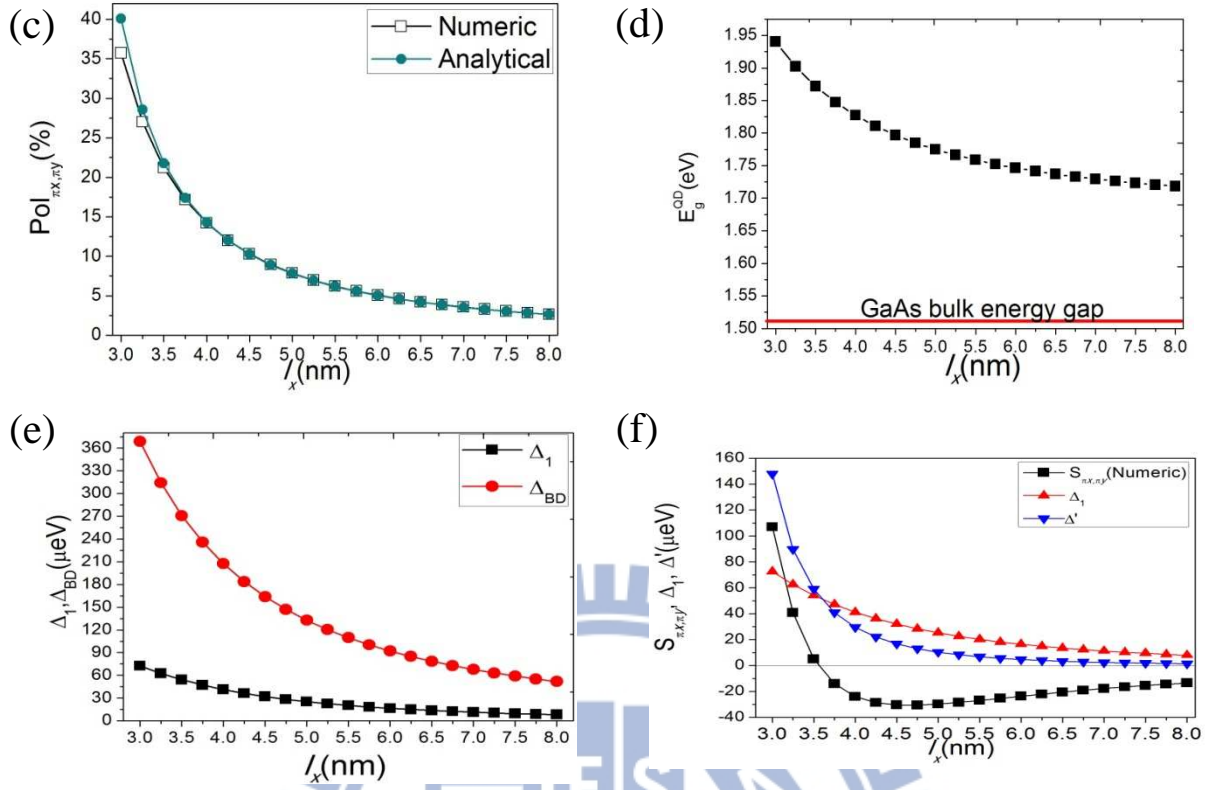


Fig. 3.1.1 (a)  $\rho_{HL}$  and  $\Delta_{HL}$  (b)  $\frac{\rho_{HL}}{\Delta_{HL}}$  (c)  $Pol_{\pi_x, \pi_y}$  with both numerical and analytical result. (d)  $E_g^{QD}$  (e)  $\Delta_{BD}$  (f)  $S_{\pi_x, \pi_y}$ ,  $\Delta_1$  and  $\Delta'$  of GaAs strain free QDs vary with size.  $l_z = 2$  nm and  $\xi' = l_y / l_x = 0.8$

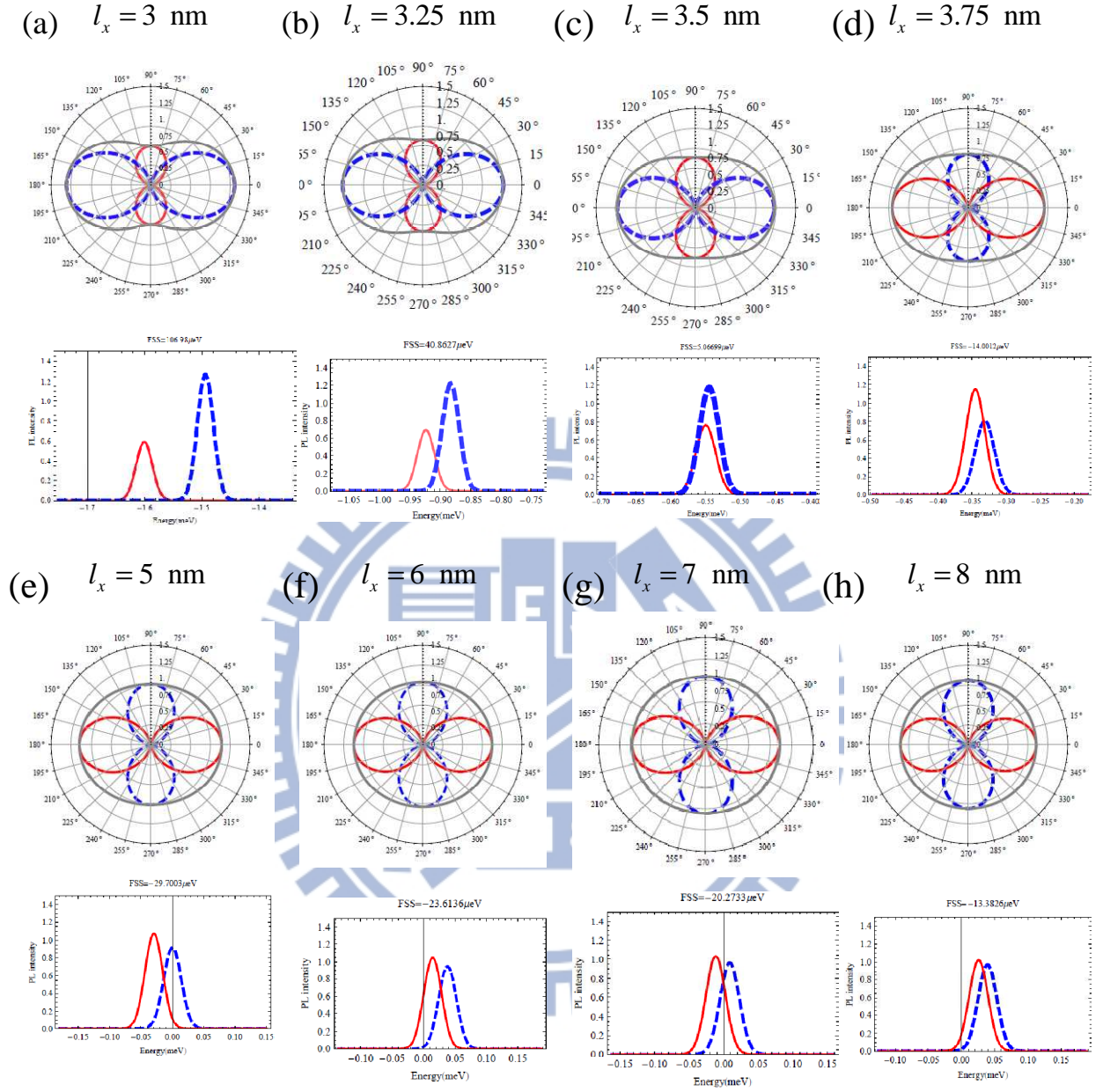


Fig. 3.1.2 GaAs QDs without strain. PL polarization and energy spectrum of QDs vary with characteristic length of (a) 3nm (b) 3.25nm (c) 3.5nm (d) 3.75nm (e) 5nm (f) 6nm (g) 7nm (h) 8nm.  $l_z = 2 \text{ nm}$  and  $\xi' = l_y / l_x = 0.8$

From Eqs . (2.1.36), (2.1.40), (2.1.43), (2.1.44)

$$\Delta_1 \propto E_p \left( \frac{1-\xi}{\xi^2} \right) \times \frac{1}{l_x^3} \times \left( 1 - \frac{3l_z}{2l_y} + \dots \right) \approx E_p \left( \frac{1-\xi}{\xi^2} \right) l_x^{-2.5} \quad (3.1.1)$$

$$\Delta_{BD} \propto \Delta_{eh,bulk}^{xc} \times \frac{a_B^{*3}}{\xi} l_x^{-2} l_z^{-1} \quad (3.1.2)$$

$$\rho_{HL}^k \propto l_x^{-2} \left( \frac{1}{\xi} - 1 \right) \quad (3.1.3)$$

$$\Delta_{HL}^k \propto \frac{1}{l_z^2} - \frac{1}{2l_x^2} - \frac{1}{2l_y^2} \propto l_z^{-2} \left( 1 - \frac{1}{l_x^2} \right) \quad (3.1.4)$$

$$\frac{\rho_{HL}^k}{\Delta_{HL}^k} \propto l_x^{-2} l_z^2 \left( 1 - \frac{1}{l_x^2} \right)^{-1} \left( \frac{1-\xi^2}{\xi^2} \right) \quad (3.1.5)$$

$$\Delta' = \frac{\rho_{HL}}{\Delta_{HL}} \Delta_{BD} \propto \Delta_{eh,bulk}^{xc} \times a_B^{*3} \left( \frac{1-\xi^2}{\xi^3} \right) \left( \frac{1}{l_z^2} - \frac{1}{2l_x^2} - \frac{1}{2l_y^2} \right)^{-1} l_x^{-4} l_z^{-1} \quad (3.1.6)$$

According to Eqs. (3.1.3) and (3.1.4),  $\rho_{HL}^k$  decreases as the size of QDs grows; in addition,  $\Delta_{HL}^k$  increases as the size grows. These analysis correlate with the analytical results shown in Fig 3.1(a). More, according to Eq. (3.1.5), the ratio  $\frac{\rho_{HL}^k}{\Delta_{HL}^k}$  decreases with an increasing size, implying a reduction of *HH- LH-* coupling. According to Eq. (2.1. 61) this ratio is directly related to the linear polarization. Thus in Fig 3.1(b), the value of Pol decreases with an increasing size. Figure 3.2 also reveals that the Pol sketches are increasingly round with a decreasing size of QDs.

According to Eqs. (3.1.1) and (3.1.2), both  $\Delta_1$  and  $\Delta_{BD}$  increase with a decreasing size. Also, according to the power of each, the trend of  $\Delta_1$  is flatter than  $\Delta_{BD}$ . However, with the factor of *HH- LH-* coupling,  $\Delta'$  increases faster

than  $\Delta_1$  with a diminishing size. Therefore, the long range interaction  $\Delta_1$  cancels the short range interaction  $\Delta'$  at the crossing point, then further short range dominates the long range interaction  $\Delta_1$  at small size region.





### 3.2 InAs/GaAs self-assembled QDs

A preliminary observation is made of the InAs/GaAs QDs *without* considering initial stress.

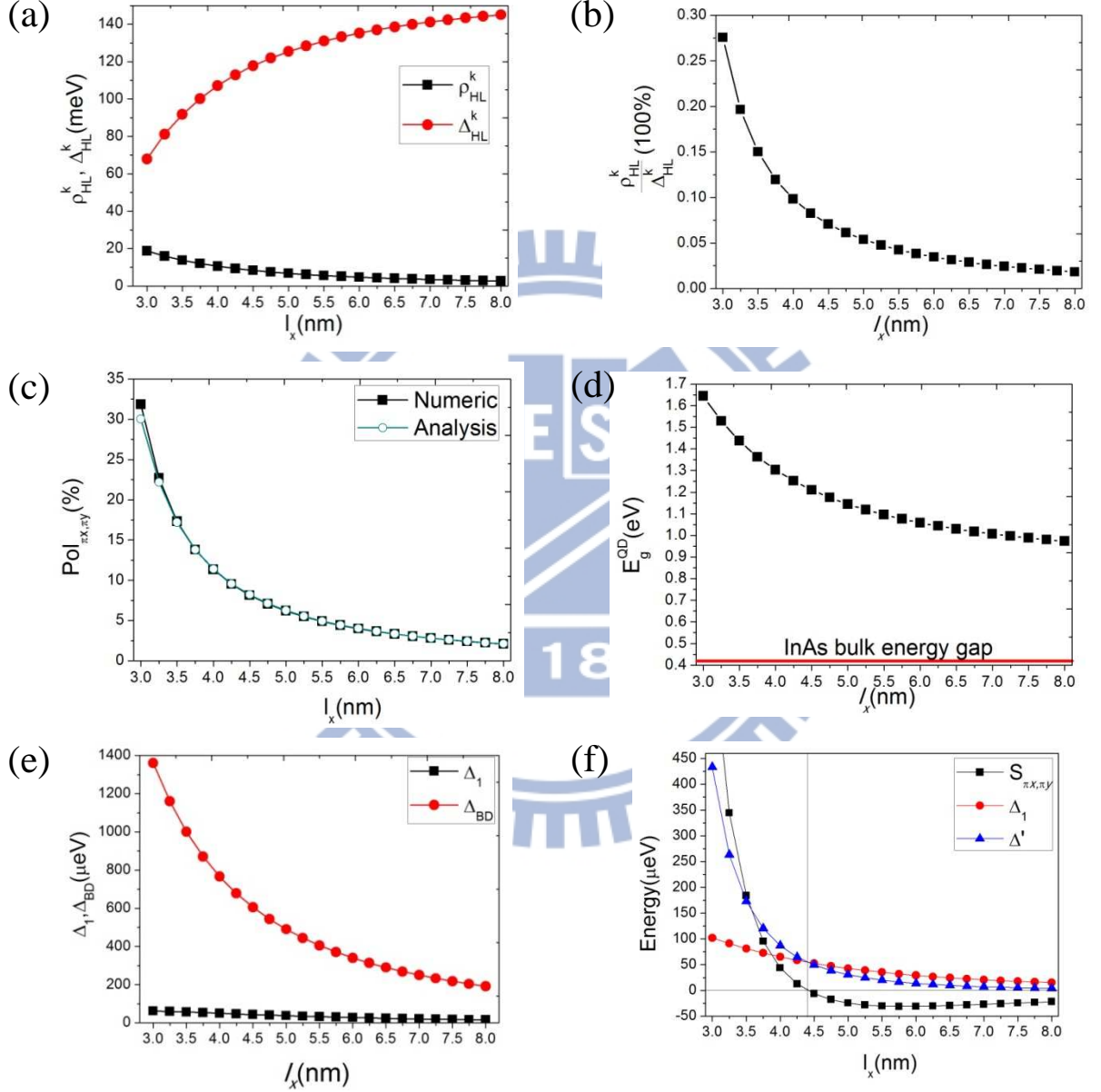


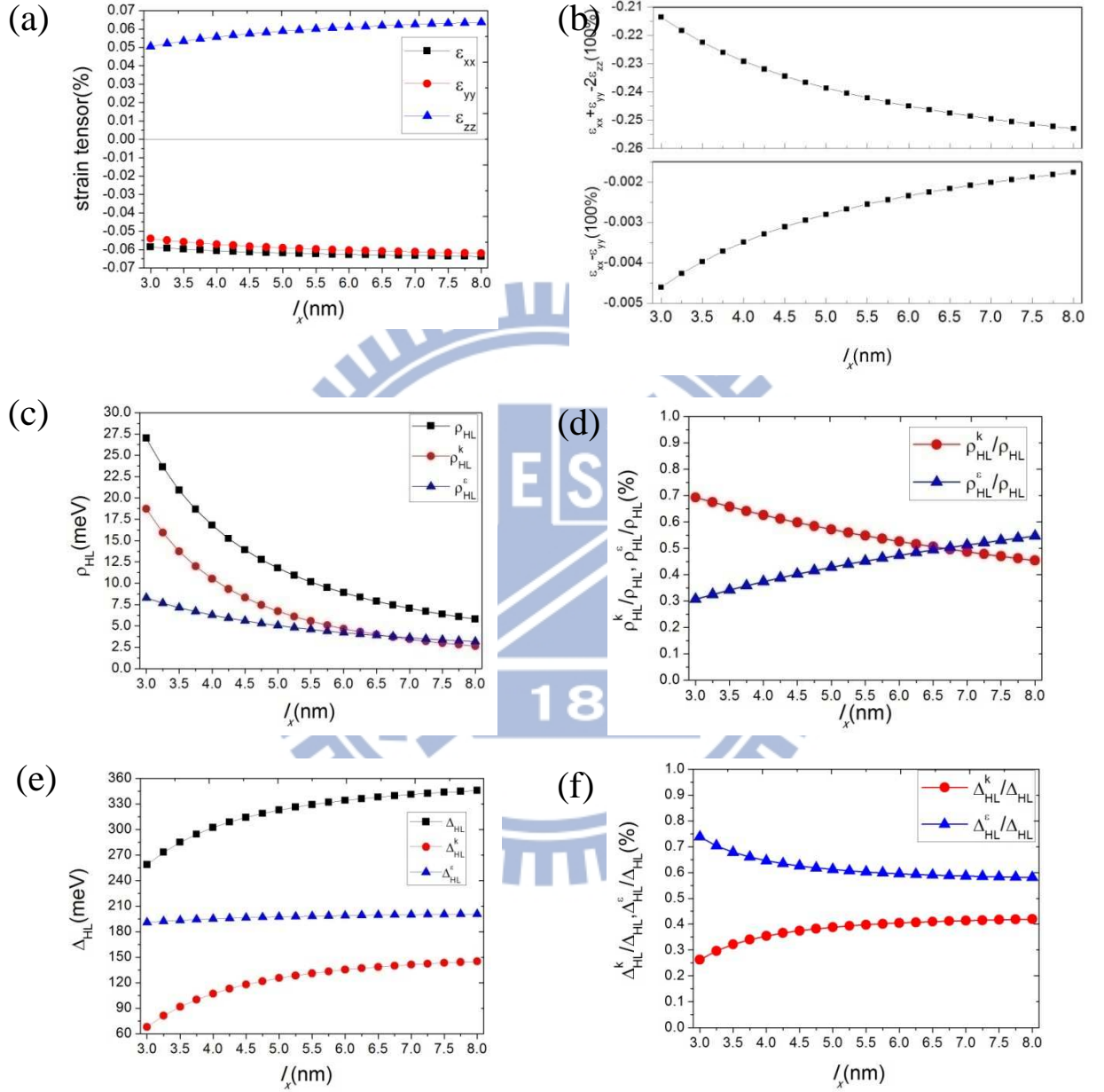
Fig. 3.2.1 (a)  $\rho_{HL}$  and  $\Delta_{HL}$  (b)  $\frac{\rho_{HL}}{\Delta_{HL}}$  (c)  $Pol_{\pi x, \pi y}$  with both numerical and

analytical result. (d)  $E_g^{QD}$  (e)  $\Delta_{BD}$  (f)  $S_{\pi x, \pi y}$ ,  $\Delta_1$  and  $\Delta'$  of InAs strain free QDs

vary with size.  $l_z = 2$  nm and  $\xi' = l_y / l_x = 0.8$



InAs/GaAs self-assembled QDs have built-in strains due to lattice mismatching. The strain tensors vary with size, as shown in Ch2.



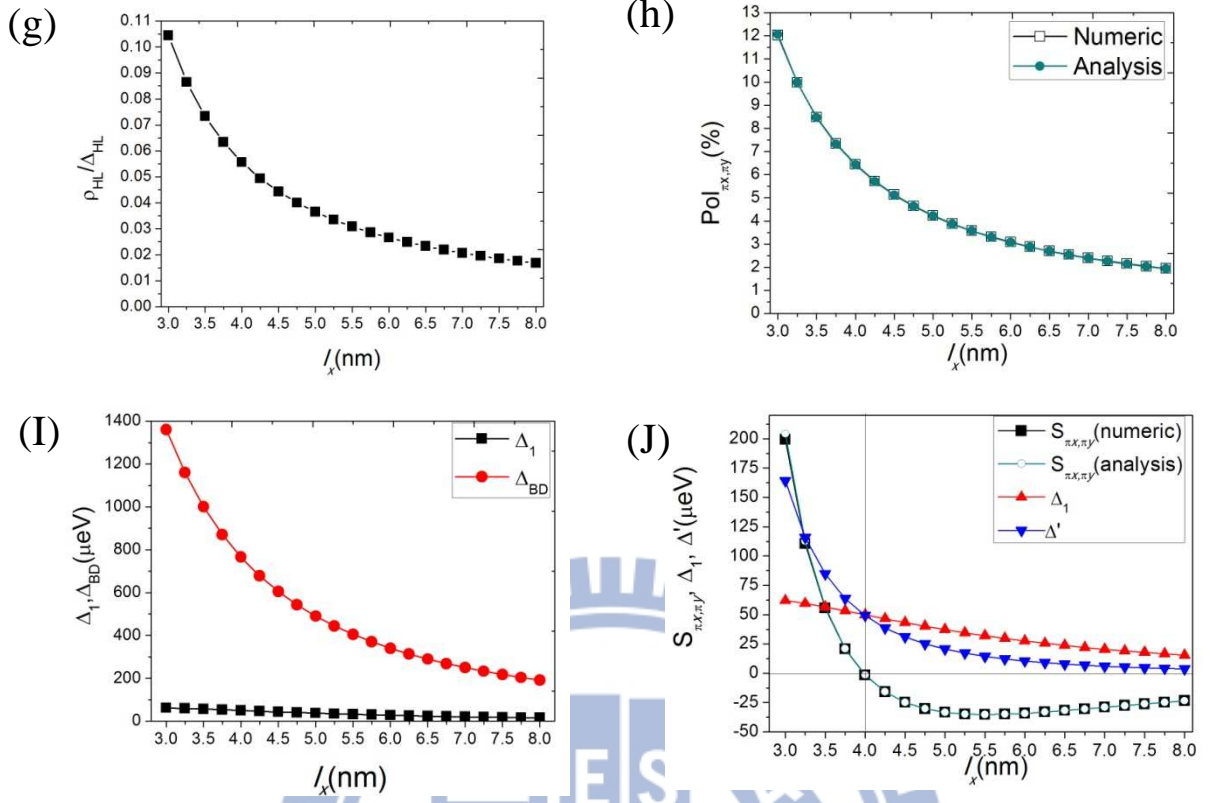


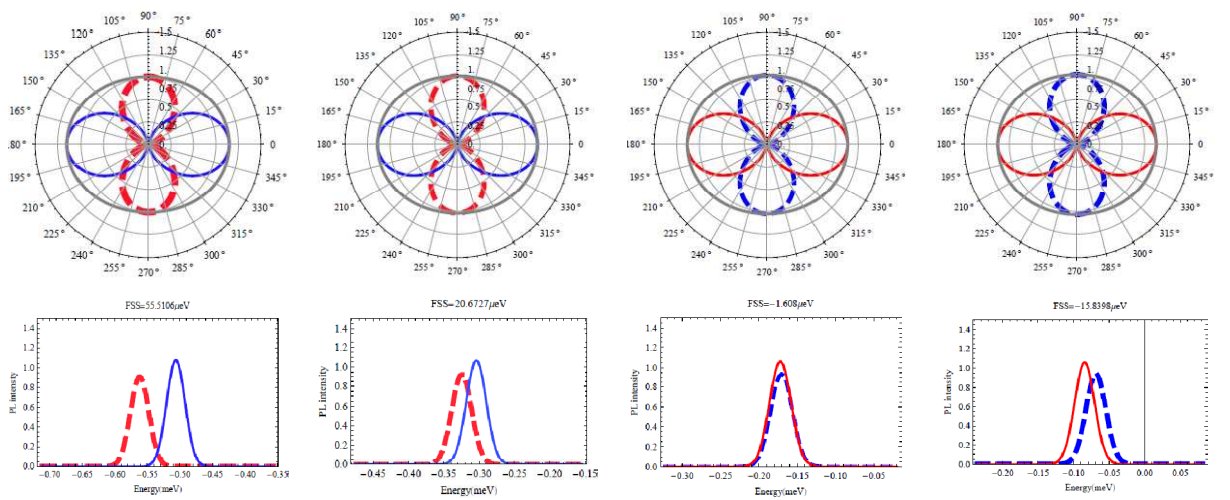
Fig. 3.2.2 InAs/GaAs with initial strain. (a) strain tensors of  $\epsilon_{xx}, \epsilon_{yy}$  and  $\epsilon_{zz}$ , (b)

$\Delta_1$ , (c)  $\rho_{HL}$ ,  $\rho_{HL}^k$  and  $\rho_{HL}^\epsilon$ , (d)  $\frac{\rho_{HL}^k}{\rho_{HL}}$  and  $\frac{\rho_{HL}^\epsilon}{\rho_{HL}}$ , (e)  $\Delta_{HL}$ ,  $\Delta_{HL}^k$  and  $\Delta_{HL}^\epsilon$ , (f)  $\frac{\Delta_{HL}^k}{\Delta_{HL}}$

and  $\frac{\Delta_{HL}^\epsilon}{\Delta_{HL}}$ , (g)  $\frac{\rho_{HL}}{\Delta_{HL}}$ , (h)  $Pol_{\pi x, \pi y}$ , (I)  $\Delta_{BD}$ , and  $\Delta_1$  (J)  $S_{\pi x, \pi y}$ ,  $\Delta_1$  and  $\Delta'$

against size with  $l_z = 2$  nm and  $\xi' = l_y / l_x = 0.8$

(a)  $l_x = 3.5$  nm (b)  $l_x = 3.75$  nm (c)  $l_x = 4$  nm (d)  $l_x = 4.25$  nm



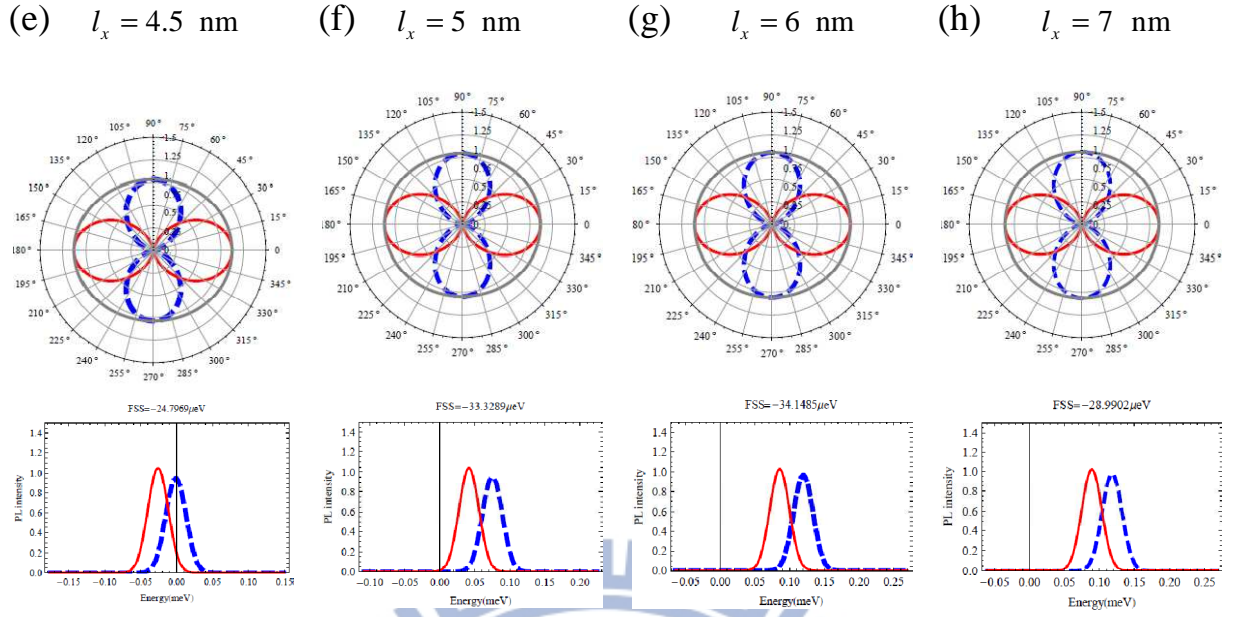


Fig. 3.2.3 Polar plots and PL spectra of InAs/GaAs QD varies with characteristic length of (a) 3.5nm, (b) 3.75nm, (c) 4nm, (d) 4.25nm, (e) 4.5nm (f) 5nm (g) 6nm (h) 7nm.

According to Eqs. (2.1. 37) and (2.1. 41)

$$\rho_{HL}^{\varepsilon} = -\frac{|d|}{2}(\varepsilon_{xx} - \varepsilon_{yy}) + i\sqrt{3}|b|\varepsilon_{xy}$$

$$\Delta_{HL}^{\varepsilon} = -|b|(\varepsilon_{xx} + \varepsilon_{yy} - 2\varepsilon_{zz})$$

In this cubic model,  $\varepsilon_{xy} = 0$ .  $\varepsilon_{xx} - \varepsilon_{yy}$  and  $\varepsilon_{xx} + \varepsilon_{yy} - 2\varepsilon_{zz}$  vary with size as shown in Figure 3.2.2(b). Fig. 3.2.2(c) and 3.2.2(e) reveals an increase in both  $\rho_{HL}$  and  $\Delta_{HL}$  relative to  $\rho_{HL}^k$  and  $\Delta_{HL}^k$  due to the initial strain. For the commonly observed size around 10~20nm width self-assembled QDs whose corresponding characteristic length is about 3~5nm. In this region,  $\Delta_{HL}^{\varepsilon}$  ( $\Delta_{HL}^k$ ) is approximately 65% (35%) in the whole  $\Delta_{HL}$ . Additionally,  $\rho_{HL}^{\varepsilon}$  ( $\rho_{HL}^k$ ) is around 40% (60%) in  $\rho_{HL}$ . This finding suggests that the initial strain's significantly

increases  $\Delta_{HL}$ , and decreases the ratio  $\frac{\rho_{HL}}{\Delta_{HL}}$ . The Pol simply follows the trend of

$\frac{\rho_{HL}}{\Delta_{HL}}$ , which increases with an decreasing size. According to Fig. 3.2.2, the polar

plots are tend to be asymmetric with the an decreasing size which agrees with the analysis results.

In the case of InAs/GaAs QDs, the energy of  $\Delta_{BD}$  is much greater than  $\Delta_1$ , which indicates that short range interaction is much more active than in GaAs/AlGaAs QDs since InAs's Bohr radius is very wide due to its Energy its narrow gap.

$$\Delta_{BD} \propto \Delta_{eh,bulk}^{xc} \times \frac{a_B^{*3}}{\xi} l_x^{-2} \quad (3.1.2)$$

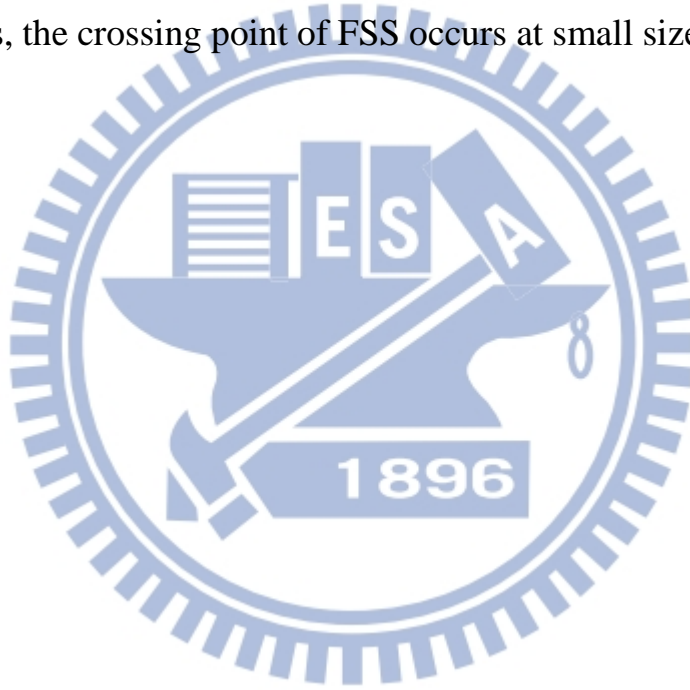
For GaAs  $a_B^* = 11 \text{ nm}$ , for InAs  $a_B^* = 34 \text{ nm}$ , this term makes  $\Delta_{BD}$  of InAs 27 times greater than that of GaAs. In the small size region,  $\Delta_{BD}$  is extremely large, subsequently making  $\Delta_1$  and  $\Delta'$  compatible with each other. Again, according to the power,  $\Delta_1$  increases faster than  $\Delta_{BD}$  with an decreasing of size, the ratio

$\frac{\rho_{HL}}{\Delta_{HL}}$  causes  $\Delta'$  to increase faster than  $\Delta_1$ . Thus a crossing occurs at around

$l_x = 3.6 \text{ nm}$ . By the region  $l_x < 3.6 \text{ nm}$ ;  $\Delta' > \Delta_1$ , thus  $F_{ss} = -\Delta_1 + \Delta'$  are positive, that is  $E_{\pi x} > E_{\pi y}$ . While  $l_x > 3.6 \text{ nm}$ ,  $\Delta' < \Delta_1$ , and  $F_{ss} = -\Delta_1 + \Delta'$  become negative. According to the results, the intensity of high energy emits along the

y-direction.

The crossing occurs with or without the initial strain. Thus, the FSS of InAs/GaAs self-assembled without initial strain varies from negative to positive and cross to zero at a large size rather than GaAs is largely owing to the very large Bohr radius. Further, the initial strains reduce heavy- and light-hole coupling. Without the initial strain,  $\Delta'$  can be slightly higher in energy; the cross point occurs at a larger  $l_x$ . Compare above two cases of GaAs/AlGaAs and InAs/GaAs QDs, the crossing point of FSS occurs at small size.





## Chapter 4 Strain effects on semiconductor bulk

### 4.1 Fundamental bulk theory

This chapter demonstrates that physical observables of semiconductor bulk under stress are varied, including the electron and valence-band structure, as well the energy gap, microscopic Bloch function and ultimately the PL polarization.

The zero energy level is set at the top of degeneracy valence-band energy at  $\Gamma$ -point with stress. Equation (2.1.4) thus becomes

$$E_n(k) = E_g + \frac{\hbar^2}{2m_e^*m_0}(k_x^2 + k_y^2 + k_z^2) + a_c(\epsilon_{xx} + \epsilon_{yy} + \epsilon_{zz}) \quad (4.1.1)$$

$E_g$ , energy gap between conduction-band and valence-band. The valence-band structures of *HH*- and *LH*- are given by four-band Luttinger Hamiltonian in Eq. (2.1.5).

The band structures are obtained by the diagonalization of the Hamiltonian.

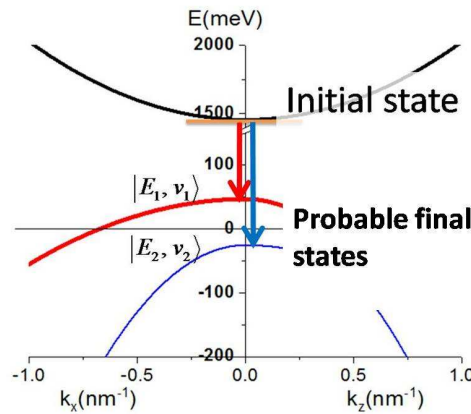


Fig. 4.1.1 An electron in the initial excited state spontaneously emit radiation, two states are probable for the emission process.

Numerical results indicate a variation of band-edge energies at  $\Gamma$ -point. The valence band edge energies of stressed bulk are obtained from the Hamiltonian at  $k=0$ . Since  $\mathcal{E}_{xz}$  and  $\mathcal{E}_{yz}$  are neglected, the  $S$  term in the Hamiltonian is neglected. The band edge energy and its corresponding eigenvector thus become.

High energy band

$$E_1 = -P_\varepsilon + \sqrt{Q_\varepsilon^2 + R_\varepsilon^2}$$

$$\left| v_1, \vec{k}=0, \varepsilon_{ij} \right\rangle = \frac{1}{N_{v1}} \left[ R_\varepsilon \left| u_{3/2}^h \right\rangle + \left( -Q_\varepsilon - \sqrt{Q_\varepsilon^2 + R_\varepsilon^2} \right) \left| u_{1/2}^h \right\rangle \right] \quad (4.1.2)$$

Low energy band

$$E_2 = -P_\varepsilon - \sqrt{Q_\varepsilon^2 + R_\varepsilon^2}$$

$$\left| v_2, \vec{k}=0, \varepsilon_{ij} \right\rangle = \frac{1}{N_{v2}} \left[ R_\varepsilon \left| u_{3/2}^h \right\rangle + \left( -Q_\varepsilon + \sqrt{Q_\varepsilon^2 + R_\varepsilon^2} \right) \left| u_{1/2}^h \right\rangle \right] \quad (4.1.3)$$

$N_{v1}$  and  $N_{v2}$  represent normalized constants.

Based on those eigenvectors, the Bloch function is composed at  $\Gamma$ -point.

The PL polarization of bulk with applied stress also adheres to the Fermi's Golden rule.

Fermi's Golden rule states that

$$I_{i \rightarrow f} \propto \left| \left\langle f \left| \hat{e} \cdot \hat{p} \right| i \right\rangle \right|^2 \delta(E - E_i + E_f)$$

$$\propto \left| \left\langle v_n, \vec{k}=0, \varepsilon_{ij} \left| \hat{e} \cdot \hat{p} \right| c \uparrow, \vec{k}=0, \varepsilon_{ij} \right\rangle \right|^2 \delta(E - E_T) \quad (4.1.4)$$

$E_T$  indicates the transition energy between conduction- and valance-bands.

$$\left| i \right\rangle = \left| c \uparrow, \vec{k}=0, \varepsilon_{ij} \right\rangle \quad (4.1.5)$$

and the final state is represented as



$$|f\rangle = |v_n, \vec{k}=0, \epsilon_{ij}\rangle \quad (4.1.6)$$

From Chang [18](Appendix A) and Eqs. (4.1.1) to (4.1.3), the transition energies of the bands are derived below:

Low transition (black to red)

$$E_{T,1} = E_g - (-P_\epsilon + \sqrt{Q_\epsilon^2 + R_\epsilon^2}) \quad (4.1.7)$$

$$I_1(\theta) \propto \frac{1}{N_{v2}} \left| \frac{R_\epsilon}{\sqrt{2}} e^{i\theta} - \frac{(-Q_\epsilon - \sqrt{Q_\epsilon^2 + R_\epsilon^2})}{\sqrt{6}} e^{-i\theta} \right|^2 \quad (4.1.8)$$

High transition (black to blue)

$$E_{T,2} = E_g - (-P_\epsilon - \sqrt{Q_\epsilon^2 + R_\epsilon^2}) \quad (4.1.9)$$

$$I_2(\theta) \propto \frac{1}{N_{v2}} \left| \frac{R_\epsilon}{\sqrt{2}} e^{i\theta} - \frac{(-Q_\epsilon + \sqrt{Q_\epsilon^2 + R_\epsilon^2})}{\sqrt{6}} e^{-i\theta} \right|^2 \quad (4.1.10)$$

$E_{T,i}$  are transition energy,  $\theta$  is the angle of  $360^\circ$  polar plot.

Moreover, the above equations are transformed in terms of stress by applying the results of stress transformation to those of strain.

$$P_\epsilon = -a_v (\epsilon_{xx} + \epsilon_{yy} + \epsilon_{zz}) = -a_v (s_{11}^{[110]} + s_{12}^{[110]} + s_{13}^{[110]})(\sigma_1 + \sigma_2) \quad (4.1.11)$$

$$Q_\epsilon = -\frac{b}{2} (\epsilon_{xx} + \epsilon_{yy} - 2\epsilon_{zz}) = -\frac{b}{2} (s_{11}^{[110]} + s_{12}^{[110]} - 2s_{13}^{[110]})(\sigma_1 + \sigma_2) \quad (4.1.12)$$

$$\begin{aligned} R_\epsilon &= \frac{d}{2} (\epsilon_{xx} - \epsilon_{yy}) - i\sqrt{3}b\epsilon_{xy} \\ &= \frac{d}{2} (s_{11}^{[110]} - s_{12}^{[110]}) \cos 2\phi_\sigma (\sigma_1 - \sigma_2) - i\sqrt{3}b \frac{1}{4} s_{66}^{[110]} \times \sin 2\phi_\sigma (\sigma_1 - \sigma_2) \end{aligned} \quad (4.1.13)$$

## 4.2 Numerical results of bulk with applied stress

This subsection discussed the results of a stressed GaAs bulk, including the bulk energy band structure, microscopic Bloch function, PL polarization and the band-edge energy variation.

### Uni-axial along [110]

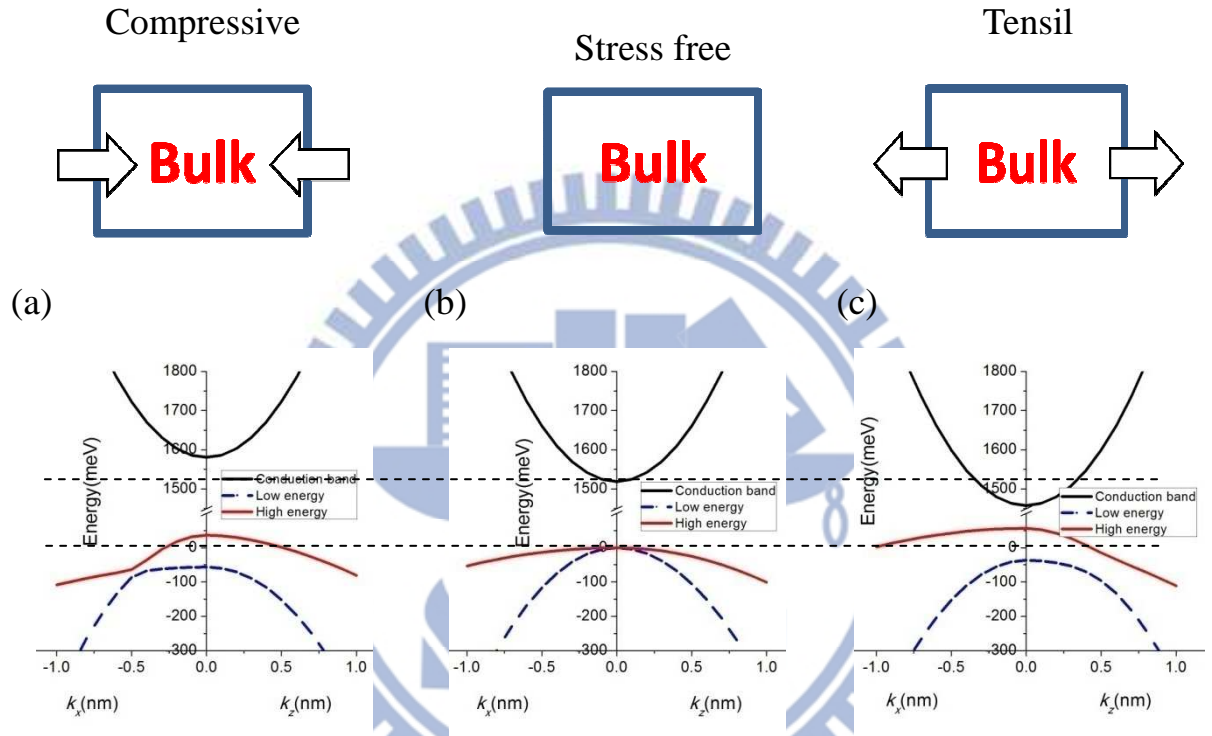


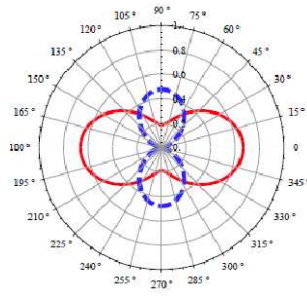
Fig. 4.2.1 GaAs bulk energy bands with stress (a) -2GPa (b) zero (c) 2GPa stress applied along [110].

Compression

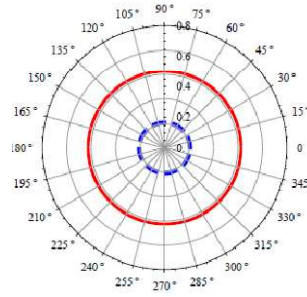
Stress free

Tensile

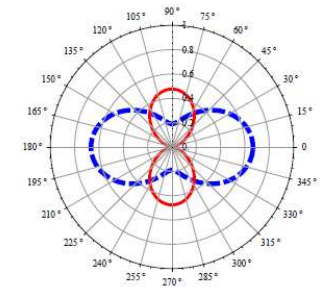
(a)



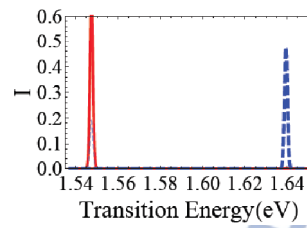
(b)



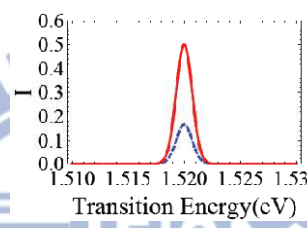
(c)



(d)



(e)



(f)

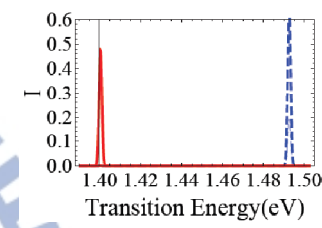


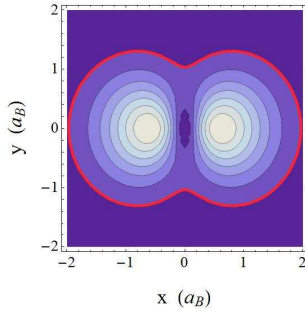
Fig. 4.2.2 PL polarization (first row) and energy spectrum (second row) of GaAs bulk with applied stress (a) -2 GPa (b) zero (c) 2 GPa (d) -2 GPa (e) zero (f) 2 GPa. Red lines denote the low transition energy, blue line denotes the high transition. Stress applied along [110]

Compression

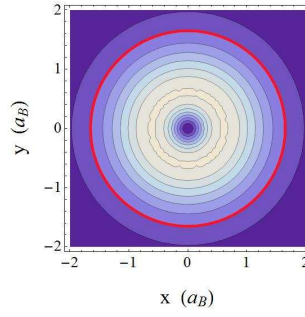
Zero stress

Tensile

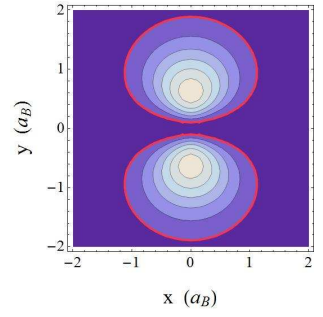
(a)



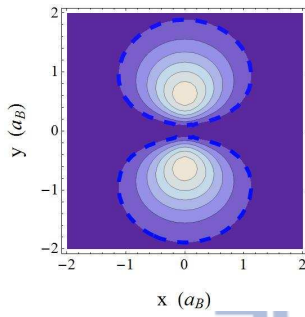
(b)



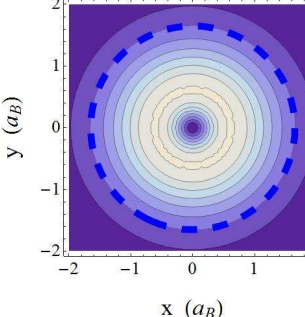
(c)



(d)



(e)



(f)

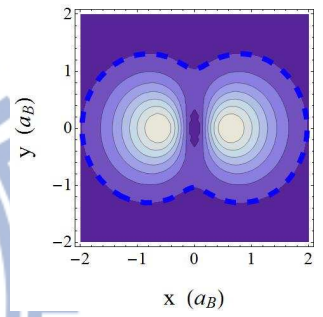
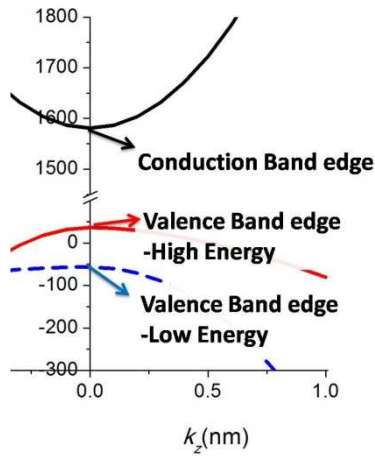
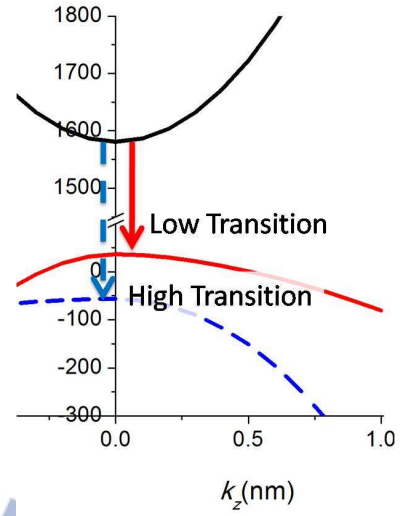


Fig. 4.2.3 Microscopic Bloch function. First row are low energy states (a) -2 GPa (b) zero (c) 2 GPa. While second row are the Bloch function of the high energy states (d) -2 GPa (e) zero (f) 2 GPa. Stress applied along [110]

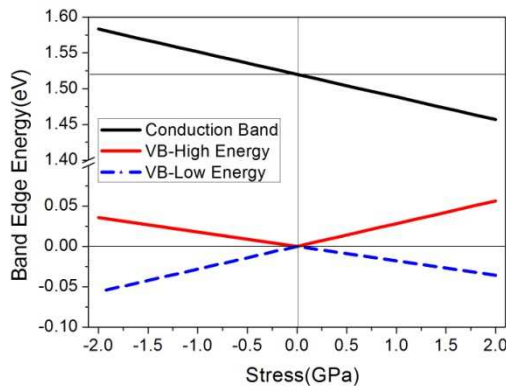
(a)



(b)



(c)



(d)

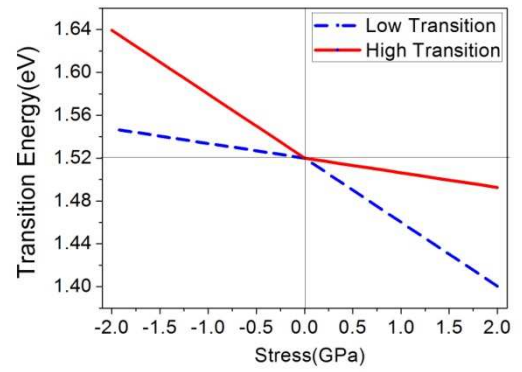


Fig. 4.2.4 (a) The chart reveals the band-edge energies at  $\Gamma$ -point. (b) The chart reveals the low transition and high transition energies. (c) Band-edge energies of three bands at  $\Gamma$ -point. (d) Transition energies, the energy difference from the conduction band to the two hole-states. Stress applied along [110] direction

## Uni-axial stress along [100]

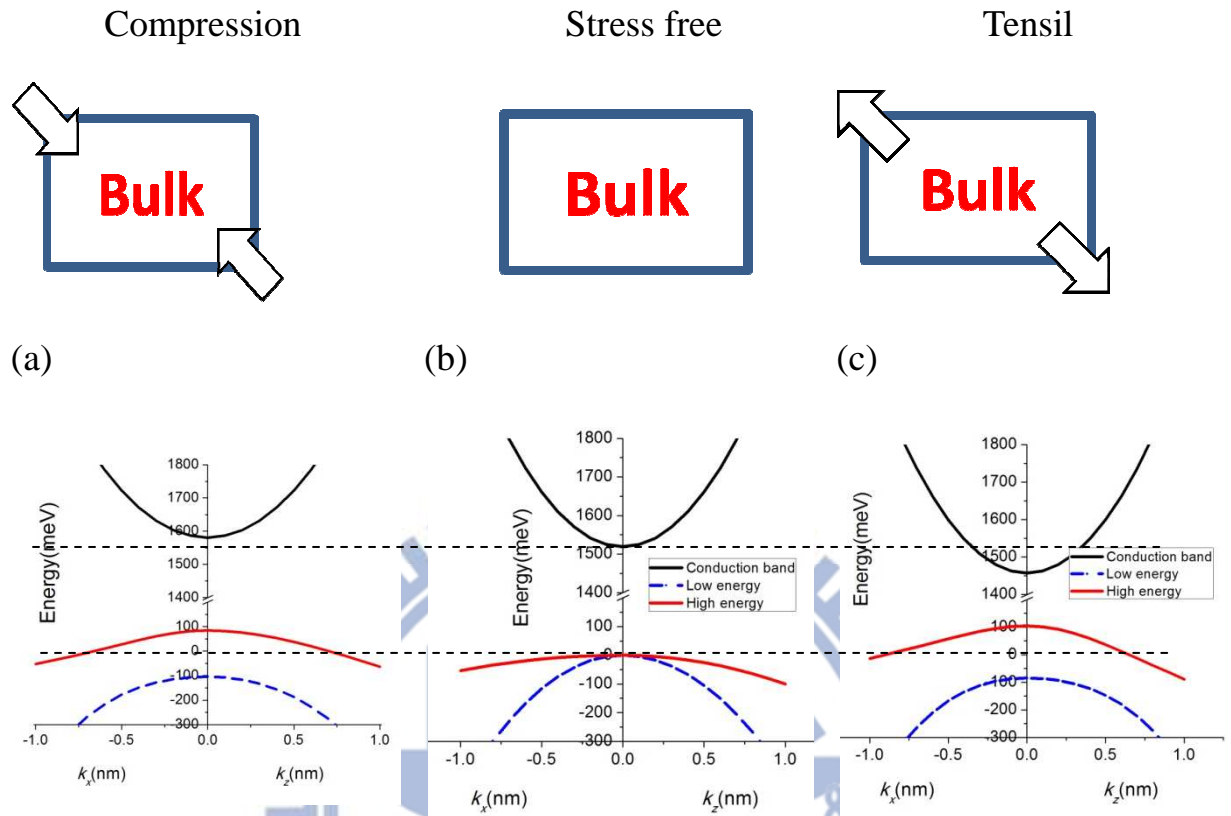
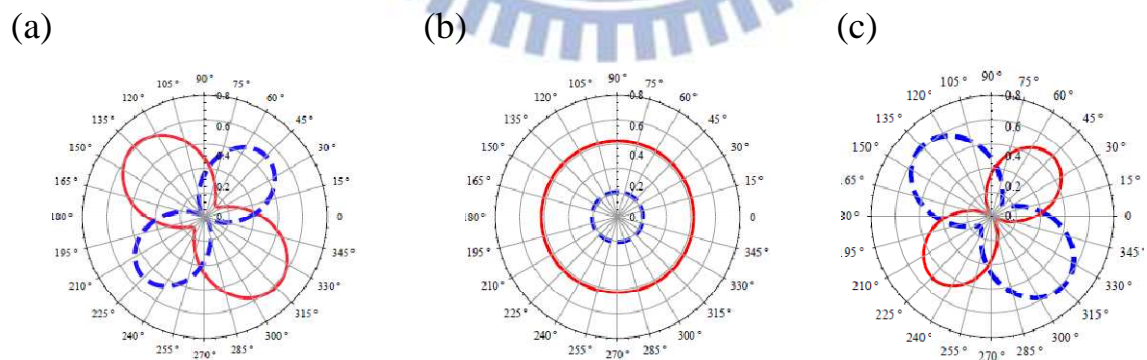


Fig. 4.2.5 GaAs bulk energy bands with stress (a) -2GPa (b) zero (c) 2GPa. Stress applied along [100].





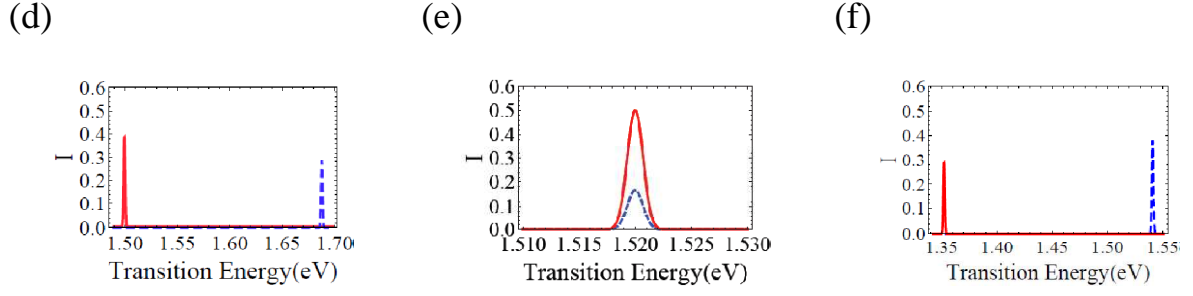


Fig. 4.2.6 PL polarization (first row) and energy spectrum (second row) of GaAs bulk with stress (a) -2GPa (b) zero (c) 2GPa (d) -2GPa (e) zero (f) 2GPa. Red lines denotes the low transition energy one, blue denotes the high transition. Stress applied along [100]

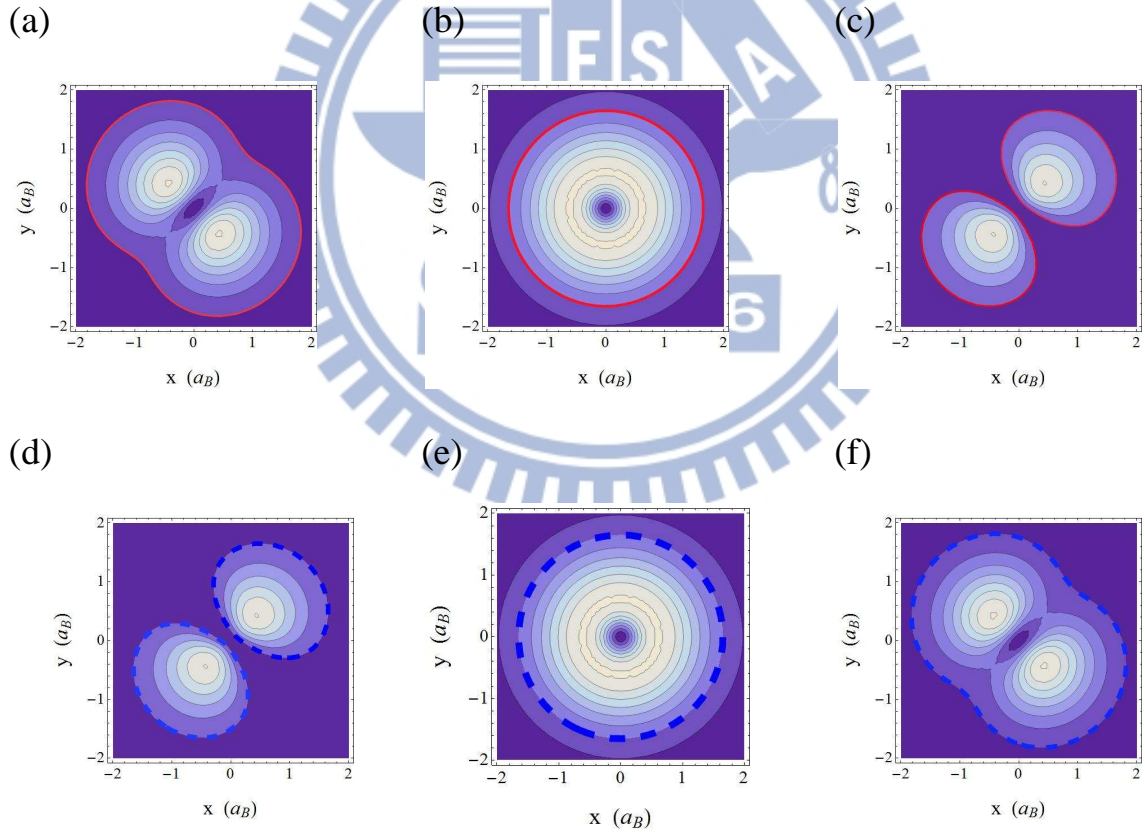


Fig. 4.2.7 Microscopic Bloch function. First row are the high energy states (a) -2GPa (b) zero (c) 2GPa . While second row are the Bloch function for the low energy hole state (d) -2GPa (e) zero (f) 2GPa. Stress applied along [100]



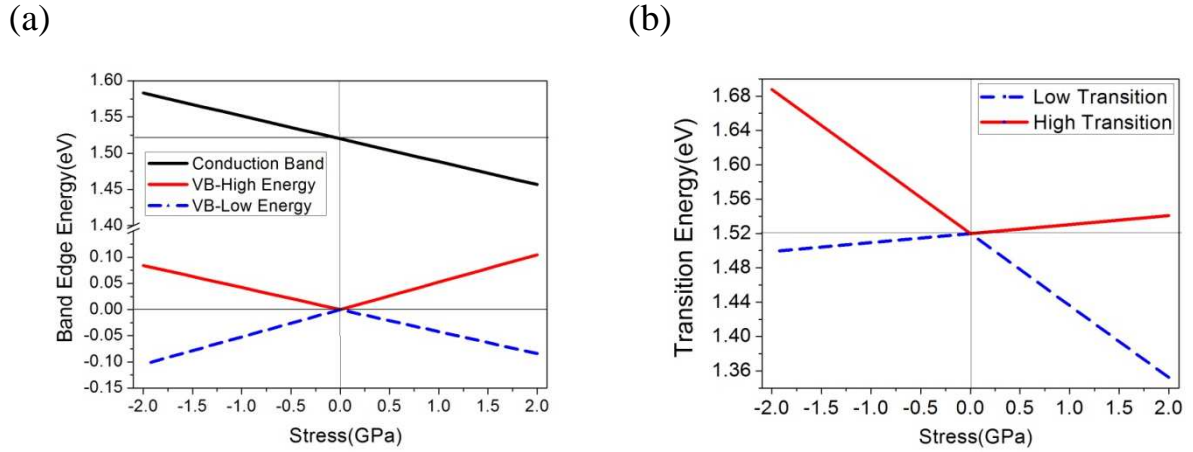


Fig. 4.2.8 Stress applied along [100] (a) band-edge energies at  $\Gamma$ -point of three bands.(b) Transition energies, the energy difference from the conduction band to the two hole-states. Stress applied along [100] direction.

An applied-stress works on the semiconductor bulk causes the slightly change of distance between atoms which distort the microscopic Bloch function. The microscopic Bloch functions reveal the charge density around nucleus and as well as the electron cloud.

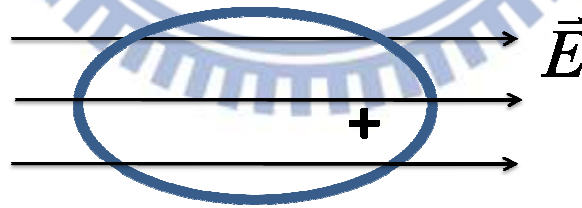


Fig. 4.2.9 “Distortion of the electron cloud in response of an applied E-field.”

(Hecht)[20]

“Distortion of the electron cloud in response to an applied E-field” (Hecht)[20].

The distortion of Bloch function indicates the existence of a built-in electric field. More, “The polarization  $\vec{P}(t)$  of a system depends upon the strength  $\vec{E}(t)$  of the applied optical field.”(Boyd)[21]

$$\vec{P}(t) = \chi \vec{E}(t) \quad (4.2.1)$$

where the constant  $\chi$  is refer to susceptibility. The shape elongation of Bloch function denotes the direction of build-in electric field, therefore, the optical polarization is along the elongation of Bloch function.



## Chapter 5 Conclusion

This study investigates the FSS and Pol of InAs/GaAs QDs self-assembled QDs and hierarchical GaAs QDs with a series of size variation. InAs/GaAs QDs have an initial strain due to lattice mismatching, in which tunes *HH-LH*-splitting energy 1.5 times higher than the strain free QDs, subsequently reducing the Pol. Meanwhile, FSS of GaAs/AlGaAs and InAs/GaAs QD were originally negative then comes crossing to zero, then again increases positively with a decreasing size. Fine structure splitting is the competition between short- and long- range, since the Bohr radius of InAs is extremely large, subsequently exacerbating the situation in which the short-range effect cancels out the long-range effect when the QD size is small.

Furthermore, the energy band of bulk InAs is constructed with an applied stress. The optical polarization, emission energy and the Bloch function under applied stress are manipulated. Analytical results indicate that the band gap decays with an increasing compressive stress. Correspondingly, the band gap rises with an increasing tensile stress. Moreover, the light emission of low energy is along the *compressed* direction and as well the microscopic Bloch function. Furthermore, the Bloch function is twisted due to the built-in electronic field caused by the stress.

As for future work, we recommend that future research further apply the stress on both InAs/GaAs QDs and GaAs QDs. By selecting an appropriate size, the FSS of InAs/GaAs can be tuned to zero. Moreover, the ground state wavefunction of 3D parabolic well is taken as basis in current study, a full

numerical computation with a large amount of basis considered which can evaluate the FSS and Pol more precisely.



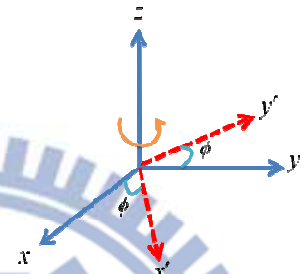
## References

1. M. Grundmann, O. Stier, and D. Bimberg, "InAs/GaAs pyramidal quantum dots: Strain distribution, optical phonons, and electronic structure", *Phys. Rev. B* **52**, 11969–11981 (1995).
2. S. Kumar, R. Trotta, E. Zallo, J. D. Plumhof, and P. Atkinson, "Strain-induced tuning of the emission wavelength of high quality GaAs/AlGaAs quantum dots in the spectral range of the 87Rb  $D_2$  lines", *Appl. Phys. Lett.* **99**, 161118 (2011).
3. R. Singh and G. Bester, "Lower Bound for the Excitonic Fine Structure Splitting in Self-Assembled Quantum Dots", *Phys. Rev. Lett* **104**, 196803 (2010).
4. S. L. Chuang, "Physics of Photonic Devices", Second Edition, Wiley (2008).
5. M. Gong, W. Zhang, G. C. Guo and L. He, "Exciton Polarization, Fine-Structure Splitting, and the Asymmetry of Quantum Dots under Uniaxial Stress", *Phys. Rev. Lett* **106**, 227401 (2011).
6. C. H. Lin, W. T. You, H. Y. Chou, S. J. Cheng, S. D. Lin, and W. H. Chang "Anticorrelation between the splitting and polarization of the exciton fine structure in single self-assembled InAs/GaAs quantum dots", *Phys. Rev. B* **83**, 075317 (2011).
7. J. F. Nye, M. A. and P. D., "Physical Properties of Crystals", 1<sup>st</sup> edition, Oxford: Clarendon Press (1957).
8. M. K. Kuo, T.R. Lin, B.T. Liao, and C.H. Yu, "Strain effects on optical properties of pyramidal InAs/GaAs quantum dots" *Physica E* **26**, 199-202 (2005).
9. S. J. Cheng, private communication, Department of Electrophysics, NCTU (2012).
10. A. V. Nenashev and A. V. Dvurechenskii, "Strain distribution in quantum dot of arbitrary polyhedral shape: Analytical solution in closed form", arXiv:0707.2183v2 (2009).
11. A. V. Nenashev and A. V. Dvurechenskii, "Strain distribution in quantum dot of arbitrary polyhedral shape: Analytical solution", *J. Appl. Phys.* **107**, 064322 (2010).
12. C. H. Ku, "Finite difference method for calculation of electronic structure of semiconductor quantum dots", MS thesis, Department of Electrophysics, NCTU (2011).
13. Y. Léger, L. Besombes, L. Maingault, and H. Mariette, "Valence-band mixing in neutral, charged, and Mn-doped self-assembled quantum dots", *Phys. Rev. B*, **76**, 045331 (2007).
14. T. Takagahara, "Theory of exciton doublet structures and polarization relaxation in single quantum dots", *Phys. Rev. B* **62**, 16840–16855 (2000).
15. M. Z. Maialle, E. A. de Andrada e Silva, and L. J. Sham "Exciton spin dynamics in quantum wells", *Phys. Rev. B* **47**, 15776 (1993).

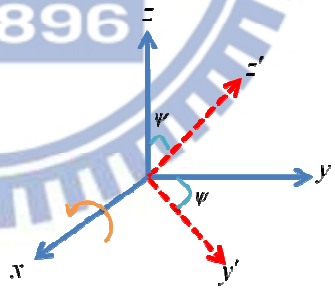
16. E. Kadantsev and P. Hawrylak, "*Theory of exciton fine structure in semiconductor quantum dots: Quantum dot anisotropy and lateral electric field*", Phys. Rev. B **81**, 045311 (2010).
17. R. Romestain and G. Fishman, "*Excitonic wave function, correlation energy, exchange energy, and oscillator strength in a cubic quantum dot*", Phys. Rev. B **49**, 1774 (1994).
18. Y. C. Chang, "*Stark effects in optical anisotropies of self-assembled quantum dots*", MS thesis, Department of Electrophysics, NCTU (2011).
19. W. D. Sheng, S. J. Cheng, and P. Hawrylak, "*Multiband theory of multi-exciton complexes in self-assembled quantum dots*", Phys. Rev. B **71**, 035316 (2005).
20. E. Hecht, "*Optics*", 4<sup>th</sup> edition, Pearson (2001).
21. R. W. Boyd, "*Nonlinear Optics*", 3<sup>rd</sup> edition, Academic Press (2008).
22. J. Ma'rqez, L. Geelhaar, and K. Jacobi, "*Atomically resolved structure of InAs quantum dots*" Appl. Phys. Lett. **78**, 2309 (2001).
23. J. Los and A. Fasolino, "*Generalization of the  $k \cdot p$  approach for strained layered semiconductor structures grown on high-index-planes*", Phys. Rev. B **53**, 4630–4648 (1996).
24. New Semiconductor Materials. Characteristics and Properties, Loffe Physico-Technical Institute, Russia (<http://www.ioffe.ru/SVA/NSM/>).
25. J. Deng, F. Ye, Q. Y. Long and C. W. Lung, "*Reliability of measuring the roughness exponent in a small-length-scale regime*". Phys. Rev. B **59**, 8 (1999).
26. H. Y. Ramirez, C. H. Lin, C. C. Chao, Y. Hsu, W. T. You, S. Y. Huang, Y. T. Chen, H. C. Tseng, W. H. Chang, S. D. Lin, and S. J. Cheng, "*Optical fine structures of highly quantized InGaAs/GaAs self-assembled quantum dots*", Phys. Rev. B **81**, 245324 (2010).
27. H. Fu, L. W. Wang, and A. Zunger, "*Excitonic exchange splitting in bulk semiconductors*", Phys. Rev. B **85**, 5568 (1999)

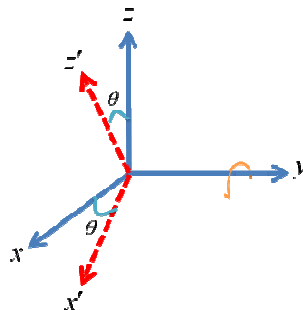
## Appendix I Rotation Matrix

Rather than a specific matrix, the rotation matrix is composed by the *rotation process*. The rotation matrices are defined first. If the xy-plane is rotated around the z-axis with an angle  $\phi$ , the rotation matrix is:

$$R_z(\phi) = \begin{bmatrix} \cos \phi & \sin \phi & 0 \\ -\sin \phi & \cos \phi & 0 \\ 0 & 0 & 1 \end{bmatrix} \quad (I.1)$$


A component in the new frame can be presented simply in terms of the old quantities. Also, following rotation around x-axis and y-axis with angles  $\psi$  and  $\theta$ , the individual matrices are as:

$$R_x(\psi) = \begin{bmatrix} 1 & 0 & 0 \\ 0 & \cos \psi & \sin \psi \\ 0 & -\sin \psi & \cos \psi \end{bmatrix} \quad (I.2)$$


$$R_y(\theta) = \begin{bmatrix} \cos \theta & 0 & -\sin \theta \\ 0 & 1 & 0 \\ \sin \theta & 0 & \cos \theta \end{bmatrix} \quad (I.3)$$


For the process that rotates around z-axis and then the y-axis and finally the x-axis rotates around  $\phi$ ,  $\theta$  and  $\psi$ , the entire process can be written as a rotation



matrix:

$$a(\psi, \theta, \phi) = R_x(\psi)R_y(\theta)R_z(\phi) \quad (\text{I.4})$$

Similarly, for the order of rotated axis comes by

1. rotate about z with angle  $\phi$
2. rotate about y with angle  $\theta$
3. rotate about new z with angle  $\gamma$

The rotation matrix becomes

$$a = R_z(\gamma)R_y(\theta)R_z(\phi) \quad (\text{I.6})$$

The frames needed can be reached by rotating the axis *no more than three times*.

For our two main purposes, first to transform the reference frame of compliance to [110] as well as transforming the reference frame of Hamiltonian. Therefore,

only  $R_z(\phi)$  is needed to form the rotation matrix. In tensor form:

$$a_{ij} = R_z(\phi) = \begin{bmatrix} \cos \phi & \sin \phi & 0 \\ -\sin \phi & \cos \phi & 0 \\ 0 & 0 & 1 \end{bmatrix} \quad (\text{I.7})$$

## Appendix II Reference frame transformation of kinetic part

Consider the Hamiltonian and its basis. Here, notations and definitions in Ref. [7] are adopted.

$$\begin{aligned} P_k &= \frac{\hbar^2 \gamma_1}{2m_0} (k_x^2 + k_y^2 + k_z^2) & Q_k &= \frac{\hbar^2 \gamma_2}{2m_0} (k_x^2 + k_y^2 - 2k_z^2) \\ R_k &= \frac{\sqrt{3}}{2} \frac{\hbar^2}{m_0} [-\gamma_2 (k_x^2 - k_y^2) + 2i\gamma_3 k_x k_y] & S_k &= \frac{\sqrt{3}\hbar^2 \gamma_3}{m_0} (k_x - ik_y) k_z \end{aligned} \quad (\text{II.1})$$

$$H_k^{LK} = - \begin{bmatrix} P_k + Q_k & -S_k & R_k & 0 \\ -S_k^\dagger & P_k - Q_k & 0 & R_k \\ R_k^\dagger & 0 & P_k - Q_k & S_k \\ 0 & R_k^\dagger & S_k^\dagger & P_k + Q_k \end{bmatrix} \begin{matrix} |J=3/2, J_z=3/2\rangle \\ |J=3/2, J_z=1/2\rangle \\ |J=3/2, J_z=-1/2\rangle \\ |J=3/2, J_z=-3/2\rangle \end{matrix} \quad (\text{II.2})$$

The basis of Hamiltonian [4]

$$\begin{aligned} \left| \frac{3}{2}, \frac{3}{2} \right\rangle &= -\frac{1}{\sqrt{2}} |(X+iY)\uparrow\rangle \\ \left| \frac{3}{2}, \frac{1}{2} \right\rangle &= \frac{-1}{\sqrt{6}} |(X+iY)\downarrow\rangle + \sqrt{\frac{2}{3}} |Z\uparrow\rangle \\ \left| \frac{3}{2}, \frac{-1}{2} \right\rangle &= \frac{1}{\sqrt{6}} |(X-iY)\uparrow\rangle + \sqrt{\frac{2}{3}} |Z\downarrow\rangle \\ \left| \frac{3}{2}, \frac{-3}{2} \right\rangle &= \frac{1}{\sqrt{2}} |(X-iY)\downarrow\rangle \end{aligned} \quad (\text{II.3})$$

The simple basis forms a convenient  $k \cdot p$  Hamiltonian relative to the basis

$|X\rangle, |Y\rangle, |Z\rangle$  [23]

$$D_{XYZ}(k) = - \begin{bmatrix} Lk_x^2 + M(k_y^2 + k_z^2) & Nk_xk_y & Nk_xk_y \\ Nk_xk_y & Lk_y^2 + M(k_x^2 + k_z^2) & Nk_yk_z \\ Nk_zk_x & Nk_xk_y & Lk_z^2 + M(k_x^2 + k_y^2) \end{bmatrix} \begin{bmatrix} |X\rangle \\ |Y\rangle \\ |Z\rangle \end{bmatrix} \quad (\text{II.4})$$

where

$$\begin{aligned} L &= \frac{\hbar^2}{2m_0}(\gamma_1 + 4\gamma_2) \\ M &= \frac{\hbar^2}{2m_0}(\gamma_1 - 2\gamma_2) \\ N &= \frac{\hbar^2}{2m_0}6\gamma_1 \end{aligned} \quad (\text{II.5})$$

Three steps to transfer the Hamiltonian to reach  $k'_x \parallel [110]$ ,  $k'_y \parallel [\bar{1}10]$ ,  $k'_z \parallel [001]$ .

1. Basis  $D_{XYZ} \Rightarrow D'_{X'Y'Z'}$
2.  $D_{XYZ}(k) \Rightarrow D'_{X'Y'Z'}(k')$
3. Re-compose  $H^{LK}(k')\{X', Y', Z'\}$

The first step transfers the matrix  $D_{XYZ}$ . The matrix is defined here as a second-rank tensor

$$\begin{aligned} D_{XYZ}(k) &\Rightarrow D_{kl} \\ D'_{X'Y'Z'}(k) &\Rightarrow D'_{ij} \end{aligned} \quad (\text{II.6})$$

Similar to the method in which stress is treated, a second-ranked tensor can be transformed via two rotation matrixes.

$$D'_{ij} = a_{ik}a_{jl}D_{kl} \quad (\text{II.7})$$

$\phi = \frac{\pi}{4}$ , the rotation matrix becomes

$$a_{ij} = \frac{1}{\sqrt{2}} \begin{bmatrix} 1 & 1 & 0 \\ -1 & 1 & 0 \\ 0 & 0 & \sqrt{2} \end{bmatrix} \quad (\text{II.8})$$

$$a_{11} = \frac{1}{\sqrt{2}} \quad a_{12} = \frac{1}{\sqrt{2}} \quad a_{13} = 0 \quad \dots$$

$$D'_{ij} = a_{ik} a_{jl} D_{kl}$$

Ex :

$$D'_{11} = \sum_{k,l=1}^3 a_{1k} a_{1l} D_{kl} \quad (\text{II.9})$$

$$= a_{11} a_{11} D_{11} + a_{11} a_{12} D_{12} + a_{11} a_{13} D_{13} +$$

$$a_{12} a_{11} \sigma''_{21} + a_{12} a_{12} \sigma''_{22} + a_{12} a_{13} D_{23} +$$

$$a_{13} a_{11} D_{31} + a_{13} a_{12} D_{32} + a_{13} a_{13} D_{33}$$

$$D'_{12} = \sum_{k,l=1}^3 a_{1k} a_{2l} D_{kl}$$

⋮

$$D'_{11} = \sum_{k,l=1}^3 a_{1k} a_{1l} D_{kl} \quad (\text{II.10})$$

$$= a_{11} a_{11} D_{11} + a_{11} a_{12} D_{12} + a_{11} a_{13} D_{13} +$$

$$a_{12} a_{11} D_{21} + a_{12} a_{12} D_{22} + a_{12} a_{13} D_{23} +$$

$$a_{13} a_{11} D_{31} + a_{13} a_{12} D_{32} + a_{13} a_{13} D_{33}$$

$$= a_{11} a_{11} D_{11} + a_{11} a_{12} D_{12} + a_{12} a_{11} D_{21} + a_{12} a_{12} D_{22}$$

$$= -\frac{1}{2} [Lk_x^2 + M(k_y^2 + k_z^2)] - Nk_x k_y - \frac{1}{2} [Lk_y^2 + M(k_x^2 + k_z^2)]$$

$$= -\frac{1}{2} (L(k_x^2 + k_y^2) + M(k_x^2 + k_y^2 + 2k_z^2) + 2Nk_{xy})$$

$$\vdots$$

By following this method, the  $k \cdot p$  Hamiltonian can be obtained with new basis of  $|X'\rangle$ ,  $|Y'\rangle$ ,  $|Z'\rangle$

$$D'_{x'yz'}(\vec{k}) = -\frac{1}{2} \begin{pmatrix} L(k_x^2 + k_y^2) + M(k_x^2 + k_y^2 + 2k_z^2) + 2Nk_xk_y & (M-L)(k_x^2 - k_y^2) & \sqrt{2}N(k_x + k_y)k_z \\ (M-L)(k_x^2 - k_y^2) & L(k_x^2 + k_y^2) + M(k_x^2 + k_y^2 + 2k_z^2) - 2Nk_xk_y & -\sqrt{2}N(k_x - k_y)k_z \\ \sqrt{2}N(k_x + k_y)k_z & -\sqrt{2}N(k_x - k_y)k_z & 2[L(k_z^2) + M(k_x^2 + k_y^2)] \end{pmatrix} \quad (\text{II.11})$$

Recall that the  $k$  terms here are still along the original reference frame. The final step must be performed to orientate around  $z$ -axis to match  $k'_x \parallel [110]$ ,  $k'_y \parallel [\bar{1}10]$ ,  $k'_z \parallel [001]$ . Where  $k$  is a first-ranked tensor, in which a rotation matrix is simply applied. Notably, the  $k$  value is represented in terms of  $k'$

$$\begin{aligned} k_i &= a_{ji} k'_j \quad (i, j=1\sim3) \\ k_x &= \frac{1}{\sqrt{2}}(k'_x - k'_y) \\ k_y &= \frac{1}{\sqrt{2}}(k'_x + k'_y) \\ k_z &= k'_z \end{aligned} \quad (\text{II.12})$$

Incorporating (II.12) into  $D'_{x'yz'}(\vec{k})$  leads to  $D'_{x'yz'}(\vec{k}')$

$$D'_{x'yz'}(\vec{k}') = -\frac{1}{2} \begin{pmatrix} k_x'^2(L+M+N) + k_y'^2(L+M-N) + 2Mk_z'^2 & 2(L-M)k'_xk'_y & 2N(k'_xk'_z) \\ 2(L-M)k'_xk'_y & k_x'^2(L+M-N) + k_y'^2(L+M+N) + 2Mk_z'^2 & 2N(k'_yk'_z) \\ 2N(k'_xk'_z) & 2N(k'_yk'_z) & 2[L(k_z'^2) + M(k_x'^2 + k_y'^2)] \end{pmatrix} \begin{pmatrix} |X'\rangle \\ |Y'\rangle \\ |Z'\rangle \end{pmatrix} \quad (\text{II.13})$$

$$D'_{x'yz'}(\vec{k}') \equiv D'_{ij} \quad (\text{II.14})$$

Finally, the 4-band  $k \cdot p$  Hamiltonian is recomposed with the basis of Slater orbital. The basis of Hamiltonian  $H'$  in the new reference frame of  $[110]$  now

becomes

$$\begin{aligned}
u'_1 \equiv u'_{3/2} &= \left| \frac{3}{2}, \frac{3}{2} \right\rangle = -\frac{1}{\sqrt{2}} |(X' + iY') \uparrow\rangle \\
u'_2 \equiv u'_{1/2} &= \left| \frac{3}{2}, \frac{1}{2} \right\rangle = \frac{-1}{\sqrt{6}} |(X' + iY') \downarrow\rangle + \sqrt{\frac{2}{3}} |Z' \uparrow\rangle \\
u'_3 \equiv u'_{-1/2} &= \left| \frac{3}{2}, \frac{-1}{2} \right\rangle = \frac{1}{\sqrt{6}} |(X' - iY') \uparrow\rangle + \sqrt{\frac{2}{3}} |Z' \downarrow\rangle \\
u'_4 \equiv u'_{-3/2} &= \left| \frac{3}{2}, \frac{-3}{2} \right\rangle = \frac{1}{\sqrt{2}} |(X' - iY') \downarrow\rangle
\end{aligned} \tag{II.15}$$

$$H'_{ij} = \langle u'_i | u'_j \rangle$$

Ex :

$$\begin{aligned}
H'_{11} &= \langle u_1 | u_1 \rangle = \left\langle \frac{3}{2}, \frac{3}{2} \left| \frac{3}{2}, \frac{3}{2} \right\rangle \right\rangle = \frac{1}{2} \langle (X' - iY') \uparrow | (X' + iY') \uparrow \rangle \\
&= \frac{1}{2} (\langle X' | X' \rangle - \langle Y' | X' \rangle + \langle X' | Y' \rangle + \langle Y' | Y' \rangle) \\
&= \frac{1}{2} \times \frac{-1}{2} (D'_{11} - D'_{21} + D'_{12} + D'_{22}) \\
&= \frac{-1}{4} [k_x'^2 (L + M + N) + k_y'^2 (L + M - N) + 2Mk_z'^2] - \frac{-1}{4} [2(L - M)k'_x k'_y] \\
&\quad + \frac{-1}{4} [2(L - M)k'_x k'_y] + \frac{-1}{4} [k_x'^2 (L + M - N) + k_y'^2 (L + M + N) + 2Mk_z'^2] \\
&= -\frac{1}{2} [k_x'^2 (L + M) + k_y'^2 (L + M) + 2Mk_z'^2] = -P'_k - Q'_k
\end{aligned} \tag{II.16}$$

$$\begin{aligned}
H'_{22} &= \langle u_2 | u_2 \rangle = \left\langle \frac{3}{2}, \frac{1}{2} \left| \frac{3}{2}, \frac{1}{2} \right\rangle \right\rangle \\
&= \left\langle \left( \frac{-1}{\sqrt{6}} (X' - iY') \downarrow - \sqrt{\frac{2}{3}} Z' \uparrow \right) \left| \left( \frac{-1}{\sqrt{6}} (X' + iY') \downarrow - \sqrt{\frac{2}{3}} Z' \uparrow \right) \right\rangle \right\rangle \\
&= \frac{1}{6} (\langle X' | X' \rangle - i \langle Y' | X' \rangle + i \langle X' | Y' \rangle + \langle Y' | Y' \rangle) + \frac{2}{3} \langle Z' | Z' \rangle \\
&= \frac{1}{6} (D'_{11} - iD'_{21} + iD'_{12} + D'_{22}) + \frac{2}{3} D'_{33} \\
&= -\frac{1}{6} (k_x'^2 (L + 5M) + k_y'^2 (L + 5M) + 2k_z'^2 (2L + M)) \\
&= -P'_k + Q'
\end{aligned} \tag{II.17}$$

$$\begin{aligned}
H'_{12} &= \langle u_1 | u_2 \rangle = \left\langle \frac{3}{2}, \frac{3}{2} \middle| \frac{3}{2}, \frac{1}{2} \right\rangle \\
&= \frac{1}{\sqrt{3}} (k'_x - ik'_y) k'_z \times N \\
&= S'
\end{aligned} \tag{II.18}$$

$$\begin{aligned}
H'_{13} &= \langle u_1 | u_3 \rangle = \left\langle \frac{3}{2}, \frac{3}{2} \middle| \frac{3}{2}, -\frac{1}{2} \right\rangle \\
&= \frac{1}{2\sqrt{3}} \left( -(k_x^2 - k_y^2) N + 2ik_x k_y (L - M) \right) \\
&= -R'
\end{aligned} \tag{II.19}$$

Based on Eqs. (II.16) and (II.17),  $P'_k$  and  $Q'_k$  are obtained

$$\begin{aligned}
P'_k &= -\frac{1}{2} (H'_{11} + H'_{22}) \\
Q'_k &= -\frac{1}{2} (H'_{11} - H'_{22})
\end{aligned} \tag{II.20}$$

Then, inserting  $L, M, N$  into Eqs. (I.16-I.19) yields the final results.

$$H_k^{LK} = - \begin{bmatrix} P'_k + Q'_k & -S'_k & R'_k & 0 \\ -S_k^{\dagger} & P'_k - Q'_k & 0 & R'_k \\ R_k^{\dagger} & 0 & P'_k - Q'_k & S'_k \\ 0 & R_k^{\dagger} & S_k^{\dagger} & P'_k + Q'_k \end{bmatrix} \begin{matrix} |J=3/2, J_z=3/2\rangle \\ |J=3/2, J_z=1/2\rangle \\ |J=3/2, J_z=-1/2\rangle \\ |J=3/2, J_z=-3/2\rangle \end{matrix} \tag{II.21}$$

$$\begin{aligned}
P'_k &= \frac{\hbar^2 \gamma_1}{2m_0} (k_x'^2 + k_y'^2 + k_z'^2) & Q'_k &= \frac{\hbar^2 \gamma_2}{2m_0} (k_x'^2 + k_y'^2 - 2k_z'^2) \\
R'_k &= \frac{\sqrt{3}}{2} \frac{\hbar^2}{m_0} \left[ -\gamma_3 (k_x'^2 - k_y'^2) + 2i\gamma_2 k'_x k'_y \right] & S'_k &= \frac{\sqrt{3}\hbar^2 \gamma_3}{m_0} (k'_x - ik'_y) k'_z
\end{aligned} \tag{II.22}$$

For simplicity, the Hamiltonian is written in which  $x$  along  $[110]$ ,  $y$  along  $[\bar{1}10]$ ,  $z$  run along  $[001]$ . Therefore, the Hamiltonian can be presented as

$$H_{k,[110]}^{LH} = - \begin{bmatrix} P_k + Q_k & -S_k & R_k & 0 \\ -S_k^{\dagger} & P_k - Q_k & 0 & R_k \\ R_k^{\dagger} & 0 & P_k - Q_k & S_k \\ 0 & R_k^{\dagger} & S_k^{\dagger} & P_k + Q_k \end{bmatrix} \begin{matrix} |J=3/2, J_z=3/2\rangle \\ |J=3/2, J_z=1/2\rangle \\ |J=3/2, J_z=-1/2\rangle \\ |J=3/2, J_z=-3/2\rangle \end{matrix} \tag{II.23}$$



$$\begin{aligned}
P_k &= \frac{\hbar^2 \gamma_1}{2m_0} (k_x^2 + k_y^2 + k_z^2) & Q_k &= \frac{\hbar^2 \gamma_2}{2m_0} (k_x^2 + k_y^2 - 2k_z^2) \\
R_k &= \frac{\sqrt{3}}{2} \frac{\hbar^2}{m_0} \left[ -\gamma_3 (k_x^2 - k_y^2) + 2i\gamma_2 k_x k_y \right] & S_k &= \frac{\sqrt{3}\hbar^2 \gamma_3}{m_0} (k_x - ik_y) k_z
\end{aligned} \tag{II.24}$$

Where  $k_x \parallel [110]$ ,  $k_y \parallel [\bar{1}10]$ ,  $k_z \parallel [001]$



### Appendix III Reference frame transformation of strain part

Orientation for the Hamiltonian in the strain part is approximately the same method with k part, the process is described. This method differs from the k part mainly in that the strain tensor is a second-ranked tensor. Some can be performed to transform it back onto the matrix form.

$$H_{\epsilon}^{LK} = - \begin{bmatrix} P_{\epsilon} + Q_{\epsilon} & -S_{\epsilon} & R_{\epsilon} & 0 \\ -S_{\epsilon}^{\dagger} & P_{\epsilon} - Q_{\epsilon} & 0 & R_{\epsilon} \\ R_{\epsilon}^{\dagger} & 0 & P_{\epsilon} - Q_{\epsilon} & S_{\epsilon} \\ 0 & R_{\epsilon}^{\dagger} & S_{\epsilon}^{\dagger} & P_{\epsilon} + Q_{\epsilon} \end{bmatrix} \begin{cases} |J=3/2, J_z=3/2\rangle \\ |J=3/2, J_z=1/2\rangle \\ |J=3/2, J_z=-1/2\rangle \\ |J=3/2, J_z=-3/2\rangle \end{cases} \quad (\text{III.1})$$

$$\begin{aligned} P_{\epsilon} &= -a_v(\epsilon_{xx} + \epsilon_{yy} + \epsilon_{zz}) & Q_{\epsilon} &= -\frac{b}{2}(\epsilon_{xx} + \epsilon_{yy} - 2\epsilon_{zz}) \\ R_{\epsilon} &= \frac{\sqrt{3}}{2}b(\epsilon_{xx} - \epsilon_{yy}) - i d \epsilon_{xy} & S_{\epsilon} &= -d(\epsilon_{xz} - i\epsilon_{yz}) \end{aligned} \quad (\text{III.2})$$

The  $k \cdot p$  Hamiltonian relative to the basis  $|X\rangle, |Y\rangle, |Z\rangle$  [23] is composed.

$$D_{XYZ}^{str} = \begin{bmatrix} l_s \epsilon_{xx} + m_s(\epsilon_{yy} + \epsilon_{zz}) & n_s \epsilon_{yx} & n_s \epsilon_{xz} \\ n_s \epsilon_{yx} & l_s \epsilon_{yy} + m_s(\epsilon_{xx} + \epsilon_{zz}) & n_s \epsilon_{yz} \\ n_s \epsilon_{zx} & n_s \epsilon_{zy} & l_s \epsilon_{zz} + m_s(\epsilon_{xx} + \epsilon_{yy}) \end{bmatrix} \begin{cases} |X\rangle \\ |Y\rangle \\ |Z\rangle \end{cases} \quad (\text{III.3})$$

According to Ref. [23], parameter  $a$  is defined in opposition to that of the text book of Chuang [4] which is refer to be the main reference of this thesis.

Therefore, the sign is changed in front of  $a$  to adapt to the textbook of Chang.

$$\begin{aligned} l_s &= +a + 2b \\ m_s &= +a - b \\ n_s &= \sqrt{3}d \end{aligned} \quad (\text{III.4})$$

Three steps to transfer the Hamiltonian to reach  $\epsilon'_{xx} \parallel [110]$ ,  $\epsilon'_{yy} \parallel [\bar{1}10]$ ,  $\epsilon'_{zz} \parallel [001]$ .

1. Basis transformation  $D_{XYZ}(\epsilon) \Rightarrow D_{X'Y'Z'}^{str}(\epsilon)$
2.  $D_{XYZ}(\epsilon) \Rightarrow D_{X'Y'Z'}^{str}(\epsilon')$

### 3. Re-compose $H'_{\epsilon'}^{LK} \{X', Y', Z'\}$

The first and third steps are the same as those in k part of in Appendix II

$$D_{XYZ}^{str} = D_{ij}^{str} \quad (III.5)$$

$$D_{ij}^{'str} = a_{ik} a_{jl} D_{kl}^{str} \quad (III.6)$$

The convenient Hamiltonian becomes

$$D_{ij}^{'str} = D_{X'Y'Z'}^{'str}(\epsilon) \quad (III.7)$$

$$= \frac{1}{2} \begin{pmatrix} l(\epsilon_{xx} + \epsilon_{yy}) + m(\epsilon_{xx} + \epsilon_{yy} + 2\epsilon_{zz}) & (m-l)(\epsilon_{xx} + \epsilon_{yy}) & \sqrt{2}n(\epsilon_{xz} + \epsilon_{yz}) \\ + 2n\epsilon_{xy} & l(\epsilon_{xx} + \epsilon_{yy}) + m(\epsilon_{xx} + \epsilon_{yy} + 2\epsilon_{zz}) & -\sqrt{2}n(\epsilon_{xz} - \epsilon_{yz}) \\ (m-l)(\epsilon_{xx} + \epsilon_{yy}) & -2n\epsilon_{xy} & \\ \sqrt{2}n(\epsilon_{xz} + \epsilon_{yz}) & -\sqrt{2}n(\epsilon_{xz} - \epsilon_{yz}) & 2[l\epsilon_{zz} + m(\epsilon_{xx} + \epsilon_{yy})] \end{pmatrix} \begin{pmatrix} |X'\rangle \\ |Y'\rangle \\ |Z'\rangle \end{pmatrix}$$

Notably, the second part requires one more procedure to transfer the second-ranked strain tensor into strain matrix form. The strain tensor in the old reference frame is presented in terms of the new one

$$\epsilon_{kl} = a_{ik} a_{jl} \epsilon'_{ij} \quad (III.8)$$

	xx	yy	zz	yz, z	xz, xz	xy, yx
tensor notation	11	22	33	23,32	31,13	12,21
matrix notation	1	2	3	4	5	6

Tensor form

matrix form

Cartesian notation

$\varepsilon_{11} = \frac{1}{2}(\varepsilon'_{11} - 2\varepsilon'_{12} + \varepsilon'_{22})$	$\varepsilon_1 = \frac{1}{2}(\varepsilon'_1 - \varepsilon'_6 + \varepsilon'_2)$	$\varepsilon_{xx} = \frac{1}{2}(\varepsilon'_{xx} - \varepsilon'_{xy} + \varepsilon'_{yy})$
$\varepsilon_{22} = \frac{1}{2}(\varepsilon'_{11} + 2\varepsilon'_{12} + \varepsilon'_{22})$	$\varepsilon_2 = \frac{1}{2}(\varepsilon'_1 + \varepsilon'_6 + \varepsilon'_2)$	$\varepsilon_{yy} = \frac{1}{2}(\varepsilon'_{xx} + \varepsilon'_{xy} + \varepsilon'_{yy})$
$\varepsilon_{33} = \varepsilon'_3$	$\varepsilon_3 = \varepsilon'_3$	$\varepsilon_{zz} = \varepsilon'_{zz}$
$\varepsilon_{23} = \frac{1}{\sqrt{2}}(\varepsilon'_{13} + \varepsilon'_{23})$	$\varepsilon_4 = \frac{1}{\sqrt{2}}(\varepsilon'_5 + \varepsilon'_4)$	$2\varepsilon_{yz} = \frac{1}{\sqrt{2}}(\varepsilon'_{xz} + \varepsilon'_{yz})$
$\varepsilon_{13} = \frac{1}{\sqrt{2}}(\varepsilon'_{13} - \varepsilon'_{23})$	$\varepsilon_5 = \frac{1}{\sqrt{2}}(\varepsilon'_5 - \varepsilon'_4)$	$2\varepsilon_{xz} = \frac{1}{\sqrt{2}}(\varepsilon'_{xz} - \varepsilon'_{yz})$
$\varepsilon_{12} = \frac{1}{2}(\varepsilon'_{11} - \varepsilon'_{22})$	$\frac{1}{2}\varepsilon_6 = \frac{1}{2}(\varepsilon'_1 - \varepsilon'_2)$	$2\varepsilon_{xy} = (\varepsilon'_{xx} - \varepsilon'_{yy})$

Inserting the result above into  $D'^{str}_{XY'Z'}(\varepsilon)$  leads to  $D'^{str}_{XY'Z'}(\varepsilon')$ .

$$D'^{str}_{XY'Z'}(\varepsilon') =$$

$$\frac{1}{2} \begin{bmatrix} \sqrt{3}d(\varepsilon'_{xx} - \varepsilon'_{yy}) + b(\varepsilon'_{xx} + \varepsilon'_{yy} - 2\varepsilon'_{zz}) & 3b\varepsilon'_{xy} & 2\sqrt{3}d\varepsilon'_{xz} \\ +a(\varepsilon'_{xx} + \varepsilon'_{yy} + \varepsilon'_{zz}) & \sqrt{3}d(-\varepsilon'_{xx} + \varepsilon'_{yy}) + b(\varepsilon'_{xx} + \varepsilon'_{yy} - 2\varepsilon'_{zz}) & \sqrt{6}d(-\varepsilon'_{xz} + \varepsilon'_{yz}) \\ 3b\varepsilon'_{yx} & +a(\varepsilon'_{xx} + \varepsilon'_{yy} + \varepsilon'_{zz}) & -2b(\varepsilon'_{xx} + \varepsilon'_{yy} - 2\varepsilon'_{zz}) + 2a(\varepsilon'_{xx} + \varepsilon'_{yy} + \varepsilon'_{zz}) \\ 2\sqrt{3}d\varepsilon'_{zx} & \sqrt{6}d(-\varepsilon'_{zx} + \varepsilon'_{zy}) & 2a(\varepsilon'_{xx} + \varepsilon'_{yy} + \varepsilon'_{zz}) \end{bmatrix} \begin{bmatrix} |X'\rangle \\ |Y'\rangle \\ |Z'\rangle \end{bmatrix} \quad (III.9)$$

Finally, recompose again the  $4 \times 4$   $k.p$  Hamiltonian  $H'^{LK}_{\varepsilon'} \{X', Y', Z'\}$ .

$$H'^{LK}_{\varepsilon'} = - \begin{bmatrix} P'_\varepsilon + Q'_\varepsilon & -S'_\varepsilon & R'_\varepsilon & 0 \\ -S'^{\dagger}_\varepsilon & P'_\varepsilon - Q'_\varepsilon & 0 & R'_\varepsilon \\ R'^{\dagger}_\varepsilon & 0 & P'_\varepsilon - Q'_\varepsilon & S'_\varepsilon \\ 0 & R'^{\dagger}_\varepsilon & S'^{\dagger}_\varepsilon & P'_\varepsilon + Q'_\varepsilon \end{bmatrix} \begin{bmatrix} |J=3/2, J_z=3/2\rangle \\ |J=3/2, J_z=1/2\rangle \\ |J=3/2, J_z=-1/2\rangle \\ |J=3/2, J_z=-3/2\rangle \end{bmatrix} \quad (III.10)$$

$$\begin{aligned} P'_\varepsilon &= -a_v(\varepsilon'_{xx} + \varepsilon'_{yy} + \varepsilon'_{zz}) & Q'_\varepsilon &= -\frac{b}{2}(\varepsilon'_{xx} + \varepsilon'_{yy} - 2\varepsilon'_{zz}) \\ R'_\varepsilon &= \frac{d}{2}(\varepsilon'_{xx} - \varepsilon'_{yy}) - i\sqrt{3}b\varepsilon'_{xy} & S'_\varepsilon &= -d[\varepsilon'_{xz} - i\varepsilon'_{yz}] \end{aligned} \quad (III.11)$$

To sum up and simplify, a Luttinger Kohn Hamiltonian of strain part can be presented as

$$H_{\varepsilon,[110]}^{LK} = - \begin{bmatrix} P_{\varepsilon} + Q_{\varepsilon} & -S_{\varepsilon} & R_{\varepsilon} & 0 \\ -S_{\varepsilon}^{\dagger} & P_{\varepsilon} - Q_{\varepsilon} & 0 & R_{\varepsilon} \\ R_{\varepsilon}^{\dagger} & 0 & P_{\varepsilon} - Q_{\varepsilon} & S_{\varepsilon} \\ 0 & R_{\varepsilon}^{\dagger} & S_{\varepsilon}^{\dagger} & P_{\varepsilon} + Q_{\varepsilon} \end{bmatrix} \begin{matrix} |J=3/2, J_z=3/2\rangle \\ |J=3/2, J_z=1/2\rangle \\ |J=3/2, J_z=-1/2\rangle \\ |J=3/2, J_z=-3/2\rangle \end{matrix} \quad (\text{III.12})$$

$$\begin{aligned} P_{\varepsilon} &= -a_v (\varepsilon_{xx} + \varepsilon_{yy} + \varepsilon_{zz}) & Q_{\varepsilon} &= -\frac{b}{2} (\varepsilon_{xx} + \varepsilon_{yy} - 2\varepsilon_{zz}) \\ R_{\varepsilon} &= \frac{d}{2} (\varepsilon_{xx} - \varepsilon_{yy}) - i\sqrt{3}b\varepsilon_{xy} & S_{\varepsilon} &= -d [\varepsilon_{xz} - i\varepsilon_{yz}] \end{aligned} \quad (\text{III.13})$$

Where  $\varepsilon_{xx} \parallel [110]$ ,  $\varepsilon_{yy} \parallel [\bar{1}10]$ ,  $\varepsilon_{zz} \parallel [001]$ .



## Appendix IV Strain modification by six-band model

The master's thesis of Chang [4] mentioned that while the strain effect is taken into consideration, the effect of split off should be considered:

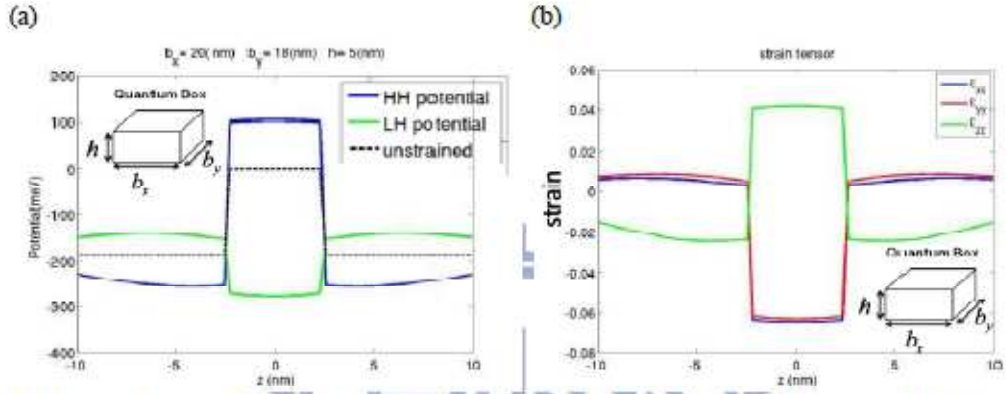


圖 3.2.7、 $b_x = 20$  (nm)、 $b_y = 18$  (nm)、 $h = 5$  (nm) 的量子盒形狀量子點。(a)輕重電洞位能。(b)使用 Comsol multiphysics 所計算的應變。

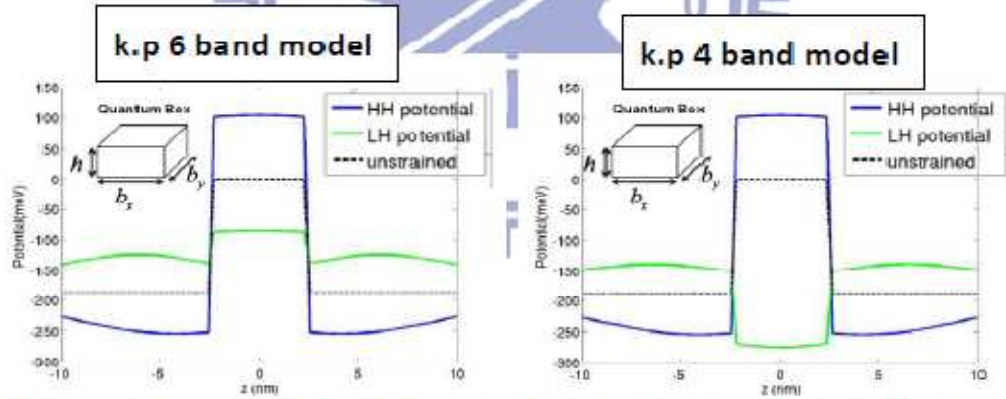


圖 3.2.8、 $b_x = 20$  (nm)、 $b_y = 18$  (nm)、 $h = 5$  (nm) 的量子盒形狀量子點的輕重電洞位能。(a)六能帶模型。(b)四能帶模型。

[18]

Fig. IV.1 shows the LH-potential is underestimated in the 4-band model which leads to the overestimation of  $\Delta_{HL}^e$ , therefore the 6 band model of strain part is used throughout this thesis.

A six-band Hamiltonian without  $R$  and  $S$  terms is given by

$$H(k=0) = \begin{bmatrix} |HH\rangle & |HH\rangle & |LH\rangle & |LH\rangle & |SO\rangle & |SO\rangle \\ P_\varepsilon + Q_\varepsilon & 0 & 0 & 0 & 0 & 0 \\ 0 & P_\varepsilon - Q_\varepsilon & 0 & 0 & -\sqrt{2}Q_\varepsilon & 0 \\ 0 & 0 & P_\varepsilon - Q_\varepsilon & 0 & 0 & \sqrt{2}Q_\varepsilon \\ 0 & 0 & 0 & P_\varepsilon + Q_\varepsilon & 0 & 0 \\ 0 & -\sqrt{2}Q_\varepsilon & 0 & 0 & P_\varepsilon + \Delta & 0 \\ 0 & 0 & \sqrt{2}Q_\varepsilon & 0 & 0 & P_\varepsilon + \Delta \end{bmatrix} \quad [4] \quad (IV.1)$$

To simplify and solve the Hamiltonian, the basis are rearranged

$$H(k=0) = \begin{bmatrix} |HH\rangle & |HH\rangle & |LH\rangle & |LH\rangle & |SO\rangle & |SO\rangle \\ P_\varepsilon + Q_\varepsilon & 0 & 0 & 0 & 0 & 0 \\ 0 & P_\varepsilon + Q_\varepsilon & 0 & 0 & 0 & 0 \\ \hline 0 & 0 & P_\varepsilon - Q_\varepsilon & 0 & 0 & \sqrt{2}Q_\varepsilon \\ 0 & 0 & 0 & P_\varepsilon - Q_\varepsilon & -\sqrt{2}Q_\varepsilon & 0 \\ 0 & 0 & 0 & -\sqrt{2}Q_\varepsilon & P_\varepsilon + \Delta & 0 \\ 0 & 0 & \sqrt{2}Q_\varepsilon & 0 & 0 & P_\varepsilon + \Delta \end{bmatrix} \quad (IV.2)$$

The eigen energy of heavy-hole is directly obtained

Further consider the rest energies of light hole and split off are set to be  $\lambda$ ,

The eigenenergies  $\lambda$  is obtained via the following steps:

$$\det \begin{vmatrix} P_\varepsilon - Q_\varepsilon - \lambda & 0 & 0 & \sqrt{2}Q \\ 0 & P_\varepsilon - Q_\varepsilon - \lambda & -\sqrt{2}Q & 0 \\ 0 & -\sqrt{2}Q & P_\varepsilon + \Delta - \lambda & 0 \\ \sqrt{2}Q & 0 & 0 & P_\varepsilon + \Delta - \lambda \end{vmatrix} = 0 \quad (IV.3)$$

then reduce the matrix to  $3 \times 3$  matrices

$$(P_\varepsilon - Q_\varepsilon - \lambda) \begin{vmatrix} P_\varepsilon - Q_\varepsilon - \lambda & -\sqrt{2}Q & 0 \\ -\sqrt{2}Q & P_\varepsilon + \Delta - \lambda & 0 \\ 0 & 0 & P_\varepsilon + \Delta - \lambda \end{vmatrix} - \sqrt{2}Q \begin{vmatrix} 0 & P_\varepsilon - Q_\varepsilon - \lambda & -\sqrt{2}Q \\ 0 & -\sqrt{2}Q & P_\varepsilon + \Delta - \lambda \\ \sqrt{2}Q & 0 & 0 \end{vmatrix} = 0 \quad (IV.4)$$

again, reduce to  $2 \times 2$  matrices

$$(P_\varepsilon - Q_\varepsilon - \lambda)(P_\varepsilon + \Delta - \lambda) \begin{vmatrix} P_\varepsilon - Q_\varepsilon - \lambda & -\sqrt{2}Q \\ -\sqrt{2}Q & P_\varepsilon + \Delta - \lambda \end{vmatrix} + \sqrt{2}Q(-\sqrt{2}Q) \begin{vmatrix} P_\varepsilon - Q_\varepsilon - \lambda & -\sqrt{2}Q \\ -\sqrt{2}Q & P_\varepsilon + \Delta - \lambda \end{vmatrix} = 0 \quad (IV.5)$$

Finally obtain the equation and lead to the result:

$$[\lambda^2 - (2P - Q + \Delta)\lambda + (P\Delta - QP - Q\Delta)]^2 = 0 \quad (IV.6)$$



$$\lambda = \frac{(2P - Q + \Delta) \pm \sqrt{\Delta^2 + 2\Delta Q + 9Q^2}}{2} \quad (\text{IV.7})$$

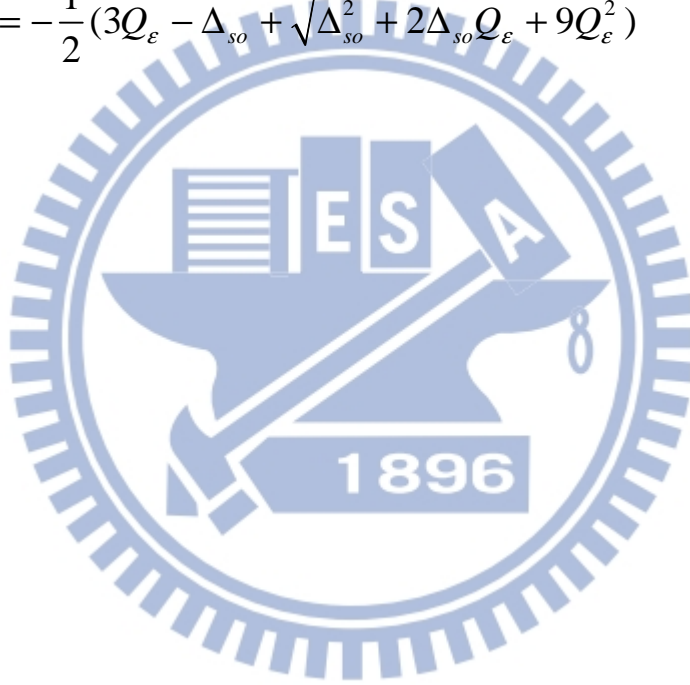
Thus the eigenenergies corresponding to the basis are:

$$E_{HH}(0) = P_\varepsilon + Q_\varepsilon \quad (\text{IV.8})$$

$$E_{LH}(0) = P_\varepsilon - Q_\varepsilon + \frac{1}{2}(Q_\varepsilon + \Delta - \sqrt{\Delta^2 + 2\Delta Q_\varepsilon + 9Q_\varepsilon^2}) \quad (\text{IV.9})$$

$$E_{SO}(0) = P_\varepsilon - Q_\varepsilon + \frac{1}{2}(Q_\varepsilon + \Delta + \sqrt{\Delta^2 + 2\Delta Q_\varepsilon + 9Q_\varepsilon^2}) \quad (\text{IV.10})$$

$$\begin{aligned} \Delta_{HL}^\varepsilon &= E_{LH}^\varepsilon - E_{HH}^\varepsilon \\ &= -\frac{1}{2}(3Q_\varepsilon - \Delta_{so} + \sqrt{\Delta_{so}^2 + 2\Delta_{so}Q_\varepsilon + 9Q_\varepsilon^2}) \end{aligned} \quad (\text{IV.11})$$



## Parameters

Quantity	Label	Unit	InAs	GaAs	Ref.
Lattice constant	$a$	nm	0.6055	0.565	[4]
Bohr radius	$a_B^*$	nm	34	11	[4]
Energy gap	$E_g$	eV	0.413	1.518	[426]
Optical matrix parameter	$E_p$	eV	21.5	28.8	[26]
Spin-orbit coupling energy	$\Delta$	eV	0.38	0.34	[4]
Static dielectric constan	$\epsilon_d$	$\epsilon_0$	15.2	12.5	[26]
CB effective mass	$m^*$	$m_0$	0.05	0.0665	[4]
Bulk exchange splitting	$\Delta_{eh,bulk}^{xc}$	$\mu eV$	2.5	20	[27]
Luttinger parameter	$\gamma_1$		19.7	6.85	[4]
Luttinger parameter	$\gamma_2$		8.4	2.1	[4]
Luttinger parameter	$\gamma_3$		9.3	2.9	[4]
CB hydrostatic def. pot	$a_c$	eV	-5.08	-8.013	[4]
VB hydrostatic def. pot	$a_v$	eV	1.00	1.16	[4]
VB shear def. pot. [100]	$b$	eV	-1.8	-1.824	[4]
VB shear def. pot. [111]	$d$	eV	-3.6	-5.062	[4]
Young's Modulus[100]	$E$	GPa	51.4	85.9	[24]
Poisson's ratio[100]	$\nu$		0.35	0.31	[24]
Elastic stiffness constant[100]	$C_{11}$	GPa	83.3	118.8	[4]
Elastic stiffness constant[100]	$C_{12}$	GPa	45.3	53.8	[4]
Elastic stiffness constant[100]	$C_{44}$	GPa	39.6	59.4	[4]
Elastic compliance constant[100]	$S_{11}^{[100]}$	$GPa^{-1}$	0.0195	0.0117	
Elastic compliance constant[100]	$S_{12}^{[100]}$	$GPa^{-1}$	-0.0069	-0.0037	
Elastic compliance constant[100]	$S_{44}^{[100]}$	$GPa^{-1}$	0.0253	0.0168	
Elastic compliance constant[110]	$S_{11}^{[110]}$	$GPa^{-1}$	0.0126	0.0082	
Elastic compliance constant[110]	$S_{12}^{[110]}$	$GPa^{-1}$	-0.000025	-0.002	
Elastic compliance constant[110]	$S_{44}^{[110]}$	$GPa^{-1}$	0.0253	0.0168	
Elastic compliance constant[110]	$S_{66}^{[110]}$	$GPa^{-1}$	0.0528	0.0308	